



HAL
open science

Optimisation des réseaux cellulaires pour les communications professionnelles critiques

Alaa Daher

► **To cite this version:**

Alaa Daher. Optimisation des réseaux cellulaires pour les communications professionnelles critiques. Réseaux et télécommunications [cs.NI]. Université Paris Saclay (COmUE), 2019. Français. NNT : 2019SACLT009 . tel-02196785

HAL Id: tel-02196785

<https://pastel.hal.science/tel-02196785>

Submitted on 29 Jul 2019

HAL is a multi-disciplinary open access archive for the deposit and dissemination of scientific research documents, whether they are published or not. The documents may come from teaching and research institutions in France or abroad, or from public or private research centers.

L'archive ouverte pluridisciplinaire **HAL**, est destinée au dépôt et à la diffusion de documents scientifiques de niveau recherche, publiés ou non, émanant des établissements d'enseignement et de recherche français ou étrangers, des laboratoires publics ou privés.

Optimisation des réseaux cellulaires pour les communications professionnelles critiques

Thèse de doctorat de l'Université Paris-Saclay
préparée à Télécom ParisTech

Ecole doctorale n°580:
Sciences et Technologies de l'Information et de la Communication (STIC)
Spécialité de doctorat: Réseaux, Information et Communication

Thèse présentée et soutenue à Paris, le 28 Mars 2019, par

ALAA DAHER

Composition du Jury :

Marceau COUPECHOUX Professeur, Télécom ParisTech	Directeur de thèse
Philippe GODLEWSKI Professeur, Télécom ParisTech	co-Directeur de thèse
Rami LANGAR Professeur, Université Paris-Est	Rapporteur
Loutfi NUAYMI Professeur, IMT Atlantique	Rapporteur
Maryline HELARD Professeur, INSA Rennes	Examinatrice
Salah Eddine EL AYOUBI Maître de Conférences, CentraleSupélec	Examinateur
Jérôme BROUET Ingénieur de Recherche, Thales	Examinateur
Jean Marc KELIF Ingénieur de Recherche, Orange Labs	Examinateur

Telecom ParisTech

Laboratory for communication and processing of information (LTCI)

Network and Computer Science department (INFRES)

**Optimizing Cellular Networks for Business
and Mission-Critical Communications**

Thesis submitted for the degree of

Doctor of Philosophy

by:

Alaa DAHER

Paris, the 28th of March 2019

Marceau COUPECHOUX	Supervisor	Professor	Telecom ParisTech
Philippe GODLEWSKI	Co-Supervisor	Professor	Telecom ParisTech
Rami LANGAR	Reviewer	Professor	University Paris East
Loutfi NUAYMI	Reviewer	Professor	IMT Atlantique
Maryline HELARD	Examiner	Professor	INSA Rennes
Salah Eddine EL AYOUBI	Examiner	Associate Professor	CentraleSupélec
Jérôme BROUET	Examiner	Research Engineer	Thales
Jean Marc KELIF	Examiner	Research Engineer	Orange Labs

J
U
R
Y

Résumé

Les communications professionnelles et critiques sont établies soit entre utilisateurs du secteur de la sûreté publique soit entre acteurs opérants des infrastructures critiques. Du fait des fortes exigences en termes de couverture, de priorité d'accès, de fiabilité et de résilience, sans oublier les services supplémentaires pour les utilisateurs professionnels, ces communications utilisent généralement les technologies PMR (*Professional Mobile Radio*). Vu la croissance des demandes de services, des changements importants sont attendus dans le domaine de la PMR. Les technologies PMR historiques échouent en effet à fournir des services à débits de données élevés, tels que les services vidéos et le transfert de photos. Ainsi, l'adaptation des technologies utilisées par les opérateurs commerciaux à la PMR apparaît comme une solution prometteuse. D'autre part, la prochaine génération de réseaux cellulaires prévoit une nouvelle variété d'applications et de services, dont les exigences de performances sont hétérogènes. Ils se classent en trois groupes: *enhanced Mobile BroadBand* (eMBB), *massive Machine-Type Communications* (mMTC) et *Ultra-Reliable Low Latency Communications* (URLLC). Récemment, les communications critiques ont été classées dans la famille URLLC des cas d'usage car elles sont prioritaires par rapport aux autres types de communications dans le réseau.

Dans ce contexte, nous concentrons à renforcer la couverture des réseaux radio fournissant des communications de groupe, service essentiel fourni par les technologies PMR, afin de satisfaire les besoins. Tout d'abord, on évalue la performance des transmissions unicast et multicast, c'est à dire, les transmissions *Multicast/Broadcast Single Frequency Network* (MBSFN) et *Single-Cell Point-To-Multipoint* (SC-PTM), en termes de qualité radio, d'efficacité spectrale du système et de couverture de cellules, tout en considérant des configurations MBSFN statiques. Puis, nous étudions un modèle analytique pour estimer le *Signal to Interference plus Noise Ratio* (SINR) dans un réseau MBSFN.

En outre, nous proposons un algorithme simple de répétitions sans requête, comme alternative à l'algorithme *Hybrid Automatic Repeat re-Quest* (HARQ), afin d'améliorer la couverture du réseau en présence de communications de groupe. En considérant les caractéristiques du canal radio, ainsi que les contraintes de délai de service, nous justifions que notre modèle fournit un important gain par rapport aux algorithmes de répétitions traditionnels.

Enfin, on évalue le compromis entre la couverture et la capacité d'un réseau utilisant les transmissions multicast, qui évolue en fonction de la taille du *cluster* de stations serveuses. On formule alors un problème d'optimisation dont l'objectif est de maintenir une probabilité de blocage acceptable du système, tout en maximisant le SINR moyen du groupe d'utilisateurs. Pour chaque groupe, on choisit le *cluster* de cellules d'une manière dynamique, en se fondant sur la minimisation d'une fonction sous-modulaire, qui prend en compte le trafic de chaque cellule du réseau à travers certains poids, ainsi que le SINR moyen du groupe. Ces poids sont optimisés au moyen de la méthode Nelder-Mead, dans le but de diriger la probabilité de blocage vers un certain seuil. Les résultats obtenus montrent l'importance du regroupement dynamique des cellules dans l'amélioration de la capacité et la couverture du système.

Abstract

Business- and mission-critical communications are communications between professional users either from the public safety sector or operating critical infrastructures. Owing to special coverage, priority access, reliability and resilience requirements, as well as additional services for professional users, these communications are conveyed by Professional Mobile Radio (PMR) networks. Driven by the demand growth, significant changes are taking place in the PMR industry. The existing PMR technologies are indeed not well suited to provide high data rates mobile services like video and photo transfers; hence, the adoption of commercial technologies for mission-critical communications is gaining strong momentum. On the other hand, the next generation cellular networks are envisioned to support a large variety of applications and services with heterogeneous performance requirements, i.e., enhanced Mobile BroadBand (eMBB), massive Machine-Type Communications (mMTC) and Ultra-Reliable Low Latency Communications (URLLC). Recently, mission-critical communications have been classified in a URLLC use case family, characterized by the need to a higher priority over other communications in the networks.

In this context, we focus on enhancing the coverage of wireless networks providing group communications, the main service allowed by PMR networks, taking advantage of the current technologies (e.g. Multimedia Broadcast/Multicast Service), to meet the mission-critical communications needs. First, we evaluate the performance of unicast and multicast transmission techniques, i.e., the Multicast/Broadcast Single Frequency Network (MBSFN) and Single-Cell Point-To-Multipoint (SC-PTM), in terms of radio quality, system spectral efficiency and cell coverage, assuming static MBSFN configurations. Then, we introduce an analytical model to derive an approximate closed-form formula of the Signal to Interference plus Noise Ratio (SINR) in a MBSFN network.

Furthermore, we propose a simple repetition scheme without request, as an alternative to Hybrid Automatic Repeat re-Quest (HARQ), in the aim of improving the network coverage in presence of group communications. By considering the wireless channel characteristics, as well as the service delay constraints, we show that our proposed scheme provides significant gains over traditional repetition schemes.

Finally, we assess the trade-off in the cluster's size of serving cells which arises between network coverage and capacity in multi-point transmissions. We formulate an optimization problem to maintain an acceptable system blocking probability, while maximizing the average SINR of the multicast group users. For group calls, a dynamic cluster of cells is selected based on the minimization of a submodular function that takes into account the traffic in every cell through some weights and the average SINR achieved by the group users. Traffic weights are then optimized using a Nelder-Mead simplex method with the objective of tracking a blocking probability threshold. Results show the importance of dynamic clustering in improving system capacity and coverage.

Contents

List of Figures	ix
List of Tables	xiii
1 Introduction	1
1.1 Mission Critical Communications	2
1.1.1 Second Generation (2G) and Professional Mobile Radio (PMR)	4
1.1.2 Fourth Generation (4G)	5
1.1.3 Fifth Generation (5G)	6
1.2 Multimedia Broadcast/Multicast Service	8
1.2.1 MBMS Transmission Techniques	8
1.2.2 System Aspect Differences Between MBSFN and SC-PTM	11
1.2.3 MBMS System Architecture	13
1.2.4 MBMS Channels	15
1.3 Thesis Contributions	17
2 SC-PTM or MBSFN for Mission-Critical Communications?	19
2.1 Introduction	20
2.2 System model	21
2.2.1 Network Model	21
2.2.2 SINR Evaluation	22
2.2.3 Spectral Efficiency	24
2.2.4 TTI Bundling	26
2.3 Simulation Results	27
2.3.1 Simulation Settings	27
2.3.2 SINR Distributions	28
2.3.3 System Spectral Efficiency	30
2.3.4 Impact of Group Size	32

2.3.5	Cell Range	33
2.3.6	TTI Bundling Gain	35
2.4	Conclusion	37
3	SINR Model for MBSFN Networks	39
3.1	Introduction	40
3.2	System model	41
3.2.1	Network model	41
3.2.2	SINR evaluation	41
3.3	Analytical Approach	43
3.3.1	Analytical model	43
3.3.2	SINR Closed-Form Formula Assuming Shadowing	45
3.4	Simulation Results	48
3.4.1	Simulation Parameters	48
3.4.2	Deterministic Path-Loss	49
3.4.3	Impact of Shadowing	49
3.5	Conclusion	53
4	A Repetition Scheme for MBSFN	55
4.1	Introduction	56
4.2	System Models	57
4.2.1	Link Level Model	58
4.2.2	Rayleigh Fading Channel	58
4.2.3	Rayleigh Fading Simulation Model	61
4.2.4	System Level Model	65
4.3	Link Level Abstraction	65
4.3.1	Overall Architecture	65
4.3.2	Effective SNR	67
4.3.3	BLER Evaluation	68
4.4	Repetition Scheme	68
4.4.1	Design Principles	68
4.4.2	Proposed Scheme	70
4.5	Simulation Results	72
4.5.1	Simulation Parameters	72
4.5.2	Validation of the Link Level Abstraction	73
4.5.3	Repetition Scheme Results for EVA50 channel	74
4.5.4	Validation of Repetition Scheme Results for EPA3 channel	77

4.5.5	Cell Radius Gain	79
4.6	Conclusion	83
5	A Dynamic Clustering Algorithm for Multi-Point Transmissions	85
5.1	Introduction	86
5.2	Model and Problem Formulation	89
5.2.1	System Model	89
5.2.2	Traffic Model and Preliminary Results	90
5.2.3	Problem Formulation	94
5.3	A Dynamic Clustering Algorithm	95
5.3.1	Main Routine	95
5.3.2	Group Call Clustering	95
5.3.3	Cell Weights Optimization	100
5.3.4	Complexity Analysis	104
5.4	Simulation Results	104
5.4.1	Simulations Settings	104
5.4.2	Group Call Multi-point Transmission	105
5.4.3	Objective Function and Blocking Probabilities	106
5.4.4	SINR Improvements	107
5.4.5	Performance Evaluation Based Minimum Group SINR	108
5.4.6	Impact of Traffic Intensity	108
5.5	Conclusion	115
	Conclusion and Further Work	117
	Publications	119
	Bibliography	121
	Appendix A Submodular Functions Minimization	131
A.1	Introduction	132
A.2	Submodular Functions	132
A.2.1	Notations	132
A.2.2	Definitions	132
A.2.3	Submodular Functions Properties	133
A.3	Submodular Function Minimization	133
A.3.1	Problem Formulation	133
A.3.2	Lovász Extension	134

A.3.3	Convex Closure	138
A.4	Equivalent Optimization Problems	140
A.4.1	Minimal Minimizer	140
A.4.2	Linear Optimization over the Base Polyhedron	143
A.5	Min-Norm Algorithm	143
A.5.1	Initialization	143
A.5.2	Linear Optimization over the Base Polyhedron	143
A.5.3	Optimality Test	144
A.5.4	Norm Minimization over the Affine Hull	144
A.5.5	Line Search	145
A.5.6	Algorithm Termination	145
	Glossary	147

List of Figures

1.1	Mission critical communication users. Source: ETELM.	2
1.2	Next generation mobile networks use case scenarios [23].	7
1.3	MBSFN definitions [34].	10
1.4	MBMS system architecture [43].	14
1.5	Enhanced channel architecture due to MBMS [47].	16
1.6	MBSFN channels mapping [32].	17
2.1	SFN212 configuration.	22
2.2	SINR CDF of different transmission modes.	29
2.3	Probability distribution of CQI indexes (Scenario I - 4 UEs/BS).	31
2.4	Probability distribution of CQI indexes (Scenario II - 4 UEs/BS).	32
2.5	Minimum SINR CDF of SC-PTM for different numbers of group users per cell.	33
2.6	Outage probability vs. cell range.	34
2.7	Maximum cell range (for a 1% outage).	35
2.8	Impact of TTI bundling on coverage (1% outage) and SSE.	36
3.1	MBSFN network model.	42
3.2	Comparison of the analytical model with simulations assuming path-loss exponents $\eta = 2.7, 3.5$ and 4	49
3.3	Comparison of the analytical model with simulations assuming cell ranges $R = 500$ m, 2500 m and 5000 m.	50
3.4	Comparison of the analytical model with simulations assuming different MBSFN area configurations.	51
3.5	Comparison of the analytical model with Monte Carlo simulations and Fenton-Wilkinson approach assuming $R = 1500$ m, $\eta = 3.5$ and $\sigma = 3, 6$ and 8 dB. Left: SINR as a function of UE-BS distance. Right: CDF of the SINR.	52
4.1	Wave's arrival angles in Jakes model.	63
4.2	Link Level Methodology.	66

4.3	Repetition Schemes.	70
4.4	Comparison between link level abstraction and link level simulations using Matlab LTE Toolbox or Vienna LTE simulator.	74
4.5	Link Level Simulations using Matlab LTE Toolbox.	75
4.6	BLER vs. SNR for various frequency hopping steps and time delays and for $L = 1, 2, 3$, and 4 repetitions for EVA50 channel, SISO case.	76
4.7	SNR thresholds for different repetition schemes at target $BLER = 10^{-1}$ for SISO case and EVA50 channel (λ_F in kHz and λ_T in ms).	77
4.8	BLER vs. SNR for MIMO 2x2 with various λ_T and λ_F , and $L = 1, 2, 3$ and 4 repetitions, for EVA50 channel.	78
4.9	BLER vs. SNR for EVA50 and MIMO 2x2 channel, with various λ_F , $\lambda_T = 1$ ms and $L = 1, 2, 3$ and 4 repetitions.	79
4.10	SNR thresholds for different repetition schemes at target $BLER=10^{-1}$ (λ_F in KHz and λ_T in ms), assuming different antenna configurations for EVA50.	80
4.11	SNR thresholds for different repetition schemes at target $BLER=10^{-1}$ (λ_F in kHz and λ_T in ms), assuming different antenna configurations for EPA3.	81
4.12	Cell range in MBSFN and SC-PTM urban networks for a target $BLER=10^{-1}$ and outage probability of 2% (λ_F in kHz and λ_T in ms) for EVA50 and SFN120. SC-PTM is with MIMO 4x4 and $\lambda_F = 720$ kHz	81
4.13	Cell range in MBSFN and SC-PTM urban networks for a target $BLER=10^{-1}$ and outage probability of 2% (λ_F in kHz and λ_T in ms) for EPA3 and SFN120. SC-PTM is with MIMO 4x4 and $\lambda_F = 720$ kHz	82
5.1	Network model: White cells are part of a MBSFN synchronization area. Cell borders are represented using Voronoi tessellation. Red stars represent User Equipments (UEs) of a group. A (multicast) group of users is served by a cluster of cells of the synchronization area.	91
5.2	Simplex operations in \mathbb{R}^2 (white dots indicate the worst vertices before operations; solid dots indicate new simplex).	101
5.3	Evolution of function $\Psi_{\mathcal{Q}}$ along the iterations of Algorithm 4.	106
5.4	Comparison of min-norm algorithm with greedy clustering to minimize function Ψ	107
5.5	Evolution of the objective function G , cell weights and blocking probabilities along the iterations of Algorithm 6.	109
5.6	Clustering evolution along Algorithm 6 iterations for a given group. The cluster serving the group is formed by the blue cells, while the white cells are interfering. The links show the best server of each UE.	110

- 5.7 Evolution of the objective function G and blocking probabilities along the iterations of globalized bounded Nelder-Mead (NM) algorithm. 111
- 5.8 Comparison of group mean, minimum and UEs SINR CDF of SC-PTM, full MBSFN cooperation transmissions with proposed clustering scheme obtained at the end of Algorithm 6. 112
- 5.9 Evaluation of the group minimum and UEs SINR using the proposed scheme, compared to a modified scheme based on exhaustive approach to evaluate function $\Psi_{\mathcal{U}}$ upon to minimum group SINR. 113
- 5.10 Impact of the traffic load on network performance. 114

- A.1 Submodular Polyhedron $P(F)$ and base polyhedron $B(F)$ for $n = 2$ (left) and $n = 3$ [122]. 133

List of Tables

2.1	SINR, MCS and Spectral Efficiency mapping table in OFDM downlink channel [55, Table 7.2.3-1], [56].	25
2.2	TTI bundling model parameters for QPSK, 16-QAM and 64-QAM modulations [57].	27
2.3	Simulation parameters.	28
2.4	Mean SSE of different transmission modes (4UEs/BS).	31
2.5	Mean SSE (in bps/Hz) of transmission modes for different numbers of group users per cell.	33
3.1	SINR analytical model simulation parameters.	48
4.1	Coherence Bandwidth of typical multi-path fading channels.	68
4.2	Coherence time of typical PMR UE speed.	69
4.3	Repetition algorithm variables.	71
4.4	Link Level simulation parameters.	73
5.1	Simulation parameters.	105

Chapter 1

Introduction

Contents

1.1 Mission Critical Communications	2
1.1.1 2G and PMR	4
1.1.2 Fourth Generation (4G)	5
1.1.3 Fifth Generation (5G)	6
1.2 Multimedia Broadcast/Multicast Service	8
1.2.1 MBMS Transmission Techniques	8
1.2.2 System Aspect Differences Between MBSFN and SC-PTM	11
1.2.3 MBMS System Architecture	13
1.2.4 MBMS Channels	15
1.3 Thesis Contributions	17

1.1 Mission Critical Communications

Business and mission-critical communications are communications between professional users either from the public safety and security sector (police, army, fire fighters), operating critical infrastructures (like metro or railway companies, airports...), or public utilities (electricity, gas, water), see Figure 1.1.

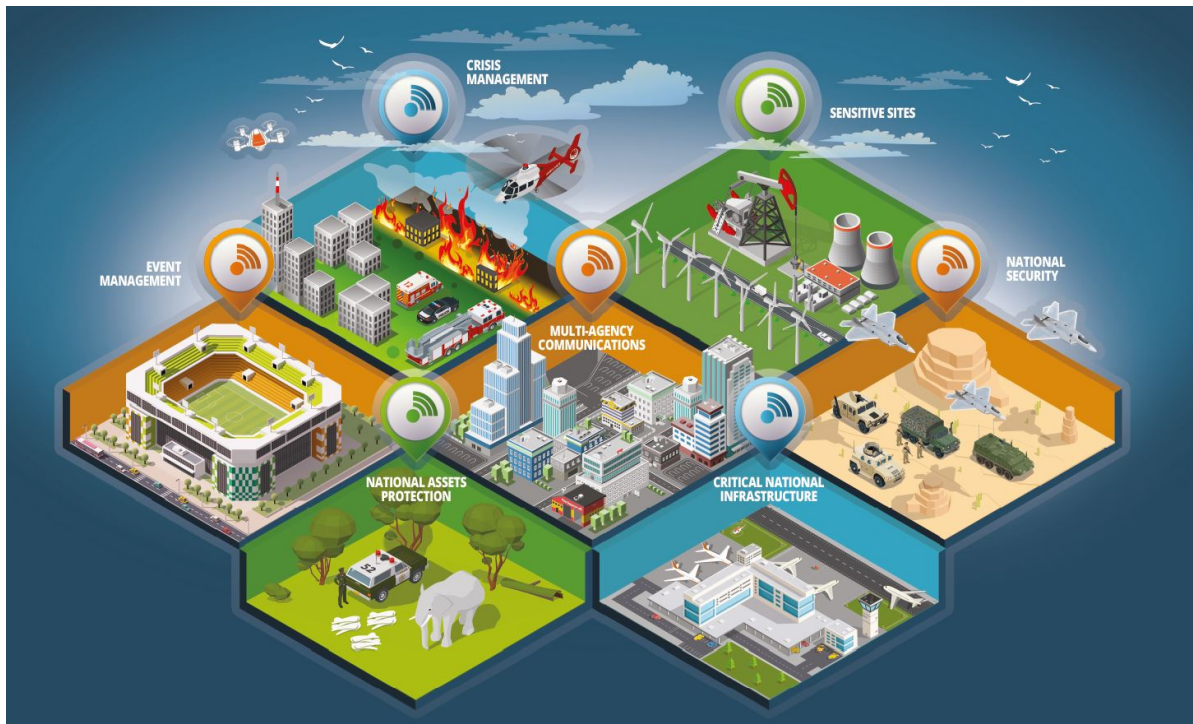


Figure 1.1 Mission critical communication users. Source: ETELM.

Effective communications are the key to a successful response to emergency and disaster situations. Indeed, the ability of the first responder emergency services to communicate among themselves affects the ability to save lives. This is reflected in increasing public investment in mission-critical communication systems. Therefore, these systems have some specific and severe requirements, such that:

- High reliability and availability: as specified in 3rd Generation Partnership Project (3GPP) Release 16, the system shall be available for 99.9999% of time [1].
- Call priority and preemption: the system shall assign different levels of priority to calls and interrupt low priority calls on arrival of high priority calls that do not find available resources.

- Coverage: coverage plays such a large role in mission-critical communication networks, since losing the signal can mean a life or death situation. In order to extend coverage range in uplink channel, high transmit power has been enabled by the system in specific bands [2].
- Resilient/Isolated network: any Base Station (BS) should be able to act alone in routing calls between network entities that stay operational, e.g., after a disaster had partially caused some network equipment to fail [3].
- Fast call setup time lower than 300 ms [4].
- Network inter-operability: communications with users located on external networks.

Moreover, unlike public cellular networks like Global System for Mobile communications (GSM), Third Generation (3G) or Fourth Generation (4G) mobile networks, mission-critical communication networks are characterized by additional services, e.g. Mission-Critical Push-To-Talk (MCPTT) [5], Mission-Critical Video (MCVideo) [6] and Mission-Critical Data (MCData) [7] including group call communication with low call setup time, mobile communication systems for railways [8], maritime communication services [9], etc.

Besides these services, group communications are one of the most important and indispensable services of mission-critical communication networks. Group communications provide an efficient management of the rescue teams, and allow sending commands and sharing information with all contributors in a disaster area. Indeed, a public safety communications system provides the means for first responders to accomplish their mission by communicating simultaneously with their collaborators in a variety of media. In such systems, individuals in a fire brigade or a police department are typically organized into groups, with different responsibilities. These groups can be predefined or formed on-demand, may have geographic areas to cover, and may be organized based on types of skills or activities to be performed. Within and across those groups, some individuals with supervisory or dispatch authority and responsibility should be able to manage and coordinate the efforts of the first responders. Further, some individuals may be able to receive multiple group communications simultaneously, using their device to listen to the one with the highest priority as signalled by the system. The network shall then allow the coexistence of many active groups at the same time, and each individual can be registered to many groups at same time. It's worthwhile to note that communication to group members is not confined to speech, as data messaging (e.g. text, image, video...) can also be sent in parallel to speech, and may be sent from a group member who is not currently speaking.

To meet these critical additional requirements and services, mission-critical communications rely on reliable and secure Professional Mobile Radio (PMR) networks.

In this context, we focus on enhancing the coverage of PMR networks providing group communications, taking advantage of the current technologies (e.g. Multimedia Broadcast/Multicast Service (MBMS)), to meet the mission-critical communication needs.

In the rest of this chapter, we introduce the main developments in the commercial mobile networks to meet the PMR networks requirements. Then, we show the main features of the MBMS introduced by the 3GPP to convey Point-To-Multipoint (PTM) transmissions. Finally, we provide the main contributions of the thesis.

1.1.1 Second Generation (2G) and PMR

Most of the deployed wireless systems for mission-critical communications are today based on PMR technologies, such as TERrestrial Trunked Radio (TETRA), TETRA for POLice (TETRAPOL), or Association of Public-safety Communications Officials-Project 25 (APCO P25), meet most of the aforementioned requirements. However, these networks are mainly devoted to provide a wide range of voice services, but have a limited possibility to provide high data rates mobile services like video streaming, files transmission (maps, databases, pictures...), ubiquitous Internet and Intranet access or Device-To-Device (D2D) communication, which have a strong impact on the efficiency and the responsiveness of the emergency services. Therefore, worldwide there is a great interest of governments and organizations involved in public safety and security towards the provision of such wide range added-value services, in PMR networks, in order to improve the situational awareness and enhance the life-saving operations.

Even if some efforts have been done to enhance PMR systems and to offer higher communication capacity, achievements are still behind those made in the commercial world that recently has developed the 3GPP Long Term Evolution (LTE) technology. Hence, there is a great consensus in adapting the LTE technology to provide IP-based broadband services with the security and reliability typical of PMR networks, which answer to the professional and critical communication needs.

Indeed, many railway researches, including the Future Railway Mobile Communication System (FRMCS) project triggered by the International Union of Railway (UIC), estimate that LTE can meet the needs for transferring railway data in the long term [10]. Moreover, governments in many countries, including the United States, Belgium and the Republic of Korea have also been surveying how to utilize the LTE system for public safety communications, either to augment their existing systems, or to provide a future migration path [11, 12].

1.1.2 Fourth Generation (4G)

The adoption of mainstream commercial technologies, such as LTE and Long Term Evolution Advanced (LTE-A), for business- and mission- critical communications has been discussed in literature [13–17]. Initially designed for public networks, the LTE standard needs some specific enhancements to meet the requirements of PMR. In this context, adopting LTE as PMR broadband technology needs that some specific applications and functionalities requested by railway as well as public safety and security operators, such as MCPTT, dispatch services, priority management, group communications and direct communications, be included in the releases of the 3GPP standard, also guaranteeing interoperability with actual PMR systems. Thus, the 3GPP has been handling various specification items for supporting the public safety features, and technical specification groups in the 3GPP have established such improvements in Release 12 and 13 specifications, which include:

- Group communications: Group Communication System Enabler (GCSE) for LTE [18] and Mission-Critical Push-To-Talk (MCPTT) over LTE [5] have been introduced into 3GPP specifications in Release 12 and Release 13 respectively, in order to support group communications together with Push-To-Talk (PTT) voice application and its evolution toward multimedia services. Further, the MBMS, introduced in Release 6, to support such communications (see Section 1.2).
- Proximity Services (ProSe): in order to enable D2D communications, without the need to have coverage from a network infrastructure, Proximity Services (ProSe) has been introduced by 3GPP under Release 12 [19, 20]. Together with group communications, D2D communications are among the key requirements for mission-critical voice services.
- Coverage: 3GPP has specified a higher power transmit class in Release 11 to improve system coverage [2].
- Enhanced Evolved Universal Terrestrial Radio Access Network (EUTRAN) sharing: intended to add flexibility in sharing network resources, 3GPP has introduced in Release 12 an enhanced resources sharing mechanism between critical and non-critical users [21].
- Isolated EUTRAN operation: in order to improve network resiliency, 3GPP has introduced in Release 13 the isolated EUTRAN operation for public safety to enable any BS to act alone in case of disasters [22].

1.1.3 Fifth Generation (5G)

Nowadays, Fifth Generation (5G) is viewed as the next revolution within the technology industry and has the potential to encompass every aspect of daily life, from a consumer, business, and industry perspective. Besides enhancing the traditional Mobile BroadBand (MBB) use case, 5G is envisioned to support a large variety applications and services, with heterogeneous performance requirements. Thus, the also known next generation mobile networks, will have to cope with a high degree of heterogeneity in terms of services, device classes, deployment types, mobility levels [23], etc.

Indeed, in addition to the classical MBB traffic demands of high throughput and capacity, where 5G networks will provide rates of up to 10 times faster than current 4G networks, it is expected that these networks will have the capacity to connect billions of objects (Internet of Things (IoT) applications), as well as providing new requirements of achieving low latency and high reliability for many services and use cases [24]. These new services are not only for human communications; actually, Machine-Type Communications (MTC) are gaining a strong momentum, as they pave the road to a broad range of use cases, which can be classified into two main categories:

- Massive Machine-Type Communications (mMTC): consists of large numbers of low-cost, small and low-power devices, with high requirements on scalability and increased battery lifetime, such as sensors and meters, and enables new services such that IoT, building automation, assisted living, etc.
- Ultra-reliable Machine-Type Communications (uMTC): also known as Ultra-Reliable Low Latency Communications (URLLC), they encompass services requiring very high reliability, ultra-reliable low latency (going down to the millisecond level [1, 23]) and uninterrupted and robust exchange of data. The URLLC enable real-time control and automation of dynamic processes (e.g. industrial factory automation, smart grid distribution, traffic management and safety), Vehicule-to-anything (V2X) applications.

Furthermore, the uMTC have been classified into many use cases families [24]. Such that the “higher reliability, higher availability and lower latency” use case family, characterized by moderate rates in most cases, and what matters most is that the messages are transmitted quickly and reliably, and that the network and its services are consistently available with minimal downtime; industrial control and drone connectivity are typical areas of this use case family. Another example of uMTC use case families is the “very low latency”, characterized by a system requirement to carrying data very quickly between the sender and receiver; this type of communication is highly needed in e.g. tactile internet [25].

Consequently, mission-critical communications have been classified in a URLLC use case family, characterized by the need to a higher priority over other communications in the networks, and require some means of enforcing this priority, e.g. fire brigade personnel having a higher priority over other users on the site of the fire. Moreover, use cases that provide coverage and services in remote or catastrophe-stricken area have been included in this family.

Figure 1.2 illustrates some usage scenarios envisioned for 5G networks.

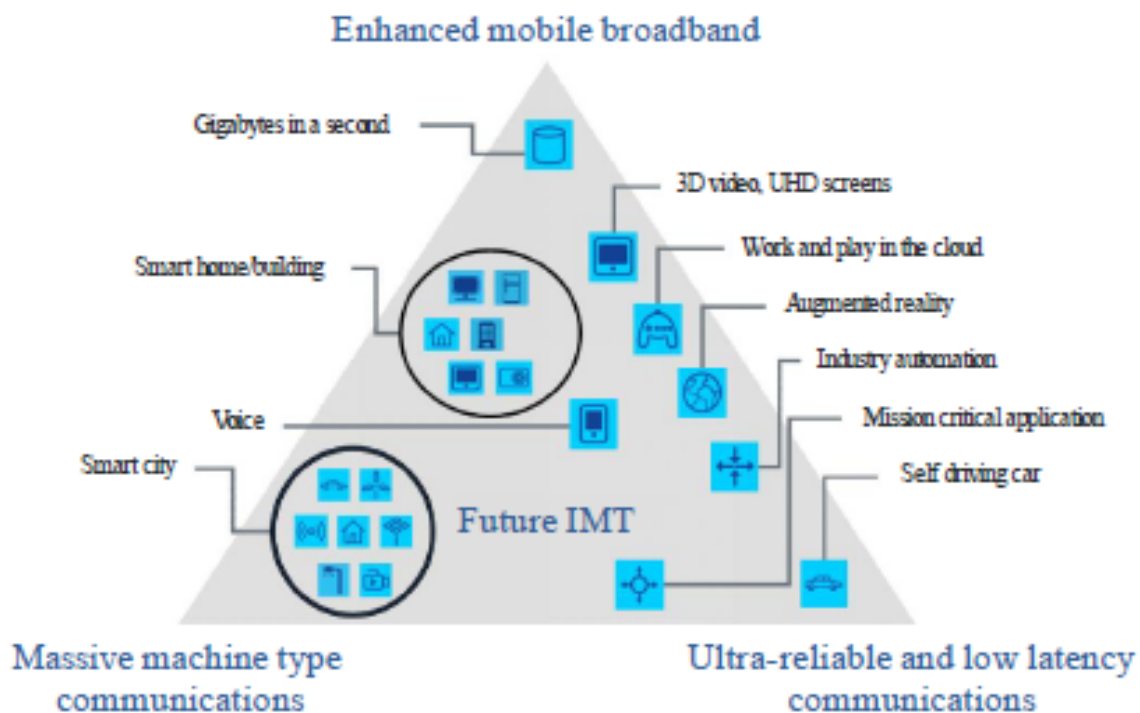


Figure 1.2 Next generation mobile networks use case scenarios [23].

By this means, 5G networks will lead the revolution of mission-critical communications. For example, with the advanced networking capabilities, first responders will go far beyond basic MCPTT to add group chat, video, file or location sharing. Moreover, fire fighters will be able to share a live video of a disaster site among team members, as well as receive videos from drones, surveillance cameras, planes and satellites in real-time. Going beyond traditional communication modalities, 5G networks will also facilitate the inclusion of other participants into a mission-critical exchange; think about all the sensors which are now becoming part of the communication network, e.g. temperature sensors, humidity sensors, wind speed and direction sensors; each of those “things” can become a life-saving thing, greatly assisting in an important critical mission. We can also see an army of robots being useful in case of nature disasters, or search and rescue operations [26].

The aforementioned studies have outlined the adoption and integration of PMR functionalities, specifications, requirements and applications in LTE and next generation networks. However, the wide coverage is an important and critical requirement for business- and mission-critical communications, while, in contrary to classical mobile networks, capacity is not the main issue in practical deployments of PMR networks, as experienced by ETELM. Thus, more resources can be used to improve system coverage, while maintaining acceptable capacity levels in PMR networks to meet their requirements. Such schemes have not been widely used in classical LTE deployments, owing to the importance of capacity in these networks. In this perspective, we introduce the multicast transmissions in mobile networks in the following section. Then, we evaluate their performance and we propose some optimization techniques to improve system coverage in the following chapters.

1.2 Multimedia Broadcast/Multicast Service

The Multimedia Broadcast/Multicast Service (MBMS) was introduced in 3GPP Release 6 to provide multimedia services over mobile networks in efficient means by sharing common radio resources among group of users [27]. By utilizing a common channel to send the same content to multiple receivers, MBMS improves the scalability of broadcast and multicast in cellular networks, and minimizes the usage of network resources.

In order to provide better coverage and throughput for cell edge users, the Multicast/Broadcast Single Frequency Network (MBSFN) was introduced in 3GPP Release 9 under the name of evolved Multimedia Broadcast/Multicast Service (eMBMS). Henceforth, for notational brevity, we use the MBMS notation.

In this section, we introduce the MBMS transmission modes, system architecture and the MBMS channels.

1.2.1 MBMS Transmission Techniques

MBMS data can be delivered either by Point-To-Point (PTP) or Point-To-Multipoint (PTM) transmissions [28]. In Point-To-Point (PTP) (or unicast) mode, a dedicated channel is established with each User Equipment (UE) to carry MBMS information, while in PTM, a common channel is used to simultaneously convey the information to multiple (multicast transmission) or all (broadcast transmission) User Equipments (UEs) requesting the corresponding data. The system level performance of PTP and PTM transmissions has been evaluated in [29], focusing on retransmission strategies. Soares et al. have proposed

in [30] a UE counting mechanism for Universal Terrestrial Radio Access Network (UTRAN) to decide the switching point between PTP and PTM modes.

Since it is expected that the radio resources increase linearly with the number of UEs receiving the same data in PTP transmission, PTM improves the resource allocation. However, PTM transmission efficiency mainly depends on the UE in the group with worst radio conditions.

The PTM transmission of MBMS data in the EUTRAN uses either Single-Cell Point-To-Multipoint (SC-PTM), or MBSFN. For each MBMS session, the Multi-cell/multicast Coordination Entity (MCE) makes the decision on whether to use SC-PTM or MBSFN in the MBMS service area, defined as the group of cells transmitting the service. In the following sections, we introduce some aspects of these transmission modes.

Multicast/Broadcast Single Frequency Network (MBSFN)

The Multicast/Broadcast Single Frequency Network (MBSFN) is a simulcast transmission technique introduced to support MBMS transmission in LTE networks. In MBSFN, a time-synchronized common waveform is transmitted simultaneously from a set of Base Stations (BSs) using the same resource blocks. The corresponding cells form the so called MBSFN area. This area can be *static*, i.e., defined a priori by the operator, or *dynamic*. In this case, the set of transmitting BSs is dynamically adapted to the UE group spatial distribution. In this context, a dynamic clustering algorithm for MBSFN networks is introduced in Chapter 5.

In such a transmission, the UE receives copies of the signal with different delays, amplitudes and phases depending on the distance to each BS. Therefore, the UE may treat the multi-cell transmissions in the same way as multi-path components of a single-cell transmission without incurring any additional complexity [31]. It can thus benefit from spatial diversity, increased useful signal power and reduced Inter-Cell Interference (ICI) (since the received signals from neighbor BSs inside the MBSFN area will be considered as constructive signals). In order to further reduce the inter-cell interference, a set of *reserved cells* around the MBSFN area can be deployed, in which there is no transmission during active MBSFN subframes. Moreover, MBSFN is designed to only support extended Cyclic Prefix (CP), which reduces Inter-Symbol Interference (ISI) to the UEs and allows the UE to combine signals from different BSs located far away from each other. These properties lead to Signal to Interference plus Noise Ratio (SINR) improvement, especially at cell edge and thus increased cell coverage [32, 33]. MBSFN uses the Multicast Traffic CHannel (MTCH) to convey the data on specific subframes.

The following definitions were introduced for MBSFN [34].

MBSFN synchronization area: An area of the network where all BSs are synchronized in order to perform MBSFN transmissions. MBSFN synchronization areas can support one or more MBSFN areas. On a given frequency layer, a BS can only belong to one MBSFN synchronization area.

Note that the MBSFN synchronization area is independent from the definition of MBMS service area.

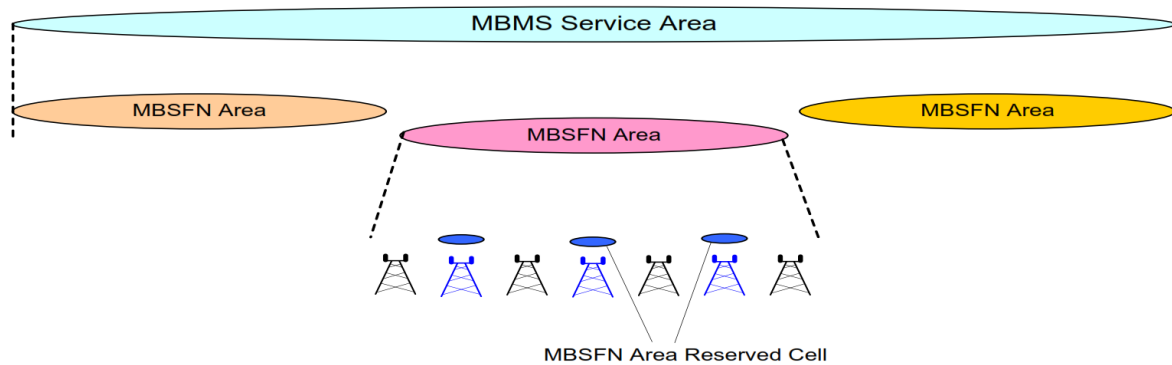


Figure 1.3 MBSFN definitions [34].

MBSFN area: The MBSFN area is a specific area where one or multiple BSs, within a MBSFN synchronization area, transmit the synchronized signals. It includes the BSs which contribute to the MBSFN transmission and advertise its availability, as well as the reserved cells. A BS can be part of several MBSFN areas [35].

MBSFN reserved cell: A cell within a MBSFN area, which does not contribute to the MBSFN transmission, is called MBSFN reserved cell. It may be allowed to transmit for other services, at limited power, on the resources allocated for the MBSFN transmission in the belonging area, in order to reduce the ICI.

Single-Cell Point-To-Multipoint (SC-PTM)

The Single-Cell Point-To-Multipoint (SC-PTM) was introduced in 3GPP Release 13 as complementary bearer type of MBMS transmission [36]. SC-PTM reuses the MBMS system architectures (logical entities and interfaces) and relies on PTM transmissions. However, the synchronized multi-BS transmission is abandoned, i.e., PTM transmission is performed on a per-cell basis. If a group of users requesting the same service is distributed over several cells, involved BSs use independently PTM for the users under their coverage and may interfere each other. Contrary to MBSFN, SC-PTM uses the Physical Downlink Shared CHannel (PDSCH), so that the multiplexing with unicast transmissions is more flexible [37]. Furthermore, SC-PTM transmission enhances coverage and transmission

efficiency by enabling the Hybrid Automatic Repeat re-Quest (HARQ) re-transmissions based on the uplink HARQ and Channel State Information (CSI) feedback from connected UEs [38]. SC-PTM can also activate the Transmission Time Interval (TTI) bundling feature that consists in sequentially transmitting multiple redundancy versions of every transport block to increase the probability of good reception. We study this feature in Chapter 2 as it does not increase the transmission delay compared to HARQ, and we introduce an alternative scheme for MBSFN networks in Chapter 4.

1.2.2 System Aspect Differences Between MBSFN and SC-PTM

In this section, we show some system aspect differences between MBSFN and SC-PTM transmission modes, in terms of allocation of the transmission area, scheduling and resource allocation, channel utilization and latency.

Static/dynamic MBMS area

As aforementioned, we designated by MBMS area the area where one or multiple BSs transmit the MBMS data, i.e., the set of BSs which are serving the UEs requesting the corresponding service. The provisioning of such area highly depends on the service to be transmitted. For some services (e.g. mobile TV), it is assumed that interested UEs are widely spread over the network and the MBMS should be delivered in a large pre-planned area, therefore, the MBSFN becomes the suitable transmission technology as it assumed that most BSs belong to the MBMS area.

On the other hand, the UEs distribution is quite different in another services (e.g. critical communications), where the interested UEs are concentrated on several (neighbor or non-neighbor) BSs; likewise, some services might be geographically restricted. In both cases, the MBSFN transmission may become non-efficient since it may occur in BSs where no interested UEs requesting the service are served by these transmitters; hence, SC-PTM is quite suitable and efficient for these services as the SC-PTM transmission area can be dynamically determined, on a per cell basis, according to the users distribution [37, 39]. Therefore, taking advantage of performance improvements achieved by MBSFN transmissions, especially in network coverage, the need arises to define an algorithm which defines the MBSFN area dynamically with respect to UEs group conditions (see Chapter 5).

Scheduling and resource allocation

For MBSFN, a subset of radio resources (up to 6 subframes per radio frame [40]) could be allocated as MBSFN subframes in LTE Orthogonal Frequency-Division Multiplexing (OFDM)

channels. However, multiplexing with unicast data in the same subframe is not allowed, even when the amount of the group data to be sent is instantaneously small. Moreover, the MBSFN subframes are rather statically configured according to service data rate, required Modulation and Coding Scheme (MCS) (depends on radio conditions of all UEs group members inside the MBSFN area) and coverage target, and can't be dynamically adjusted according to the number of active groups and their traffic load. Thus, radio resources configured for MBMS might be unnecessarily wasted when provisioned for some services.

However, both SC-PTM and unicast transmissions use PDSCH and they have the same radio frame structure, hence the radio resources could be flexibly shared between these transmission schemes in the same radio frame, leading to prevent any waste in spectrum resources that can be fully utilized [37, 41]. Hence, SC-PTM can be seen as a solution to improve system capacity and scalability compared to MBSFN transmissions (see Chapter 2). Although the capacity is not the main issue in PMR, however, SC-PTM transmissions must be considered, in PMR, as normal enablers for multicast transmissions since they allowed some techniques to improve system coverage, e.g. TTI bundling, which are not adopted for MBSFN in current standards. Moreover, SC-PTM may represent a benchmark for a trade-off analysis between system's coverage and capacity, presented in Chapter 5.

Physical channel utilization

Multicast/Broadcast Single Frequency Network (MBSFN) is only transmitted on single antenna port, and it is expected that the reference signals should be redesigned in order to support multiple antenna port transmission for MBSFN. While SC-PTM transmission is more flexible than MBSFN due to the support of multiple antenna port transmission, since it is based on PDSCH, i.e., transmit diversity could be applied for SC-PTM to increase the radio efficiency [37].

Moreover, MBSFN subframes only support extended Cyclic Prefix (CP) to enable the signal combining of the synchronized transmissions from multiple BSs in a large area. However, the longer CP of OFDM symbols implies a lower code rate for a given MCS, or a lower MCS has to be used to achieve the same BLock Error Rate (BLER) (compared to normal CP) for a given SINR, which leads to a system capacity lost. When the MBMS area is small or only consists of one cell, the use of extended CP is actually not needed; thus, SC-PTM is more flexible than MBSFN in such scenario of small areas due to the support of normal CP [42].

Latency

Single-Cell Point-To-Multipoint (SC-PTM) can support shorter latency, comparing to MBSFN, when establishing new MBMS sessions; in fact, the time to setup and notify the receiving group members of the MBMS bearer setup for a new group communication, in MBSFN transmission, is dominated by the Multicast Control Channel (MCCH) modification period, which can take the value 5.12 s or 10.2 s [37].

Network planning

The network planning and deployment for SC-PTM is quite easier than that of MBSFN, since MBMS data is sent on a per cell basis and synchronization between multiple sites is not required [37].

1.2.3 MBMS System Architecture

Although SC-PTM and MBSFN will bring capacity and Quality of Service (QoS) gains to the mobile networks, their implementations need costly modifications to the network architecture. Therefore, in order to support MBMS operation in radio networks, 3GPP has introduced new logical network entities, as well as user and control plane interfaces to interconnect them. An evolved architecture is then introduced, as depicted in Figure 1.4. LTE network is comprised of the access network and the core network, known as Evolved Universal Terrestrial Radio Access Network (EUTRAN) and Evolved Packet Core (EPC) respectively. Within EUTRAN, the BSs are the collectors of the information that has to be transmitted over the air-interface. In the following, we summarize some functionalities of other network entities that contribute in MBMS operation.

Multi-cell/multicast Coordination Entity (MCE)

The MCE is a logical control entity involved in the session control signaling. It is responsible for allocation of time and frequency resources used by BSs in the MBSFN area (refer to Section 1.2.1) for multi-cell MBMS transmission, as well as the selection of the MCS, used on the radio bearers, that guarantees the coverage requirements. The MCE is also responsible for services admission control; indeed, it can decide to un-establish the radio bearers of the new MBMS service if the radio resources are not sufficient, or may preempt radio resources from other radio bearers of ongoing MBMS services [32, 34]. Furthermore, it coordinates the transmission of synchronized signals from different BSs, and decides to use SC-PTM or MBSFN (refer to Section 1.2.1) in the transmission of the MBMS data. A

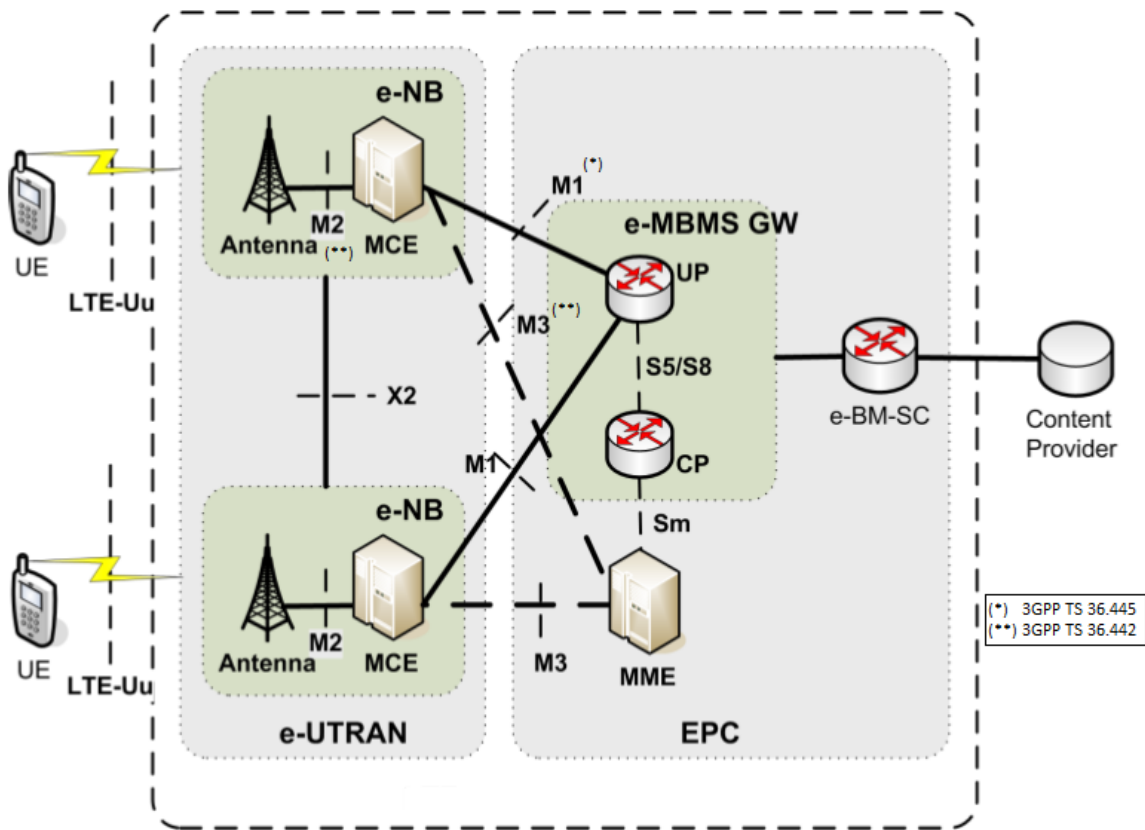


Figure 1.4 MBMS system architecture [43].

BS is served by a single MCE, which can be integrated as part of the BS, or as stand-alone entity (as in Figure 1.4). Moreover, the dynamic clustering algorithm of the MBSFN area, proposed in Chapter 5, can be implemented in the MCE, owing to its crucial role in MBMS session control [34].

eMBMS GateWay (eMBMS-GW)

The eMBMS GateWay (eMBMS-GW) is physically located between the evolved Broadcast/Multicast Service Center (eBM-SC) and the BS. Its main function is the forwarding of MBMS user data packets to each BS transmitting the service by means of IP multicast, by allocating an IP multicast address, for each MBMS session, to which the BS should join to receive MBMS user data. Furthermore, the eMBMS-GW performs MBMS session control signaling (session start/update/stop) towards the EUTRAN via the Mobility Management Entity (MME) to set up MBMS radio bearers [32, 34]. It is logically split into two domains: the first is related to user plane, while the other is related to control plane. Likewise, it is connected to EUTRAN by two distinct interfaces, namely M1 and M3 respectively.

evolved Broadcast/Multicast Service Center (eBM-SC)

The eBM-SC is the entry point for content providers, or any external broadcast/multicast source, into the Evolved Packet Core (EPC). Indeed, it is the entity in charge of introducing the multimedia content into the network. For this purpose, it plays the role of traffic shaping and authorizing content provider and terminal requests, as well as the scheduling of broadcast and multicast sessions. Also, it controls the security, billing, in addition to the start and end of MBMS transmissions. Finally, the eBM-SC synchronizes the transmitted data among BSs by means of SYNC protocol [32].

1.2.4 MBMS Channels

In SC-PTM, similarly with unicast transmissions, the MBMS data is carried over PDSCH, and the corresponding downlink assignments are dynamically provided by Physical Downlink Control CHannel (PDCCH). Each SC-PTM session is identified by a Group-Radio Network Temporary Identifier (RNTI), shared among a group of UEs to allow them receiving the transmitted MBMS data [44].

On the other side, a MBSFN area can provide many MBMS services. Based on their QoS, these services are classified into groups. Hence, all services in one group, having the same QoS requirement, are multiplexed in time domain and transmitted using the same MCS, by a specific transport channel for MBMS at the Medium Access Control (MAC) layer, so-called Multicast CHannel (MCH), mapped on the Physical Multicast CHannel (PMCH) of the physical layer [34, 45, 46]. Regarding the air interface, there are two logical channels related to MBMS in downlink: Multicast Traffic CHannel (MTCH) and Multicast Control CHannel (MCCH). Both channels are mapped on the MCH and used by UEs that receive MBMS traffic [45]. The relationship between the logical, transport and physical downlink channels for MBMS is shown in Figure 1.5.

Some functions of these channels are described in the following sections.

Multicast Traffic CHannel (MTCH)

The MTCH is a PTM downlink channel used to carries data, corresponding to a certain MBMS, to the UEs, via Radio Link Control (RLC) Unacknowledged Mode (UM) due to the broadcast nature of the transmission, where feedback is not available from the UE in the uplink [45, 47]. A MBSFN area can support many MBMS services, resulting in multiple MTCH belonging to one area; the BS multiplexes these channels at MAC layer [46].

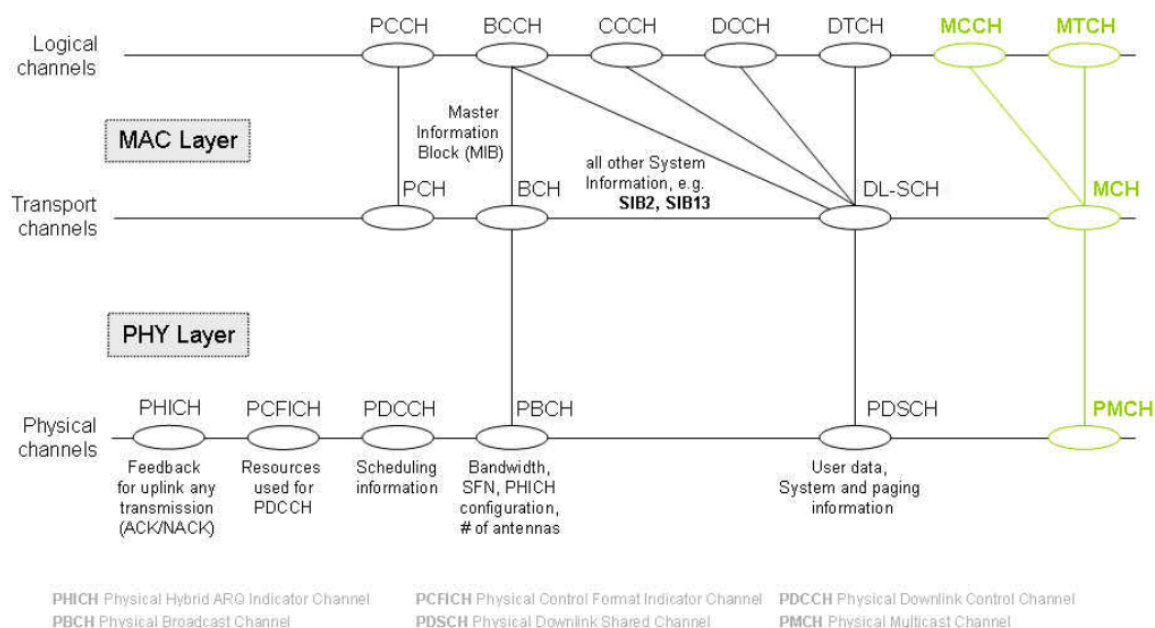


Figure 1.5 Enhanced channel architecture due to MBMS [47].

Multicast Control Channel (MCCH)

The MCCH is a PTM downlink channel used to provide the MBMS control information of one or several MTCH, from the network to UEs, including the subframe allocation (positions and number) assigned to MCH, as well as the used MCS [45–47]. Note that there is four MCS allowed for the MCCH: MCS index 2, 7 (both Quadrature Phase Shift Keying (QPSK)), 13 (16-Quadrature Amplitude Modulation (QAM)), 19 (64-QAM) [47].

In each MBSFN area, there is always one MCCH, associated to one or multiple MTCH, multiplexed onto the MCH (as depicted in Figure 1.6). For MCCH and MTCH, the UE shall not perform RLC re-establishment when moving between cells of the same MBSFN area [34]. As for the MTCH, MCCH uses RLC UM in the transmission [47].

Multicast Channel (MCH)

The MCH is used to transport multiple MBMS, multiplex in time-domain, and assigned to one group due to their equivalent QoS requirement, in one MBSFN area.

A MBSFN area contains one or more MCH, and the time in which all MCH share the resources is named Common Subframe Allocation (CSA) and given in the unit of radio frame. The CSA pattern is periodically repeated with the CSA period. The MCH Subframe Allocation (MSA) for every MCH carrying MTCH is defined by the CSA pattern, the CSA

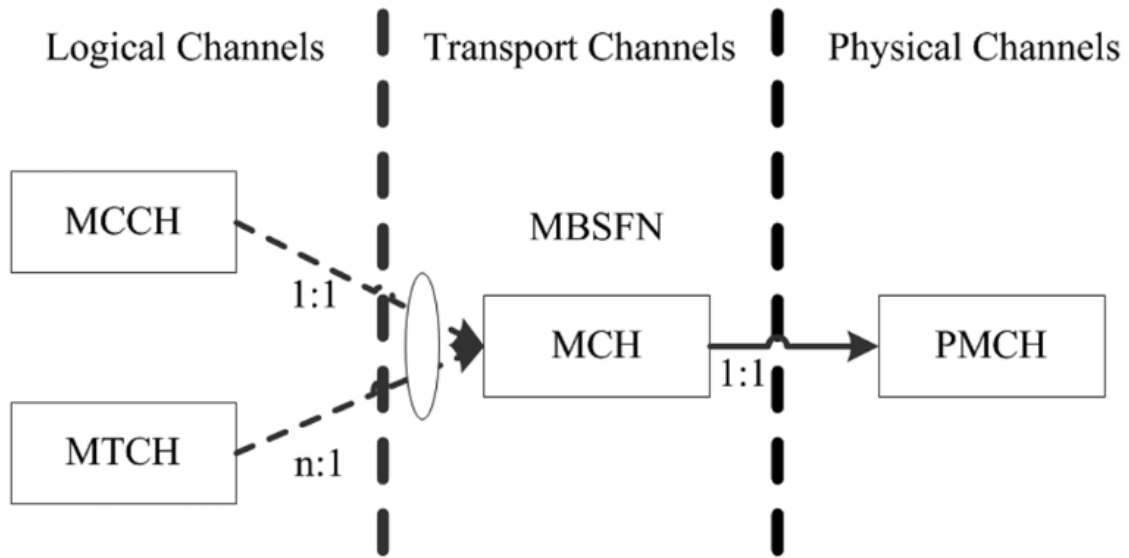


Figure 1.6 MBSFN channels mapping [32].

period and the MSA end, that are all signalled on MCCH. The MSA end indicates the last subframe of the MCH within the CSA period [34].

Physical Multicast CHannel (PMCH)

The MCH, which carries the MBSFN data, is finally mapped into the PMCH. In each PMCH subframe, only one MCH can be allocated. This physical channel has different characteristics than PDSCH, such that the extended CP and the modified reference signal pattern.

Moreover, unlike PDSCH used in SC-PTM transmissions, the advanced link adaptation schemes, such as MCS adaptation to UE Channel Quality Indicator (CQI) and TTI bundling, are not adopted for PMCH in the current 3GPP Releases. We show that, in Chapters 2 and 4, applying such technologies for MBSFN transmissions will lead to a higher spectral efficiency, improved scalability and coverage.

1.3 Thesis Contributions

This thesis primary objective is to propose and evaluate the main techniques that improve mobile networks coverage, a crucial requirement for business- and mission-critical communications.

In this context, the aforementioned radio transmission techniques of multicast/broadcast communications presented in Section 1.2.1 with their main characteristics and differences, are evaluated in Chapter 2 in terms of radio quality and coverage gain, and their impact on

the system capacity and System Spectral Efficiency (SSE) is shown, under different UEs distribution scenarios and network configurations. Moreover, we show the ability of TTI bundling to trade-off coverage for capacity, so it can provide a flexible solution to improve the network coverage.

Since Multicast/Broadcast Single Frequency Network (MBSFN) is envisioned to be a key technology for business- and mission- critical communications, the need arises to define simple and efficient dimensioning rules for such networks. The SINR is an important key performance parameter since other metrics such as outage probability and capacity can be deduced from it. Thus, in Chapter 3, we introduce an analytical model to derive an approximate closed-form formula of the SINR in a MBSFN. The proposed model takes into account ISI due to the different propagation delays between the UE and its serving BSs.

In Chapter 4, we propose a simple repetition scheme without request as an alternative to Hybrid Automatic Repeat re-Quest (HARQ) for group communications. When transport blocks are re-transmitted several times, a trade-off arises between coverage and capacity on the one hand, coverage and delay on the other hand. The performance of our scheme is evaluated using a link layer abstraction based on the Mean Instantaneous Capacity (MIC) together with BLER vs. Signal to Noise Ratio (SNR) curves in Additive White Gaussian Noise (AWGN). With this approach, we obtain very quick results for various schemes. We carefully design our repetition scheme by considering the channel characteristics and the service delay constraints. The proposed scheme could be adopted by next generation MBSFN or SC-PTM networks in order to increase the coverage of mission-critical networks.

In MBSFN networks, the full cooperation among all cells of an area achieves the highest cooperative gain, but has stringent impact on system capacity. A trade-off in the cluster's size of serving cells thus arises between high SINR and network capacity. To assess this trade-off, we formulate in Chapter 5 an optimization problem to maintain an acceptable system blocking probability, while maximizing the average SINR of the multicast group users. For every multicast group to be served, a dynamic cluster of cells is selected based on the minimization of a submodular function that takes into account the traffic in every cell through some weights and the average SINR achieved by the group users. Traffic weights are then optimized using a Nelder-Mead simplex method with the objective of tracking a blocking probability threshold. The proposed clustering scheme is compared to full cooperation and to SC-PTM schemes. Results show the importance of dynamic clustering in improving system capacity and coverage.

Finally, the results of these studies are summarized along with the perspectives for the future work in Section 5.5.

Chapter 2

SC-PTM or MBSFN for Mission-Critical Communications?

Contents

2.1	Introduction	20
2.2	System model	21
2.2.1	Network Model	21
2.2.2	SINR Evaluation	22
2.2.3	Spectral Efficiency	24
2.2.4	TTI Bundling	26
2.3	Simulation Results	27
2.3.1	Simulation Settings	27
2.3.2	SINR Distributions	28
2.3.3	System Spectral Efficiency	30
2.3.4	Impact of Group Size	32
2.3.5	Cell Range	33
2.3.6	TTI Bundling Gain	35
2.4	Conclusion	37

2.1 Introduction

One of the main services of Professional Mobile Radio (PMR) is the group communication; in general, a number of first responders for public safety, or railway company agents, etc., need to form a group for communicating with each other or sharing the common data for collaboration on their mission. A such service can be seen as a Multimedia Broadcast/Multicast Service (MBMS), firstly introduced by 3rd Generation Partnership Project (3GPP) for Universal Mobile Telecommunication System (UMTS) in Release 6, as a Point-To-Multipoint (PTM) content delivery to provide multimedia services over mobile networks in efficient means by taking advantage of the broadcast nature of the radio channel [48].

Multimedia Broadcast/Multicast Service (MBMS) flows are transmitted either by Multicast/Broadcast Single Frequency Network (MBSFN), or Single-Cell Point-To-Multipoint (SC-PTM). The MBSFN technology is a natural enabler for such services because it offers PTM communications. In this approach, several Base Stations (BSs) transmit the same signal to group users and thus increase their Signal to Interference plus Noise Ratio (SINR), especially at cell edge. In MBSFN, the transmission of MBMS data can occur in cells, in which there are no user interested in receiving the session, thus, radio resource waste can occur. Moreover, the transmitting cells should be synchronized, which imposes additional delays in session's establishment. SC-PTM has thus been proposed in 3GPP Release 13 as an alternative to overcome these issues. In SC-PTM, multicast transmission is performed on a per cell basis, which aims at increasing the System Spectral Efficiency (SSE) [36].

The performance of MBSFN and SC-PTM has been discussed in literature and recent 3GPP technical reports. In [49], an analytical model for the capacity and coverage estimations in MBSFN transmission were proposed. Alexiou et al. presented in [50] a study on performance and cost analysis of different MBSFN deployments, but mainly focus on forward error correction impact. Different selection techniques of Modulation and Coding Scheme (MCS) have been evaluated for MBSFN assuming Channel State Information (CSI) feedback, e.g. in [32, 33]. In references [32, 33, 49, 50], SC-PTM is however not considered.

Some system aspect differences between MBSFN and SC-PTM have been presented in Section 1.2.2. Authors of [28, 38] focus on the gains brought by Hybrid Automatic Repeat re-Quest (HARQ). In [28], deployment strategies of MBSFN are not investigated although they have crucial impact on its performance. The 3GPP report [51] is the closest to our study in this chapter. A performance comparison of SC-PTM, MBSFN and unicast transmission modes are presented. The authors show that SC-PTM outperforms MBSFN in terms of SSE,

owing to the efficient use of radio resources only in cells in which there are User Equipment (UE) interested in receiving the session. However, the authors didn't consider the selection of appropriate MCS for each MBSFN session, since the CSI feedback is not adopted by the standard. Also, the trade-off between coverage gain ensured by MBSFN and transmission reliability in terms of outage probability has not been investigated; although this trade-off is crucial for mission critical communications [52].

System aspect differences between multicast transmission modes have been presented in Section 1.2.1. In this chapter, we evaluate the performance of MBSFN, SC-PTM and unicast transmissions in different UE's distribution scenarios and network configurations, in terms of SINR distribution, SSE, outage probability and cell range. We study the trade-off between coverage and reliability, and we provide engineering rules for the deployment of group communication services. We also show the impact of the Transmission Time Interval (TTI) bundling feature.

The rest of this chapter is organized as follows: In Section 2.2, we introduce the system model and parameters in Section 2.2. Section 2.3 presents and discusses the simulation results. Finally, conclusions are summarized in Section 2.4.

2.2 System model

In this section, we introduce our system model, the SINR and Spectral Efficiency (SE) evaluation formulas of unicast, SC-PTM and MBSFN transmissions, as well as the model used in our study to evaluate the TTI bundling gains.

2.2.1 Network Model

We consider the downlink of a cellular network with omnidirectional BSs implementing either MBSFN, SC-PTM or unicast transmissions. Let \mathcal{X} be the set of all cells (or BSs) in the network.

In MBSFN transmission, we consider several network deployment configurations. We designate by "SFN_{atr}" a given configuration, where there are "a" rings of cells with active User Equipments (UEs) requesting the considered service, "t" rings of cells transmitting synchronously the service without active UEs, and "r" rings of reserved cells. In such network, there are also "o" rings of cells which are outside the MBSFN area. Let \mathcal{X}_a , \mathcal{X}_t , \mathcal{X}_r and \mathcal{X}_o be the sets of BSs inside cell rings "a", "t", "r" and "o" respectively; hence: $\mathcal{X} = \mathcal{X}_a \cup \mathcal{X}_t \cup \mathcal{X}_r \cup \mathcal{X}_o$. To simplify, let $\mathcal{X} = \mathcal{X}_a \cup \mathcal{X}_t$. An example of such configuration is illustrated in Figure 2.1.

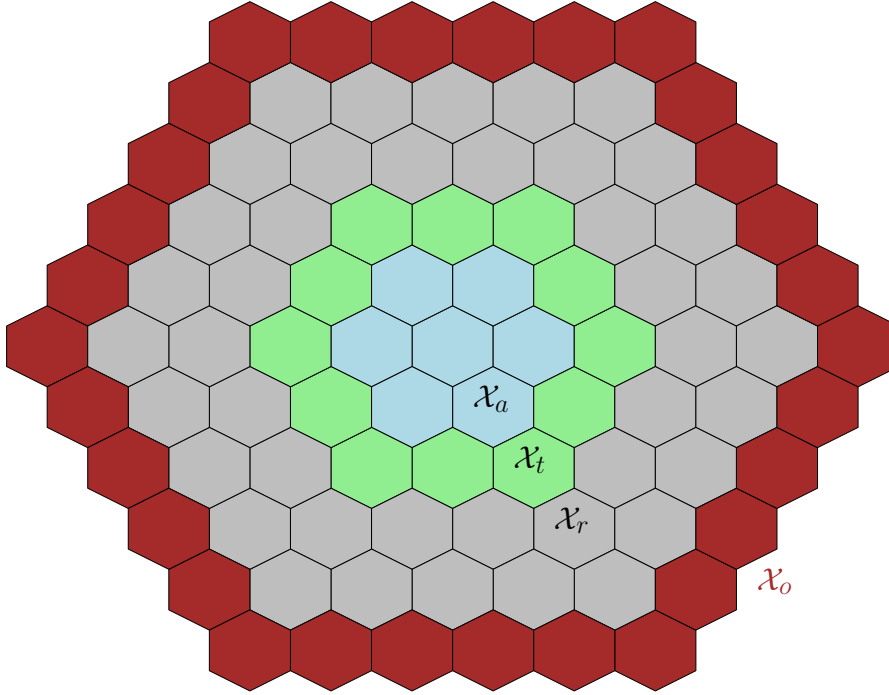


Figure 2.1 SFN212 configuration.

In SC-PTM and unicast transmissions, the MBMS data is transmitted in BSs supporting active UEs, and all other BSs act as interfering transmitters.

2.2.2 SINR Evaluation

In this section, we introduce the SINR formulas for unicast, SC-PTM and MBSFN transmissions.

Unicast

In a unicast transmission, the SINR experienced by UE u is given by:

$$\gamma_{ucst}(u) = \frac{g_{0u}P_0}{\sum_{b \in \mathcal{X} \setminus \{0\}} g_{bu}P_b + \mathcal{N}}, \quad (2.1)$$

where $b = 0$ is the index of the Base Station (BS) providing the maximum receive power to UE u , called serving BS or *best server*; P_b is the transmit power of BS b ; and g_{bu} is the channel gain between BS b and UE u ; and \mathcal{N} is the thermal noise power given by [53]: $\mathcal{N} = \mathcal{N}_0W$, where \mathcal{N}_0 denotes the white noise power spectral density, and W the system bandwidth. More specifically, $g_{bu} = \kappa d_{bu}^{-\eta} X_{bu}$, d_{bu} is the distance between b and u , $X_{bu} = 10^{\xi_{bu}/10}$ is a

log-normal random variable characterizing shadowing, ξ_{bu} is a zero-mean Gaussian random variable with standard deviation σ in dB; κ is a constant and η is the path-loss exponent.

Note that the Inter-Symbol Interference (ISI) is assumed to be negligible in unicast and SC-PTM transmissions, owing to the Cyclic Prefix (CP).

SC-PTM

In a SC-PTM transmission, the SINR of user u is defined in the same way as for unicast transmission since all BSs that do not serve u are interfering:

$$\gamma_{sc-ptm}(u) = \gamma_{ucst}(u). \quad (2.2)$$

MBSFN

In SC-PTM and unicast transmissions, the signals originating from all BSs except the serving BS are viewed as Inter-Cell Interference (ICI). On the contrary, in MBSFN, the signal received from an BS of the MBSFN area is part of the useful received signal, provided that the propagation delay does not exceed the CP duration.

To account for this, we define the weight function of the useful portion of a received MBSFN signal as [49]:

$$\omega_{bu} = \begin{cases} 0 & \tau_{bu} < -T_U \\ 1 + \frac{\tau_{bu}}{T_U} & -T_U \leq \tau_{bu} < 0 \\ 1 & 0 \leq \tau_{bu} < T_P \\ 1 - \frac{\tau_{bu} - T_P}{T_U} & T_P \leq \tau_{bu} < T_P + T_U \\ 0 & \text{otherwise} \end{cases} \quad (2.3)$$

where τ_{bu} is the difference in propagation delay between signals from BS b and serving BS 0 at UE u , i.e., $\tau_{bu} = \frac{d_{bu} - d_{0u}}{c}$; c is the light propagation speed. Variable T_U is the duration of the useful part of Orthogonal Frequency-Division Multiplexing (OFDM) symbol and T_P is the duration of the OFDM CP.

Therefore, the SINR experienced by UE u , in a MBSFN transmission, can be expressed as [49]:

$$\gamma_{mbsfn}(u) = \frac{\sum_{b \in \mathcal{X}} \omega_{bu} g_{bu} P_b}{\sum_{b \in \mathcal{X}} (1 - \omega_{bu}) g_{bu} P_b + \sum_{b \in \mathcal{X}_o} g_{bu} P_b + \mathcal{N}}. \quad (2.4)$$

2.2.3 Spectral Efficiency

The Modulation and Coding Scheme (MCS) plays a crucial role in the Spectral Efficiency (SE) evaluation [49, 54]. In the downlink channel of Long Term Evolution (LTE) systems, the Channel Quality Indicator (CQI) index is fed back to the BS in order to assign the appropriate MCS. The estimated CQI index relies on the SINR experienced by the user u and can be obtained by:

$$CQI_u = \max\{i | \gamma_{th,i} \leq \gamma(u), \text{ for } i = 1 \dots M\}, \quad (2.5)$$

where M is the total number of CQI, and is 15 in 3GPP Release 15 specifications [55]; $\gamma_{th,i}$ is the SINR switching threshold for the CQI i , and $\gamma(u)$ is the SINR experienced by the user u (i.e. $\gamma_{ucst}(u)$, $\gamma_{sc-ptm}(u)$ or $\gamma_{mbsfn}(u)$). These thresholds depend on transmission chain parameters, thus, different sets of thresholds have been provided in literature. In [56], Fan et al. provided a set of thresholds determined with similar system parameters of ours.

On the other hand, each CQI index is defined by a modulation and a coding rate fixed in 3GPP standards [55, Table 7.2.3-1]. Therefore, the corresponding spectral efficiency is obtained by multiplying the coding rate by the number of bits sent with the associated modulation; e.g., the efficiency of CQI 3 is given by: $\frac{193}{1024} \times 2 = 0.377$.

The SINR thresholds [56], modulation order, code rate and efficiency [55] of each CQI index are summarized in Table 2.1.

In PTM transmissions, the UEs of a group listen to a common channel, share the same time and frequency resources, as well as same MCS. Thus, different MCS selection approaches, under different goals, have been proposed in the literature [32, 33], such that:

- The MCS that ensures the maximum SE over all the users of the group.
- The MCS that achieves a target SE.
- The MCS ensuring that even the UE with the lowest SINR receive the data.

However, in the context of mission-critical communications, the latter approach is the one that ensures the best coverage, owing to the fact that all UEs, even those with the lowest SINR, will receive the MBMS data. Therefore, in multicast transmissions, we select the MCS based on the minimum SINR among those experienced in a group, from which we determine the SE of the group. Moreover, because of the possible multi-cell transmission, resources are used in several cells for a given group. To take into account these two effects and to be able to compare the transmission schemes, we need to define a System Spectral Efficiency (SSE).

CQI Index	Modulation Order	Code Rate (x1024)	Efficiency (bps/Hz)	SINR Threshold γ_{th} (dB) w/ 10% BLER
0	Out of Range			
1	QPSK	78	0.1523	-9.478
2		120	0.2344	-6.658
3		193	0.377	-4.098
4		308	0.601	-1.798
5		449	0.877	0.399
6		602	1.1758	2.424
7	16-QAM	378	1.4766	4.489
8		490	1.9141	6.367
9		616	2.4063	8.456
10	64-QAM	466	2.7305	10.266
11		567	3.3223	12.218
12		666	3.9023	14.122
13		772	4.5234	15.849
14		873	5.1152	17.786
15		948	5.5547	19.809

Table 2.1 SINR, MCS and Spectral Efficiency mapping table in OFDM downlink channel [55, Table 7.2.3-1], [56].

Let consider a user u served by the reference cell of index 0. Let \mathcal{U}_0 the group of users to which u belongs and which are served by BS 0. At least, let $\mathcal{U}_{\tilde{x}}$ be the group users that are served by the MBSFN area of u .

Unicast

In unicast transmissions, the SE (in bps/Hz), $SE_{ucst}(u)$, is derived from $\gamma_{ucst}(u)$, based on the appropriate MCS (see Table 2.1). Note that SE does not depend on the rest of the group. In order to take into account the fact that the information is sent to every user separately, the SSE is defined by dividing the SE by $|\mathcal{U}_0|$, and taking the expectation as follows:

$$SSE_{ucst} \triangleq \mathbb{E}\left[\frac{SE_{ucst}(u)}{|\mathcal{U}_0|}\right] \quad (2.6)$$

where the expectation is taken over user locations, group characteristics (spatial distribution, size), cells, and channel variations.

SC-PTM

In this case, the MCS chosen for UE u depends on the smallest SINR in \mathcal{U}_0 , so that $SE_{sc-ptm}(\mathcal{U}_0) = SE(\min_{u \in \mathcal{U}_0} \gamma_{sc-ptm}(u))$. As SC-PTM uses a common resource for all users in \mathcal{U}_0 , we can define:

$$SSE_{sc-ptm} \triangleq \mathbb{E}[SE_{sc-ptm}(\mathcal{U}_0)]. \quad (2.7)$$

MBSFN

Here, the MCS chosen for u depends on the smallest SINR in \mathcal{X} , so that

$$SE_{mbsfn}(\mathcal{X}) = \frac{6}{7} SE(\min_{u \in \mathcal{X}} \gamma_{mbsfn}(u)), \quad (2.8)$$

where the factor $\frac{6}{7}$ accounts for the longer CP with MBSFN. Indeed, MBSFN uses only extended CP (6 OFDM symbols per time slot), while unicast and SC-PTM transmissions employ normal CP (7 OFDM symbols per time slot); thus, to account for the resource waste introduced by the longer CP, the SE of MBSFN transmissions is multiplied by the factor $\frac{6}{7}$.

Moreover, to consider the reserved resources in reserved cells, as well as the resources used in BSs which transmit the MBSFN signal without serving any UE, the SSE in MBSFN is defined as follows [51]:

$$SSE_{mbsfn} \triangleq \mathbb{E}[SE_{mbsfn}(\mathcal{X})] \frac{|\mathcal{X}_a|}{|\mathcal{X}_a| + |\mathcal{X}_t| + |\mathcal{X}_r|}. \quad (2.9)$$

Let consider a MBSFN area formed by 5 cells, where the active UEs are distributed in 2 cells only ($|\mathcal{X}_a| = 2$ and $|\mathcal{X}_t| = 3$). Moreover, 3 additional cells are considered as reserved to improve the transmission ($\mathcal{X}_r = 3$). In such scenario, the number of resources used over the network to transmit the MBMS data is 8, assuming that the target service requires 1 resource per cell. Otherwise, in a SC-PTM transmission, the same scenario requires only 2 resources, since the users are distributed over 2 cells. Hence, Equation (2.9) is introduced to account for this resource waste in MBSFN transmissions.

2.2.4 TTI Bundling

Transmission Time Interval (TTI) bundling is a feature highly related to HARQ, in the sense that several redundancy versions of a transport block are sequentially transmitted. There is however no feedback from the receiver. This is thus an attractive option for delay sensitive reliable group communications. TTI bundling can be adopted for SC-PTM and unicast, whereas MBSFN standards have not adopted so far such techniques. For each TTI

transmission, an improvement of the BLock Error Rate (BLER) is expected, as it provides UE additional information. In [57], Ikuno et al. estimate the SINR gain for a given BLER target that can be achieved when HARQ with Incremental Redundancy (IR) is used, compared to a transmission without HARQ. We evaluate the gain of TTI bundling based on this study assuming a fixed number of re-transmissions. As a consequence, the SINR after the i -th re-transmission can be written:

$$\gamma^{(i)}(u) = \gamma(u) + \gamma_{ttib-gain}^{(i)} \quad (2.10)$$

where $\gamma(u)$ is given by Equation (2.1) or Equation (2.2) depending on the transmission scheme. Figures of $\gamma_{ttib-gain}^{(i)}$ are given by [57]:

$$\gamma_{ttib-gain}^{(i)} = v_{mode}^{(i)} \cdot ECR + \varepsilon_{mode}^{(i)} \quad (2.11)$$

where ECR refers to the Effective Code Rate (ECR) specified for each MCS level and given in Table 2.1; $v_{mode}^{(i)}$ and $\varepsilon_{mode}^{(i)}$ are two parameters depending on re-transmission order (i) as well as modulation level and summarized in Table 2.2.

Modulation	i	$v_{mode}^{(i)} \cdot 10^{-2}$	$\varepsilon_{mode}^{(i)}$
QPSK	1	0.0804	2.89
	2	0.1628	4.57
	3	0.2006	5.62
16-QAM	1	0.042	1.17
	2	0.8435	0.74
	3	0.9464	1.15
64-QAM	1	0.8996	-1.23
	2	1.2288	-0.71
	3	1.2728	0.15

Table 2.2 TTI bundling model parameters for QPSK, 16-QAM and 64-QAM modulations [57].

2.3 Simulation Results

2.3.1 Simulation Settings

The simulator considers an hexagonal urban city cellular network composed of a central cell and 10 rings of adjacent BSs (331 omni-directional BSs in total). It performs Monte

Carlo simulations by varying at each snapshot channel gains and UE locations. The UEs of a group are distributed either in the central cell only (Scenario I), or in central cell as well as the first ring of adjacent cells (Scenario II). We vary the group size by considering 1, 2, 4, 8 or 10 UEs per cell in both scenarios (typical figures for mission-critical communications).

Moreover, PMR networks operate at carrier frequency $f_c = 700 \text{ MHz}$, thus, Hata model ($150 \text{ MHz} \leq f_c \leq 1500 \text{ MHz}$) is assumed for path-loss evaluations, in a urban environment; therefore, κ and η parameters are given by [58]:

$$\kappa_{dB} = 69.55 + 26.161 \log_{10}(f_c) - 13.82 \log_{10}(h_b) - 3.2[\log_{10}(11.75h_u)^2], \text{ in dB,}$$

$$\eta = 4.49 - 0.655 \log_{10}(h_b),$$

where h_b and h_u refer to BS and UE antenna heights respectively (in m).

The parameters used in the performed simulations are presented in Table 2.3.

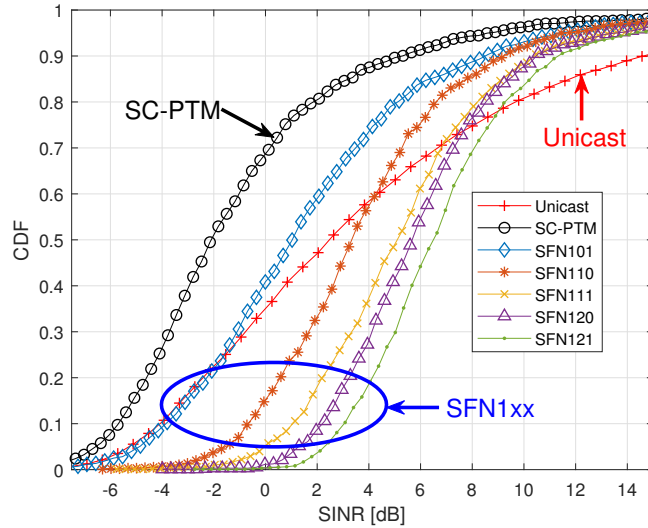
Parameter	Assumption
System model	Macro-cells, urban city
Cellular layout	Hexagonal grid
Number of cells	331 omnidirectional BSs
Cell range	1 Km
Channel Bandwidth (W)	5 MHz
BS Tx power (P)	40 dBm (10 W)
Nb. of group users per cell	1,2,4,8 or 10 UE per BS
White noise power spectral density (\mathcal{N}_0)	-174 dBm/Hz
Shadowing standard deviation (σ)	6 dB
BS antenna height (h_b)	55 m
UE antenna height (h_u)	1.5 m
TTI bundling model	IR with 1, 2, 3 re-Tx, BLER=10%
$T_{CP,mbsfn}$	16.7 μs
$T_{CP,sc-ptm}, T_{CP,uncst}$	5.2 and 4.7 μs
Useful signal frame length, T_U	66.7 μs

Table 2.3 Simulation parameters.

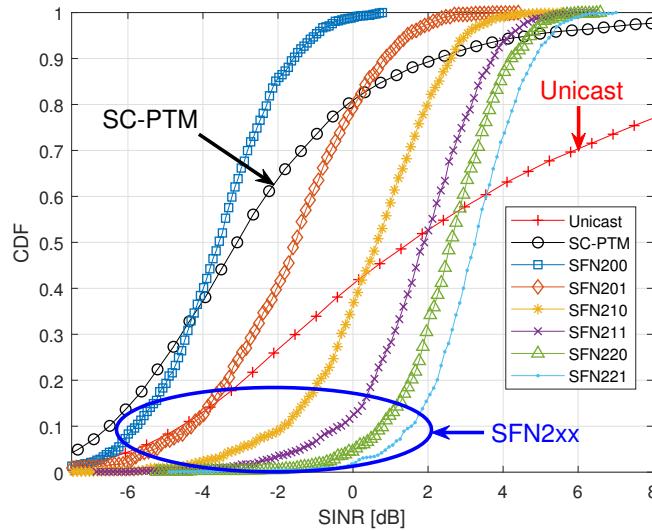
2.3.2 SINR Distributions

To compare the performance of different transmission modes, we first consider 4UE/BS for both Scenarios I and II. Figures 2.2a and 2.2b show the Cumulative Distribution Function

(CDF) of the SINR in unicast, and the minimum SINR in SC-PTM and MBSFN transmission modes, i.e., $\gamma_{ucst}(u)$, $\min_{p \in \mathcal{X}_0} \gamma_{sc-ptm}(p)$ and $\min_{p \in \mathcal{X}} \gamma_{mbsfn}(p)$ in Scenarios I and II, respectively.



(a) Scenario I (4 UEs in central cell).



(b) Scenario II (4 UEs/cell in central and first ring cells).

Figure 2.2 SINR CDF of different transmission modes.

Multicast/Broadcast Single Frequency Network (MBSFN) benefits from the synchronous transmission from adjacent BSs and/or the use of reserved cells as shown on Figure 2.2a. We observe that the introduction of one ring of reserved cells increases the SINR by 3 dB approximately (see SFN101 vs. SC-PTM). Furthermore, an additional SINR gain of 1 to

2 dB can be obtained by transmitting the signal synchronously on same resources from BSs of this ring (see SFN110 vs. SFN101). Reserving the resources of the second ring while transmitting the synchronous signal in the first one (SFN111) improves SINR with 1 to 2 dB compared to SFN110. Moreover, transmitting the synchronous signal from two adjacent rings (SFN120 and SFN 121) improves SINR by 1 to 2 dB compared to single ring transmission (SFN110 and SFN111). All in all, about 9 dB can be gained over SC-PTM with SFN121 for 50% of the groups. For a small group of 4 UEs co-located in a single cell, SFN110 is sufficient to improve the median SINR over unicast.

From Section 2.2, we see that unicast SINR distribution does not depend on the group size, that SC-PTM SINR depends only on the number of group users in reference cell, whereas MBSFN SINR depends on the number of group users in the whole MBSFN area. As a consequence, although the group size has increased, the SC-PTM SINR distribution is not affected in Scenario II because the number of UEs per cell is constant. On the contrary, all MBSFN SINR distributions are shifted to the left. In the best case, MBSFN improves the SINR by 6 dB over SC-PTM (SFN221). SFN211 is now needed for MBSFN to outperform unicast median SINR.

As a conclusion, in terms of minimum SINR, SC-PTM may be preferred over MBSFN for groups, whose users are distributed over many cells. From our simulations we have observed that if the group is distributed over more than 2 rings around the central cell, SC-PTM outperforms SFNX00 (with $X \geq 3$).

2.3.3 System Spectral Efficiency

Tables 2.4a and 2.4b show the mean SSE evaluated for different transmission modes (we assume here that CSI feedback and MCS adaptation is possible in MBSFN).

Although unicast provides roughly a double mean SE with respect to multicast transmissions, it uses resources proportional to the number of group users in the cell. MBSFN uses four times less resources than unicast in every cell but uses more resources in the network since some BSs without group users also transmit. It also suffers from a longer CP. In Scenario I, the former effect does not compensate the latter one so that unicast outperforms MBSFN in terms of SSE. Among MBSFN configurations, SFN110 offers the best SSE, which suggests that reserved cells and an extra ring of transmitting BSs are not required. SC-PTM outperforms both unicast and MBSFN in terms of SSE because it uses less resources than unicast in every cell and less resources in the network than MBSFN. The degradation of the SINR with SC-PTM observed in the previous section does not compensate these effects. In fact, the higher SINR values in SFN110 scenario (Figure 2.3) leads to higher MCS levels compared to SC-PTM. Thus, we note that 65% of groups are served by CQI indexes 5-7 in

Transmission mode	Mean SSE (bps/Hz)
Unicast	0.36
SC-PTM	0.56
SFN101	0.14
SFN110	0.17
SFN111	0.08
SFN120	0.08
SFN121	0.04

(a) Scenario I

Transmission mode	Mean SSE (bps/Hz)
Unicast	0.36
SC-PTM	0.56
SFN200	0.30
SFN201	0.17
SFN210	0.24
SFN211	0.15
SFN220	0.17
SFN221	0.11

(b) Scenario II

Table 2.4 Mean SSE of different transmission modes (4UEs/BS).

SFN110, while indexes 2-4 are used in SC-PTM transmissions to serve approximately the same groups number.

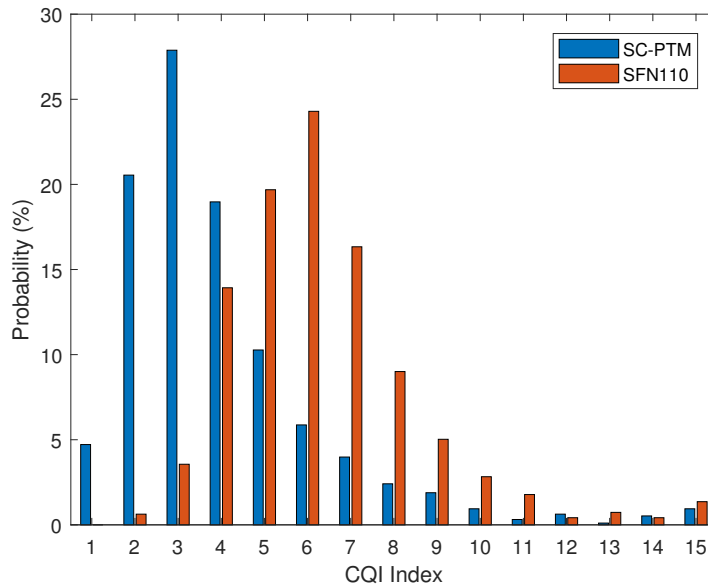


Figure 2.3 Probability distribution of CQI indexes (Scenario I - 4 UEs/BS).

In Scenario II, users are distributed over more cells, which increases the MBSFN SSE, whereas unicast and SC-PTM SSEs are on the contrary not affected. For example, the SSE of SFN200 is now comparable to unicast. From our simulations, we observe that MBSFN performance however saturates for an increasing number of rings (SFNX00 configuration with $X \geq 3$) and never outperforms unicast. This can be explained by the unfavorable MCS selection scheme in MBSFN, which is not compensated by the use of less resources with

respect to unicast. Indeed, increasing the size of the MBSFN area increases largely the probability of low MCS levels, and neglect the selection of higher ones; e.g., in Figure 2.4, we show that 90% of the groups adopt CQI indexes 4-6 in SFN210 transmissions, while CQI 8-15 are not used by any group. SFN210 is the best MBSFN configuration for the same reason as for Scenario I.

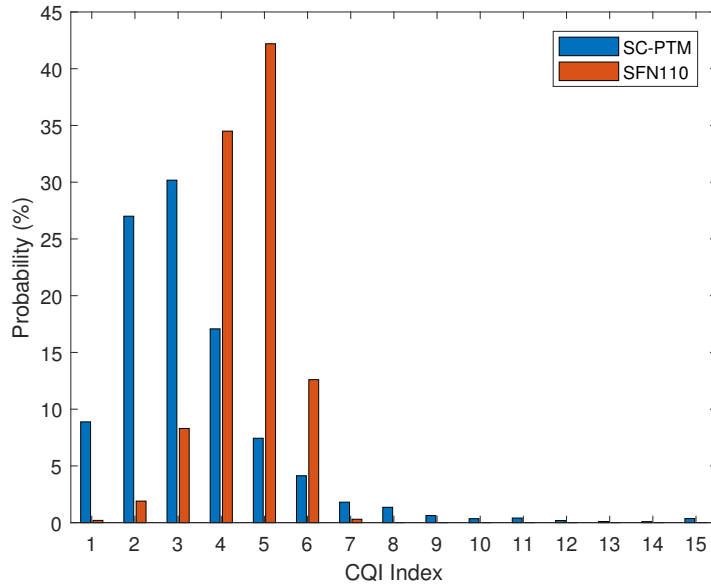


Figure 2.4 Probability distribution of CQI indexes (Scenario II - 4 UEs/BS).

As a conclusion for this section, MBSFN performance in terms of SSE is increasing with the number of group users. Reserved cells and transmitting cells without group users should be avoided for an increased SSE. If the number of group users per cell is small, MBSFN may not outperform unicast transmission. SC-PTM outperforms MBSFN in terms of SSE. As this effect is the inverse of the one observed for SINR distributions, the transmission mode choice will depend on whether the operator wants to favor coverage or capacity.

2.3.4 Impact of Group Size

In Figure 2.5, we vary the number of group users per cell and show the SINR distributions for SC-PTM. As we consider the minimum SINR for the group, it is clear that the radio quality decreases as the number of UEs increases. We also observe that the standard deviation is reduced. The degradation of the SINR implies a degradation of the SE and thus of the SSE as shown in Table 2.5. Unicast transmission is outperformed by multicast transmissions after about 10 group users per cell.

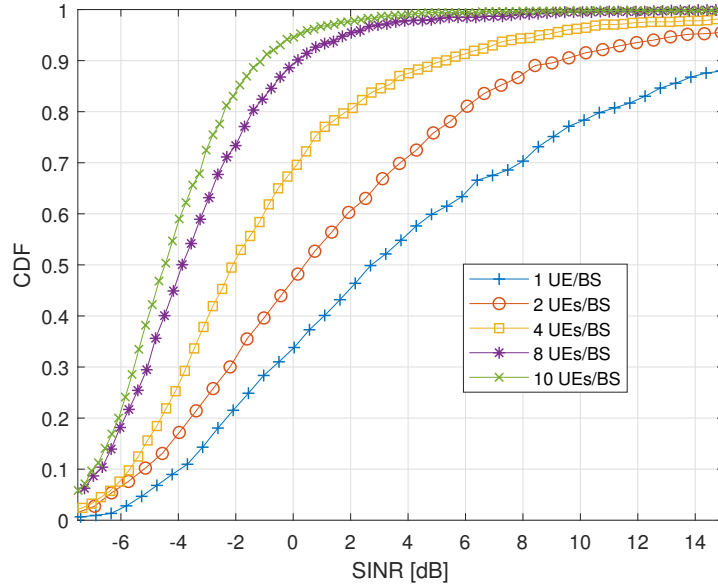


Figure 2.5 Minimum SINR CDF of SC-PTM for different numbers of group users per cell.

Nb. of group users per cell	1	2	4	8	10
Unicast	1.47	0.72	0.36	0.18	0.14
SC-PTM	1.47	0.93	0.56	0.33	0.29
SFN110	0.29	0.22	0.17	0.12	0.11
SFN210	0.37	0.30	0.24	0.21	0.20

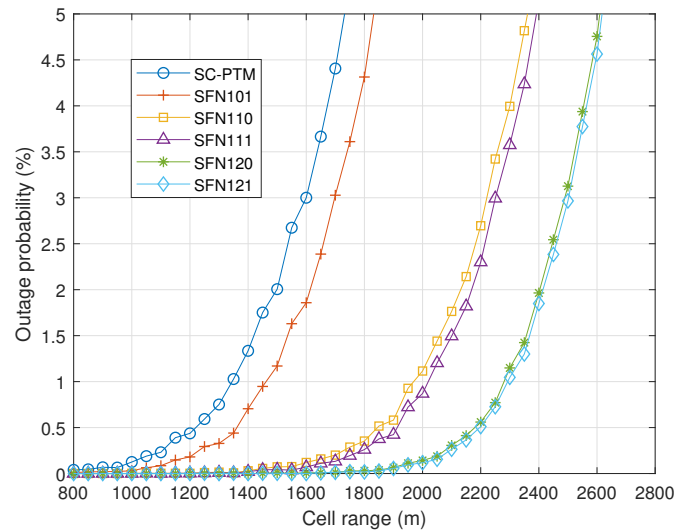
Table 2.5 Mean SSE (in bps/Hz) of transmission modes for different numbers of group users per cell.

2.3.5 Cell Range

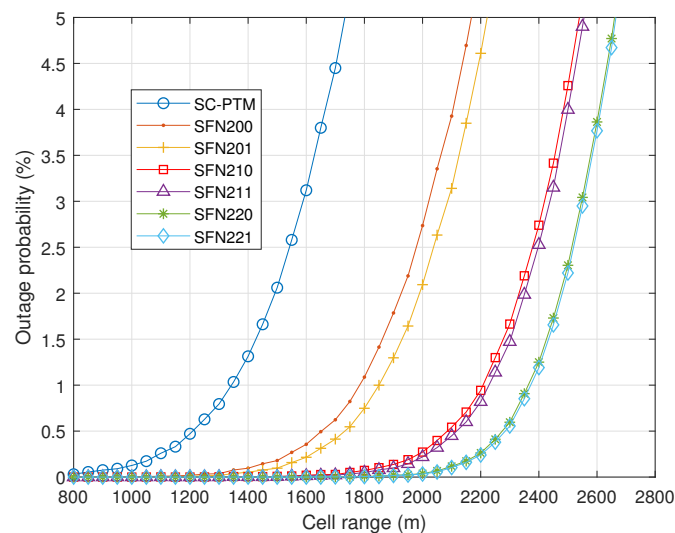
In this section, we evaluate achievable cell ranges depending on the chosen transmission modes. We first define the outage probability as the probability that a UE experiences an SINR lower than a certain threshold γ_{th} (taken as -9.478 dB in our simulations, see Table 2.1). Note that we consider here individual SINR and not the minimum SINR of the group. Figure 2.6 shows the outage probabilities in terms of cell range.

Figures 2.7a and 2.7b show the achievable cell range of different transmission modes, in Scenarios I and II respectively, assuming a maximum outage of 1% (typical value for critical communication services).

In both scenarios, we notice the significant coverage gain of MBSFN transmissions with respect to SC-PTM. Cell range of 1350 m can be achieved with SC-PTM, while MBSFN



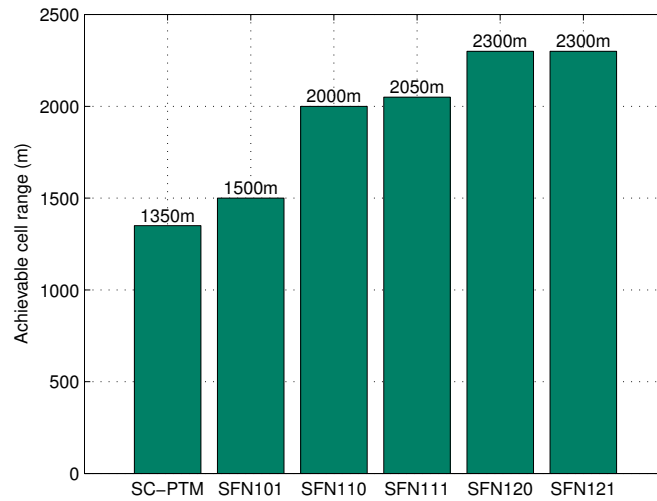
(a) Scenario I



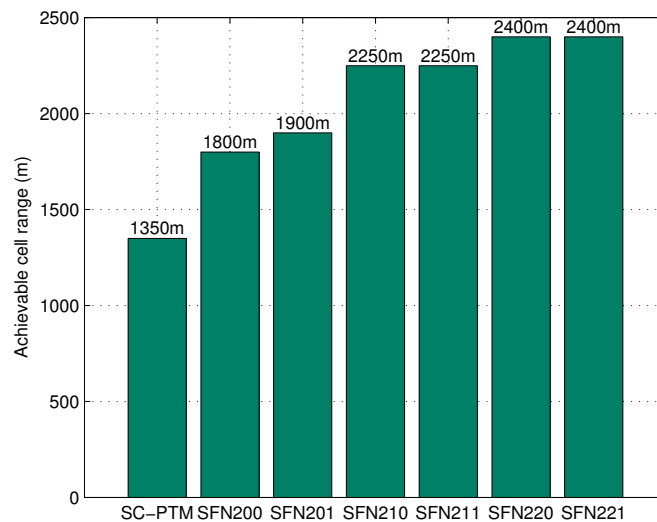
(b) Scenario II

Figure 2.6 Outage probability vs. cell range.

allows cell range up to 2300 m (+70%) in the best case in Scenario I. A 78% gain is achieved in Scenario II (as more rings of cells are transmitting). Moreover, the use of reserved cells in MBSFN transmissions does not improve significantly the cell coverage (e.g., SFN110 vs SFN111, SFN210 vs SFN211).



(a) Scenario I



(b) Scenario II

Figure 2.7 Maximum cell range (for a 1% outage).

2.3.6 TTI Bundling Gain

Figure 2.8 shows cell ranges with SC-PTM with or without TTI bundling compared to cell ranges with SFN110 and SFN210 (assuming again a maximum outage of 1%). We use Equation (2.10) with always a fixed number of retransmissions (1, 2 or 3). MBSFN is assumed without TTI bundling.

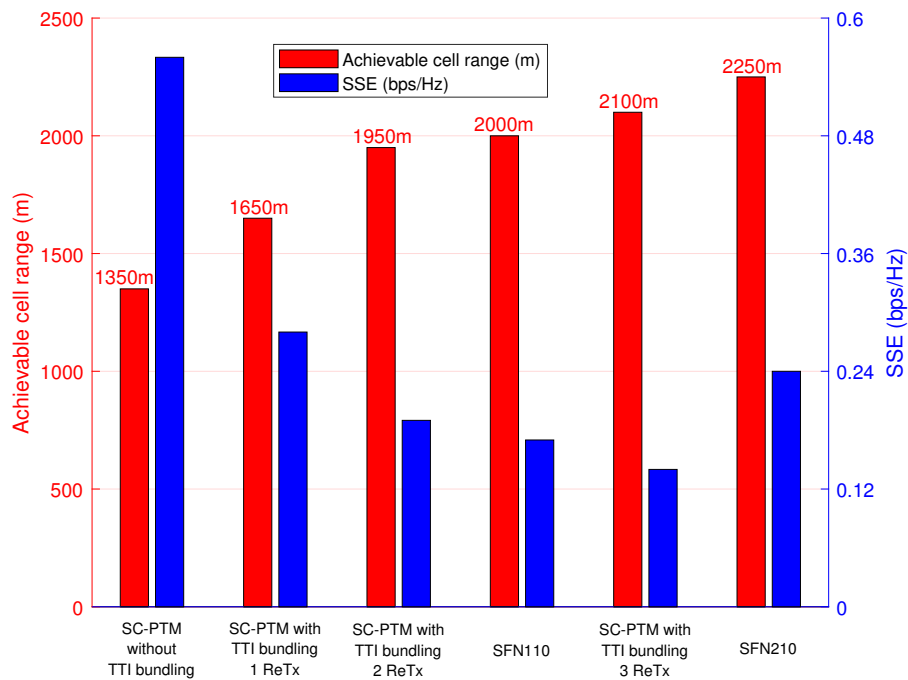


Figure 2.8 Impact of TTI bundling on coverage (1% outage) and SSE.

We note that SC-PTM with TTI bundling with 3 retransmissions provides a coverage gain of 750 m and 100 m compared to SC-PTM without TTI bundling and SFN110 but at the cost of a reduced SSE due to retransmissions. By playing with the number of TTI bundling retransmissions, we see that it is possible to find a trade-off between SSE and coverage as per the operator needs.

2.4 Conclusion

In this chapter, a performance comparison between Multicast/Broadcast Single Frequency Network (MBSFN), Single-Cell Point-To-Multipoint (SC-PTM) and unicast transmissions for mission-critical communications has been presented in terms of Signal to Interference plus Noise Ratio (SINR) gain, System Spectral Efficiency (SSE) and outage probability. Our main conclusions for the scenarios considered in this chapter are the following:

- In terms of minimum group SINR, SC-PTM may be preferred to MBSFN for groups, whose users are distributed over many cells;
- SC-PTM outperforms both unicast and MBSFN in terms of SSE because it uses less resources than unicast in every cell and less resources than MBSFN in the network; it should thus be preferred when the resource is scarce;
- In other scenarios, MBSFN provides huge gains in terms of cell range;
- The trade-off between capacity and coverage can be tuned by varying the number of Transmission Time Interval (TTI) bundling retransmissions with SC-PTM.

We have also provided MBSFN design rules in this chapter:

- The gain provided by reserved cells in terms of coverage is negligible, along with significant radio resource waste. Thus, reserved cells should be avoided;
- Transmitting cells without group users bring significant coverage gain. As the cost in terms of SSE is huge, a single ring of transmitting cells without group users is sufficient.

Chapter 3

SINR Model for MBSFN Networks

Contents

3.1	Introduction	40
3.2	System model	41
3.2.1	Network model	41
3.2.2	SINR evaluation	41
3.3	Analytical Approach	43
3.3.1	Analytical model	43
3.3.2	SINR Closed-Form Formula Assuming Shadowing	45
3.4	Simulation Results	48
3.4.1	Simulation Parameters	48
3.4.2	Deterministic Path-Loss	49
3.4.3	Impact of Shadowing	49
3.5	Conclusion	53

3.1 Introduction

Owing to the system improvements presented in Chapters 1 and 2, Multicast/Broadcast Single Frequency Network (MBSFN) is envisioned to be a key technology for business- and mission-critical communications. On the other hand, radio network planning is one of the key steps before deployment. Dimensioning tools are based on the characterization of the Signal to Interference plus Noise Ratio (SINR), the important key performance parameter, since other metrics, such as outage probability, capacity and spectral efficiency, can be derived from it, as shown in Chapter 2. The need thus arises for simple, fast and accurate method to compute the SINR as a function of the main MBSFN network parameters.

The SINR has been evaluated analytically in the literature for single-cell as well as multi-cell transmissions. In [49], authors propose a model for Inter-Symbol Interference (ISI) in a MBSFN network but do not provide a model for the SINR. Ohmann et al. provide in [59] an approximate SINR distribution but don't take into account ISI and do not provide a simple closed-form formula for the SINR as a function of the distance between the User Equipment (UE) and its closest serving Base Station (BS). A closed-form formula for the outage probability in MBSFN networks has been provided by Talarico et al. in [60]; the ISI is however not considered.

Our work in this chapter is inspired by [61, 62]. In [61], a fluid model is proposed to evaluate the so called other-cell interference factor, and a closed-form formula has been provided to derive outage probability. Furthermore, authors of [62] derive an analytical formula of the Signal to Interference Ratio (SIR) using Fenton-Wilkinson approach, considering the shadowing impact. However, both studies consider single-cell transmissions, while our evaluation studies MBSFN, a multi-cell transmission technique.

In this chapter, we introduce an analytical model, that allows quick calculations of the SINR in MBSFN transmissions. Our model takes into account ISI due to the different propagation delays between the UE and its serving Base Stations (BSs). The comparison with Monte Carlo simulations shows that our approach provides accurate results when shadowing standard deviation is low. When shadowing is highly variable, our model, while less accurate, outperforms the traditional approach based on Fenton-Wilkinson [63] used in literature to evaluate the shadowing impact. This phenomenon is due to the fact that several BSs serve the same UE so that shadowing on every individual link compensate. We show that our model is simpler and provides more accurate results.

The chapter is organized as follows: in Section 3.2, we introduce MBSFN and the network model. We define our analytical model and apply Fenton-Wilkinson in Section 3.3.

Section 3.4 presents and discusses the simulation results. Finally, conclusions are summarized in Section 3.5.

3.2 System model

In this section, we present the network model for MBSFN transmissions and SINR calculations.

3.2.1 Network model

Multicast/Broadcast Single Frequency Network (MBSFN) has been defined as a downlink multi-cell transmission technique, where a time-synchronized common waveform is transmitted from multiple cells, which leads to significant improvement in SINR. The group of BSs which contribute to the simulcast transmission constitutes the so-called MBSFN area (see Section 1.2.1). Moreover, MBSFN networks can support a group of reserved cells; such a cell may be allowed to transmit for other services on the resource allocated to MBSFN transmission, but at restricted power. We recall from Section 2.2.1 that \mathcal{X} is the set of all cells (or BSs) in the network, \mathcal{X} the set of BSs inside the MBSFN area, \mathcal{X}_r the set of reserved cells, and \mathcal{X}_o the set of other cells not involved in MBSFN transmission. Hence, $\mathcal{X} = \mathcal{X} \cup \mathcal{X}_r \cup \mathcal{X}_o$. In Figure 3.1, we approximate the regions shown in Figure 2.1 by a disk and concentric circular rings.

3.2.2 SINR evaluation

The SINR experienced by UE u , in a MBSFN transmission, has been introduced in Section 2.2.2. As aforementioned, to evaluate the useful portion of a received MBSFN signal, the weight function has been provided in Equation (2.3), in terms of τ_{bu} , the difference in propagation delay between signals received from an BS b and the serving BS 0 at UE u .

Assume that the distance r_0 to the closest serving BS is known and serves as a reference for other signals, then this weight function can be modified for any BS at a distance r from the UE as follows:

$$\Gamma(r, r_0) = \begin{cases} 1 & r_0 \leq r < r_0 + cT_p \\ -\frac{r - r_0 - c(T_p + T_U)}{cT_U} & r_0 \leq r - cT_p < r_0 + cT_U \\ 0 & \text{otherwise} \end{cases} \quad (3.1)$$

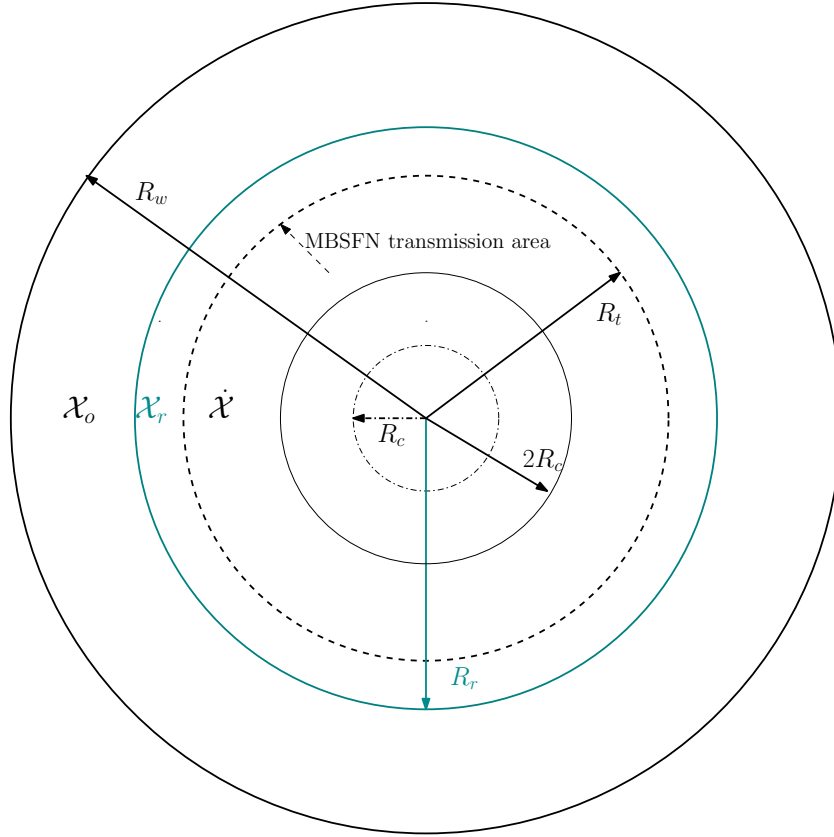


Figure 3.1 MBSFN network model.

Moreover, the SINR experienced by UE u can be expressed by (similarly to Equation (2.4)):

$$\gamma_u = \frac{p_{t,U}(u)}{p_{t,I}(u) + p_{o,I}(u) + \mathcal{N}} \quad (3.2)$$

where $p_{t,U}(u)$ and $p_{t,I}(u)$ denotes respectively the sum of useful and interference portions of signals received from BSs in \mathcal{X} , while $p_{o,I}(u)$ refers to the power of received signals transmitted by BSs in \mathcal{X}_o . Parameter \mathcal{N} is the thermal noise power given by $\mathcal{N} = \mathcal{N}_0 W$, where \mathcal{N}_0 denotes the white noise power spectral density, and W the system bandwidth. More specifically, useful and interfering signal powers are given by:

$$p_{t,U}(u) = \sum_{b \in \mathcal{X}} \omega_{bu} \kappa P_b r_{bu}^{-\eta} X_{bu}, \quad (3.3)$$

$$p_{t,I}(u) = \sum_{b \in \mathcal{X}} (1 - \omega_{bu}) \kappa P_b r_{bu}^{-\eta} X_{bu}, \quad (3.4)$$

$$p_{o,I}(u) = \sum_{b \in \mathcal{X}_o} \kappa P_b r_{bu}^{-\eta} X_{bu}, \quad (3.5)$$

where, as introduced in Equation (2.1), P_b is the transmit power of BS b assumed to be constant across BSs; κ is a constant; η is the path-loss exponent (η is typically strictly greater than 2 and for technical reasons we assume $\eta \neq 3$); $X_{bm} = 10^{\xi_{bm}/10}$ is a log-normal random variable characterizing shadowing and ξ_{bm} is a zero-mean Gaussian random variable with standard deviation σ in dB.

3.3 Analytical Approach

In this section, we extend the fluid model presented in [61, 62] to MBSFN.

3.3.1 Analytical model

The fluid model approach, developed in [61], consists in replacing a given fixed discrete number of transmitters (BSs) by an equivalent continuum of transmitters over the network area. In MBSFN, this approach means that the useful and interference portions of signals transmitted by BSs inside the MBSFN area (\mathcal{X}), in addition to interference signals received from interfering BSs outside of MBSFN area (\mathcal{X}_o) are now considered as continuum fields. In an homogeneous and regular cellular network, we denote ϱ the constant BS density.

We first consider a central cell of radius R (see Figure 3.1). Around this cell, there is a MBSFN area of radius $R_t \geq R_c$ (R_c is the half inter-BS distance). Around this area, there is a ring of reserved cells between disks of radius R_t and R_r . At last, the network is assumed to be a disk of radius $R_n \geq R_r$.

In a first approach, we ignore shadowing and approximate in Equation (3.2) every sum by an integral:

$$\begin{aligned} p_{o,l}(r_0) &= \int_0^{2\pi} \int_{R_r-r_0}^{R_n-r_0} \varrho \kappa P_b r^{-\eta} r dr d\theta \\ &= 2\pi \varrho \kappa P_b \frac{(R_r - r_0)^{2-\eta} - (R_n - r_0)^{2-\eta}}{\eta - 2}, \end{aligned} \quad (3.6)$$

where r is the distance from UE u to a given transmitting position. Received powers can now be expressed as functions of the single variable r_0 . We apply the same technique to

$p_{t,U}(u)$ and $p_{t,I}(u)$:

$$\begin{aligned} p_{t,U}(r_0) &= \kappa P_b r_0^{-\eta} + \int_0^{2\pi} \int_{2R_c-r_0}^{R_t-r_0} \varrho \kappa P_b \Gamma(r, r_0) r^{-\eta} r dr d\theta \\ &= 2\pi \varrho \kappa P_b \left(\frac{r_0^{-\eta}}{2\pi \varrho} + \frac{(2R_c - r_0)^{2-\eta}}{\eta - 2} - \Phi(r_0) \right), \end{aligned} \quad (3.7)$$

$$\begin{aligned} p_{t,I}(r_0) &= \int_0^{2\pi} \int_{2R_c-r_0}^{R_t-r_0} \varrho \kappa P_b (1 - \Gamma(r, r_0)) r^{-\eta} r dr d\theta \\ &= 2\pi \varrho \kappa P_b \left(\Phi(r_0) - \frac{(R_t - r_0)^{2-\eta}}{\eta - 2} \right), \end{aligned} \quad (3.8)$$

where $\Phi(r_0)$ is defined as follows:

$$\Phi(r_0) = \frac{(2R_c - r_0)^{2-\eta}}{\eta - 2} - \int_{2R_c-r_0}^{R_t-r_0} \Gamma(r, r_0) r^{-\eta} r dr. \quad (3.9)$$

To evaluate these integrals, we consider several sub-cases.

Case 1: $r_0 > \frac{1}{2}[R_t - cT_p]$

The signals transmitted by BSs $b \in \mathcal{X}$ arrive at UE u with no excessive delay; thus, ISI can be totally removed. In this case:

$$\Phi(r_0) = \frac{(R_t - r_0)^{2-\eta}}{\eta - 2}. \quad (3.10)$$

Case 2: $\frac{1}{2}[2R_c - cT_p] < r_0 < \frac{1}{2}[R_t - c(T_p + T_u)]$

In this case, the first ring around BS 0 contributes only to the useful signal, while other BSs from the MBSFN area may contribute to the interference depending on their distance to the UE. We obtain:

$$\Phi(r_0) = \frac{[r_0 + cT_p]^{3-\eta} - [r_0 + c(T_p + T_u)]^{3-\eta}}{cT_u(\eta - 2)(\eta - 3)}. \quad (3.11)$$

Case 3: $\frac{1}{2}[2R_c - cT_p] < r_0$ and $\frac{1}{2}[R_t - c(T_p + T_u)] < r_0 < \frac{1}{2}[R_t - cT_p]$

In this case, all BSs from the MBSFN area are interfering except the first ring, which contributes only to useful signal. We obtain Equation (3.12).

$$\Phi(r_0) = \frac{(r_0 + cT_P)^{3-\eta}}{cT_U(\eta-2)(\eta-3)} + \frac{r_0 + c(T_P + T_U)}{cT_U} \frac{(R_t - r_0)^{2-\eta}}{\eta-2} - \frac{(R_t - r_0)^{3-\eta}}{cT_U(\eta-3)}. \quad (3.12)$$

Case 4: $r_0 < \frac{R_t - c(T_P + T_U)}{2}$ and $\frac{2R_c - c(T_P + T_U)}{2} < r_0 < \frac{2R_c - cT_P}{2}$

All BSs $b \in \mathcal{X}$ signals, including the first ring, have useful and interfering parts. We obtain Equation (3.13).

$$\Phi(r_0) = \frac{(2R_c - r_0)^{3-\eta}}{cT_U(\eta-3)} - \frac{r_0 + cT_P}{cT_U} \frac{(2R_c - r_0)^{2-\eta}}{\eta-2} - \frac{(r_0 + c(T_P + T_U))^{3-\eta}}{cT_U(\eta-2)(\eta-3)}. \quad (3.13)$$

Case 5: $r_0 > \frac{1}{2}[R_t - c(T_P + T_U)]$ and $\frac{1}{2}[2R_c - c(T_P + T_U)] < r_0 < \frac{1}{2}[2R_c - cT_P]$

Only the signals received from first ring BSs include useful and interfering portions, while the signals transmitted from other BSs in the MBSFN area are completely interfering. We obtain Equation (3.14).

$$\Phi(r_0) = \frac{(2R_c - r_0)^{3-\eta} - (R_t - r_0)^{3-\eta}}{cT_U(3-\eta)} - \frac{r_0 + cT_P}{cT_U} \frac{(2R_c - r_0)^{2-\eta}}{\eta-2} + \frac{r_0 + c(T_P + T_U)}{cT_U} \frac{(R_t - r_0)^{2-\eta}}{\eta-2}. \quad (3.14)$$

Case 6: $r_0 \leq \frac{2R_c - c(T_P + T_U)}{2}$

In this case, all signals transmitted by BSs $b \in \mathcal{X} \setminus \{0\}$ arrive with excessive delays, so that they completely interfere with the signal transmitted by the serving BS. Thus:

$$\Phi(r_0) = \frac{(2R_c - r_0)^{2-\eta}}{\eta-2}. \quad (3.15)$$

3.3.2 SINR Closed-Form Formula Assuming Shadowing

In this section, we propose an approximation of the SINR in MBSFN transmissions based on Fenton-Wilkinson method, in order to analyze the shadowing impact.

Sum of Log-normal Random Variables

Several classical techniques have been proposed in order to approximate a sum of log-normal random variables, e.g., Schwartz-Yeh [64] and Beaulieu et al. [65]. The former involves complex recursive calculations, while the latter assumes identical means and standard

deviations for the considered random variables. On the contrary, the Fenton-Wilkinson [63] method provides a closed-form formula for non-identical distributed log-normal random variables.

We consider the sum $S = \sum_i \alpha_i X_i$, where α_i is a constant, $X_i = 10^{\xi_i/10}$ is a log-normal random variable, and ξ_i is a zero-mean random variable with standard-deviation σ in dB. Each term of S follows a log-normal distribution with mean $a \nu_i$ and variance $a^2 \sigma^2$, where $a = \ln(10)/10$ and $\nu_i = \frac{1}{a} \ln(\alpha_i)$. The Fenton-Wilkinson method approximates the sum S itself by a log-normal random variable with mean $a \nu$, and variance $a^2 \sigma_s^2$, where:

$$a \nu = \ln \left(\sum_i e^{a \nu_i} \right) + \frac{a^2 \sigma^2}{2} - \frac{a^2 \sigma_s^2}{2}, \quad (3.16)$$

$$a^2 \sigma_s^2 = \ln \left[(e^{a^2 \sigma^2} - 1) \frac{\sum_i e^{2a \nu_i}}{(\sum_i e^{a \nu_i})^2} + 1 \right]. \quad (3.17)$$

These two expressions simplify to:

$$a \nu = \ln \left(\sum_i \alpha_i \right) + \frac{a^2 \sigma^2}{2} - \frac{a^2 \sigma_s^2}{2}, \quad (3.18)$$

$$a^2 \sigma_s^2 = \ln \left[(e^{a^2 \sigma^2} - 1) \frac{\sum_i \alpha_i^2}{(\sum_i \alpha_i)^2} + 1 \right]. \quad (3.19)$$

Fenton-Wilkinson Approach for Shadowing

The Fenton-Wilkinson based method was applied for single-cell transmissions in [62], and it has exhibited accurate results when shadowing standard deviation is low.

In our model, which deals with multi-cell transmissions, we assume that all BSs transmit with the same power P_b , the SINR in Equation (3.2) can be formulated as:

$$\begin{aligned} \gamma_u &= \left(\frac{\sum_{b \in \mathcal{X}} (1 - \omega_{bu}) r_{bu}^{-\eta} X_{bu}}{\sum_{b \in \mathcal{X}} \omega_{bu} r_{bu}^{-\eta} X_{bu}} + \frac{\sum_{b \in \mathcal{X}_o} r_{bu}^{-\eta} X_{bu}}{\sum_{b \in \mathcal{X}} \omega_{bu} r_{bu}^{-\eta} X_{bu}} + \frac{\mathcal{N}}{\sum_{b \in \mathcal{X}} \omega_{bu} \kappa P_b r_{bu}^{-\eta} X_{bu}} \right)^{-1} \\ &= (\wp_U + \wp_I + \wp_{\mathcal{N}})^{-1}, \end{aligned} \quad (3.20)$$

where \wp_U , \wp_I and $\wp_{\mathcal{N}}$ denote useful, interference and noise terms respectively.

To compute the characteristics of these terms, let us define the following functions:

$$\begin{aligned}\ell(\boldsymbol{\omega}, \mathbf{r}, \eta, \mathcal{X}) &= \sum_{i \in \mathcal{X}} \omega_i r_i^{-\eta} \\ \hbar(\boldsymbol{\omega}, \mathbf{r}, \eta, \sigma, \mathcal{X}) &= \left((e^{a^2 \sigma^2 / 2} - 1) \frac{\sum_{i \in \mathcal{X}} \omega_i^2 r_i^2}{(\sum_{i \in \mathcal{X}} \omega_i r_i)^2} + 1 \right)^{-\frac{1}{2}}\end{aligned}\quad (3.21)$$

where $a = \ln(10)/10$, \mathcal{X} denotes a set of BSs, $\boldsymbol{\omega}$ and \mathbf{r} are two vectors representing the weighting function and the distance between UE u and every element of \mathcal{X} .

Using Fenton-Wilkinson approach, we approximate φ_U, φ_I and $\varphi_{\mathcal{N}}$ as log-normal random variables. Thus, Equations (3.22), (3.23) and (3.24), provide the corresponding mean and variance respectively:

$$\begin{aligned}a v_U &= \ln \left(\frac{\ell(\mathbf{1} - \boldsymbol{\omega}, \mathbf{r}, \eta, \mathcal{X}) \cdot \hbar(\mathbf{1} - \boldsymbol{\omega}, \mathbf{r}, \eta, \sigma, \mathcal{X})}{\ell(\boldsymbol{\omega}, \mathbf{r}, \eta, \mathcal{X}) \cdot \hbar(\boldsymbol{\omega}, \mathbf{r}, \eta, \sigma, \mathcal{X})} \right), \\ a^2 \sigma_U^2 &= -2 \ln \left[\hbar(\mathbf{1} - \boldsymbol{\omega}, \mathbf{r}, \eta, \sigma, \mathcal{X}) \cdot \hbar(\boldsymbol{\omega}, \mathbf{r}, \eta, \sigma, \mathcal{X}) \right].\end{aligned}\quad (3.22)$$

$$\begin{aligned}a v_I &= \ln \left(\frac{\ell(\mathbf{1}, \mathbf{r}, \eta, \mathcal{X}_o) \cdot \hbar(\mathbf{1}, \mathbf{r}, \eta, \sigma, \mathcal{X}_o)}{\ell(\boldsymbol{\omega}, \mathbf{r}, \eta, \mathcal{X}) \cdot \hbar(\boldsymbol{\omega}, \mathbf{r}, \eta, \sigma, \mathcal{X})} \right), \\ a^2 \sigma_I^2 &= -2 \ln \left[\hbar(\mathbf{1}, \mathbf{r}, \eta, \sigma, \mathcal{X}_o) \cdot \hbar(\boldsymbol{\omega}, \mathbf{r}, \eta, \sigma, \mathcal{X}) \right].\end{aligned}\quad (3.23)$$

$$\begin{aligned}a v_{\mathcal{N}} &= - \left[\ln \frac{PK}{\mathcal{N}} + \ln \ell(\boldsymbol{\omega}, \mathbf{r}, \eta, \mathcal{X}) + \frac{a^2 \sigma^2}{2} + \ln \hbar(\boldsymbol{\omega}, \mathbf{r}, \eta, \sigma, \mathcal{X}) \right], \\ a^2 \sigma_{\mathcal{N}}^2 &= -2 \ln \hbar(\boldsymbol{\omega}, \mathbf{r}, \eta, \sigma, \mathcal{X}).\end{aligned}\quad (3.24)$$

Finally, we determine the mean and variance of γ_u as follows:

$$\begin{aligned}
a v_{\gamma_u} &= - \left[\ln \left(\sum_{l \in \{U, I, \mathcal{N}\}} e^{a v_l + a^2 \sigma_l^2 / 2} \right) - \frac{a^2 \sigma_{\gamma_u}^2}{2} \right], \\
a^2 \sigma_{\gamma_u}^2 &= \ln \left[\frac{\sum_{l \in \{U, I, \mathcal{N}\}} (e^{a^2 \sigma_l^2} - 1) e^{2a v_l + a^2 \sigma_l^2}}{\left(\sum_{l \in \{U, I, \mathcal{N}\}} e^{a v_l + a^2 \sigma_l^2 / 2} \right)^2} + 1 \right]. \tag{3.25}
\end{aligned}$$

3.4 Simulation Results

In this section, we compare our model to Monte Carlo simulations and compare it to the Fenton-Wilkinson approach.

3.4.1 Simulation Parameters

As in Section 3.4, we consider an hexagonal urban city cellular network composed of a central cell and 10 rings of adjacent BSs (331 omni-directional BSs in total). The User Equipments (UEs) are distributed in the MBSFN area, formed by the central cell in addition to 2 rings of adjacent cells (reserved cells are not considered in this first setting). Hata model (Urban, BS antenna height of 55 m, UE antenna height of 1.5 m) is assumed for path-loss evaluations. The system simulation parameters that were taken into account for our simulations are presented in Table 3.1.

Parameter	Assumption
Cell range (R)	500 m, 1500 m or 5000 m
BS density (ρ)	$(3\sqrt{3}R^2/2)^{-1}$
Half distance between 2 eNBs (R_c)	$R\sqrt{3}/2$
MBSFN area radius (R_t)	$5R\sqrt{3}/2$
Shadowing standard deviation (σ)	0dB, 3dB, 6dB or 8dB
Cyclic Prefix length, T_p	16.7 μ s
Useful signal frame length, T_U	66.7 μ s

Table 3.1 SINR analytical model simulation parameters.

3.4.2 Deterministic Path-Loss

Figure 3.2 shows the comparison between the analytical model and the SINR evaluated by simulations without shadowing ($\sigma = 0$ dB), for different path-loss exponent η . We observe that the analytical model matches very well the simulations, for different realistic values of η .

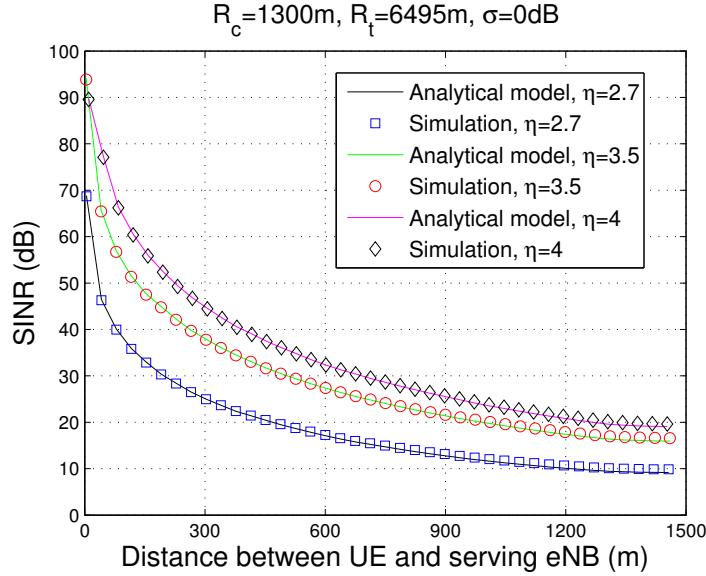


Figure 3.2 Comparison of the analytical model with simulations assuming path-loss exponents $\eta = 2.7, 3.5$ and 4 .

In Figure 3.3, we show that our model is accurate for various cell ranges, from 500 m (as envisioned for mission-critical deployments) to 5000 m (a typical value for classical MBSFN networks).

Moreover, we evaluate our analytical model for different MBSFN configurations. We consider two different configurations: SFN110 and SFN121; in the first one, only the first ring of adjacent BSs to the central cell transmit the MBSFN signals, while in the second, we assume two rings of transmitting cells with an additional single ring of reserved cells, which do not transmit on MBSFN resources. Figure 3.4 shows that in both configurations the model matches well the simulation results.

3.4.3 Impact of Shadowing

In this section, the SINR is evaluated by simulation, taking the impact of shadowing into consideration. We compare these simulations with our model and with the Fenton-Wilkinson approach. In the latter method, ν_{γ_u} as in Section 3.3.2 is plotted as a function of the distance

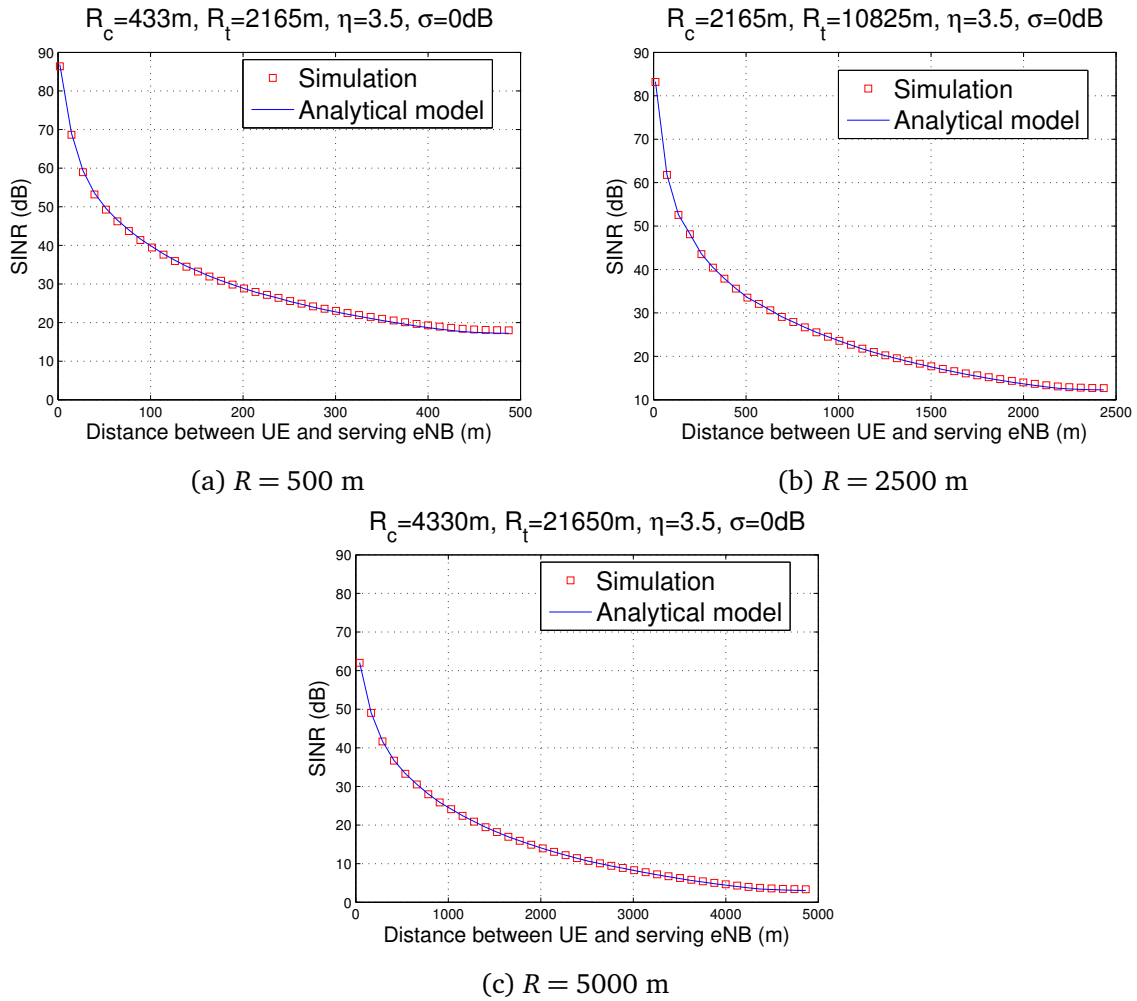


Figure 3.3 Comparison of the analytical model with simulations assuming cell ranges $R = 500\text{ m}$, 2500 m and 5000 m .

to the reference serving BS. Figure 3.5 shows the variation of the SINR with respect to the distance to the serving BS (left) and the Cumulative Distribution Function (CDF) of the SINR (right) for various realistic shadowing standard deviations.

As expected, the accuracy of the two approaches decreases with increasing σ . For $\sigma = 3\text{ dB}$, our model matches very well with simulations. There is at most 3 dB difference at $\sigma = 6\text{ dB}$. The maximum difference reaches 5 dB for $\sigma = 8\text{ dB}$ (at 500 m from the BS). In terms of CDF, our model is more accurate for high SINRs than for very low SINRs. However, in all cases our analytical model does better than Fenton-Wilkinson, which is the reference method in the literature for taking into account shadowing. Owing to its simplicity, our model can be preferred.

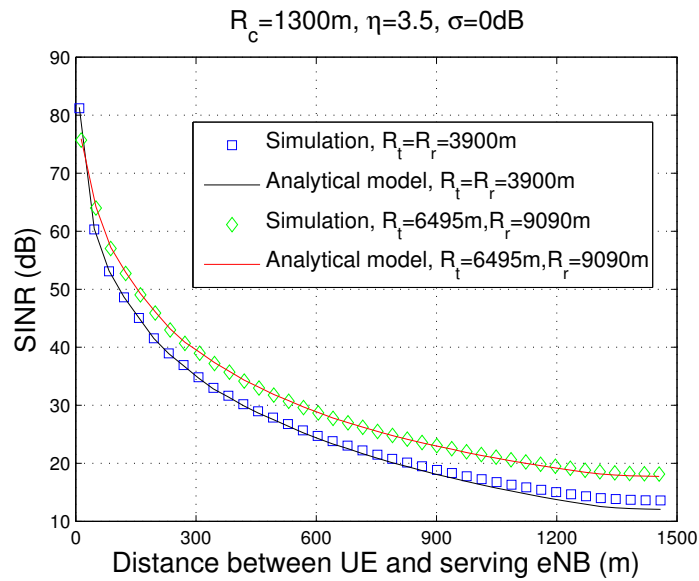


Figure 3.4 Comparison of the analytical model with simulations assuming different MBSFN area configurations.

We note from the comparison with simulated distributions that our model may become inaccurate for the evaluation of low outage probabilities. It provides however accurate overall SINR distributions at a click speed. These distributions can be used for performance evaluation when link adaptation is performed without relying on time expensive simulations. Moreover, as experienced from our simulations presented in Chapter 4, we note that considering -9.478 dB as an outage Signal to Noise Ratio (SNR) threshold [56] is quite optimistic, regarding Professional Mobile Radio (PMR) system requirements.

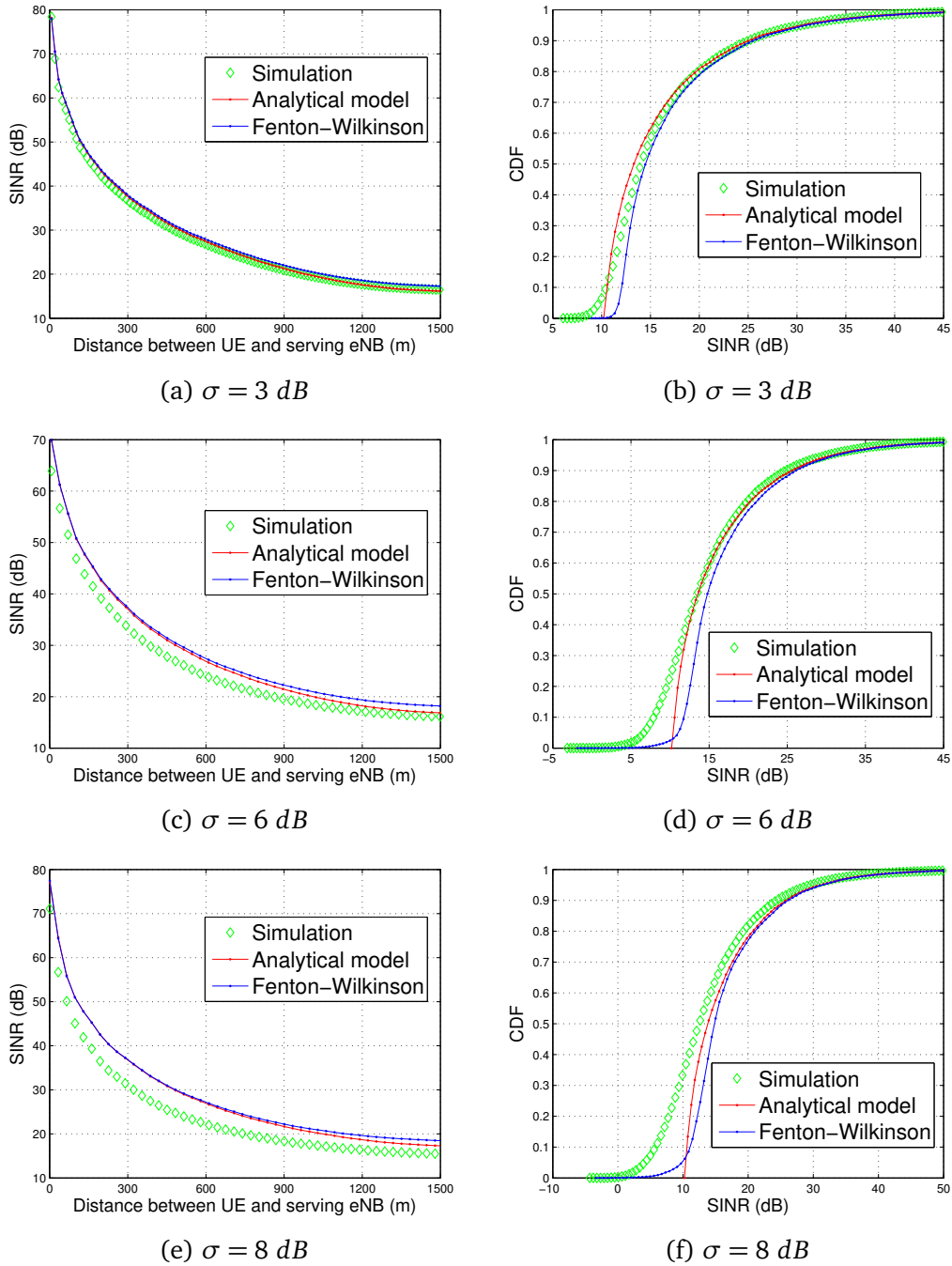


Figure 3.5 Comparison of the analytical model with Monte Carlo simulations and Fenton-Wilkinson approach assuming $R = 1500 \text{ m}$, $\eta = 3.5$ and $\sigma = 3, 6$ and 8 dB . Left: SINR as a function of UE-BS distance. Right: CDF of the SINR.

3.5 Conclusion

In this chapter, we have proposed a Signal to Interference plus Noise Ratio (SINR) model for Multicast/Broadcast Single Frequency Network (MBSFN) based mission critical communications. Our model takes into account Inter-Symbol Interference (ISI) due to the different propagation delays between the User Equipment (UE) and its serving Base Station (BS), as well as the MBSFN area size. Closed-form formulas for the expression of the SINR as a function of the distance to the nearest serving BS makes the proposed model particularly appealing for fast dimensioning processes. Monte Carlo simulations show that our approach is very accurate when shadowing is low. At high shadowing standard deviation, our model does better than the classical Fenton-Wilkinson approach.

Chapter 4

A Repetition Scheme for MBSFN

Contents

4.1 Introduction	56
4.2 System Models	57
4.2.1 Link Level Model	58
4.2.2 Rayleigh Fading Channel	58
4.2.3 Rayleigh Fading Simulation Model	61
4.2.4 System Level Model	65
4.3 Link Level Abstraction	65
4.3.1 Overall Architecture	65
4.3.2 Effective SNR	67
4.3.3 BLER Evaluation	68
4.4 Repetition Scheme	68
4.4.1 Design Principles	68
4.4.2 Proposed Scheme	70
4.5 Simulation Results	72
4.5.1 Simulation Parameters	72
4.5.2 Validation of the Link Level Abstraction	73
4.5.3 Repetition Scheme Results for EVA50 channel	74
4.5.4 Validation of Repetition Scheme Results for EPA3 channel	77
4.5.5 Cell Radius Gain	79
4.6 Conclusion	83

4.1 Introduction

A performance evaluation of the point-to-multipoint technologies envisioned for Professional Mobile Radio (PMR) has been presented in Chapter 2. The coverage improvements achieved by Multicast/Broadcast Single Frequency Network (MBSFN) are compared with capacity gains attained with Single-Cell Point-To-Multipoint (SC-PTM). We show that the coverage vs. capacity trade-off which arises between these transmission modes may be compensated by the data repetition. Contrary to classical mobile networks, capacity is not the main issue in practical deployments of PMR networks¹. In this chapter, we thus focus on coverage improvement in presence of group calls by proposing a repetition scheme based on Chase Combining (CC) and Maximum Ratio Combining (MRC).

Hybrid Automatic Repeat re-Quest (HARQ) is a classical technique to improve communication reliability. For a given Block Error Rate (BLER) target, the required Signal to Interference plus Noise Ratio (SINR) is lowered as the number of re-transmissions increases. The gain achieved in terms of SINR can then be translated in terms of cell coverage. In [66], the authors show that HARQ with full Incremental Redundancy (IR) offers the best throughput performance for high modulation schemes but at the cost of higher memory requirement. On the contrary, HARQ with CC is favored, when lower modulation schemes are assumed and memory is a limiting factor. As MBSFN uses robust Modulation and Coding Schemes (MCSs), CC is a natural choice. In [67], an enhanced HARQ scheme for Orthogonal Frequency-Division Multiplexing (OFDM) systems has been introduced, based on modulation constellation diversity, which consists of changing the bit interleaving mode such as the data sequence is changed, when data is requested for re-transmissions. The authors show that the proposed scheme improves system's coverage and throughput performance, compared to a scheme employing CC, when frequency diversity is applied as well. However, the modulation constellation diversity effect is not useful if Quadrature Phase Shift Keying (QPSK) is used in OFDM system, and the scheme degenerates into a frequency diversity scheme. In [68], Kumagai et al. presented a maximal ratio combining Automatic Repeat re-Quest (ARQ) scheme for OFDM, in which the frequency is changed at every re-transmission in order to benefit from frequency diversity. Moreover, several studies have shown gains in both average system capacity and cell-edge data rates, when introducing the frequency diversity to the packet scheduler [69, 70].

HARQ suffers however from multiple drawbacks when group calls are considered. As the transmission is multicast, re-transmissions should be performed according to the multiple feedbacks from the User Equipments (UEs) in the group. Such scheme can matter in terms

¹As experienced by ETELM.

of radio resource efficiency and transmission delays for group communications; since the re-transmission should take place when at least one Non-ACKnowledgement (NACK) is sent from the UEs in the group, it may occur more frequently as the number of UEs per group increases. Moreover, the control signaling overhead on the feedback channel may drastically increase. Also MBSFN standards have not adopted so far the possibility of a feedback channel on the uplink.

Motivated by gains brought by Transmission Time Interval (TTI) bundling alternative scheme evaluated in Chapter 2 for SC-PTM transmissions, we propose in this chapter an alternative approach which relies on CC repetitions without any feedback for MBSFN. This technique is widely used in Internet of Things (IoT) standards Sigfox, LoRa and NarrowBand-Internet of Things (NB-IoT) for simplicity reasons and sometimes because of the absence of feedback [71]. Here, for PMR networks, we design the time and frequency shifts to be adopted for every repetition based on the channel characteristics and video codec constraints. The number of repetitions and their time-frequency distance is the result of a trade-off between coverage and capacity on the one hand, and between coverage and delay on the other hand. In Chapter 2, we adopted results from literature to evaluate the SINR gains provided by TTI bundling, while in this chapter, we rely on a simplified performance evaluation model, which allows us to obtain quick results without implementing the whole transmission reception chain to evaluate our system, and to test various proposed repetition schemes. We show by link and system level simulations that the proposed scheme provides a substantial gain in terms of SINR, and hence is an attractive option to enhance the network coverage for delay sensitive reliable group communications.

The rest of the chapter is organized as follows: in Section 4.2, we introduce the system models used in our evaluation. Next, we present the abstractions considered at link level to cope the transmission chain complexity in Section 4.3. In Section 4.4, we describe the proposed repetition scheme. Section 4.5 presents and discusses the simulation results. Finally, conclusions are summarized in Section 4.6.

4.2 System Models

In order to evaluate our proposed scheme, we rely on both link level and system level approaches.

4.2.1 Link Level Model

We consider an OFDM downlink channel. The received signal on the n -th subcarrier during the i -th OFDM symbol is given by:

$$r_n[i] = \sqrt{p_n} \Omega_n[i] s_n[i] + w_n[i], \quad (4.1)$$

where $n = 1, \dots, N_{sc}$ and $i = 1, \dots, N_{sym}$, N_{sc} is the number of subcarriers in a Resource Block (RB), N_{sym} the number of symbols in a subcarrier, p_n the power allocated to the n -th subcarrier, $\Omega_n[i]$ the complex channel gain of samples received at the n -th subcarrier during the i -th OFDM symbol, $s_n[i]$ is the symbol transmitted over the n -th subcarrier of the i -th symbol, and $w_n[i]$ is the noise modeled as zero-mean Gaussian random variable with variance $\sigma_{\mathcal{N}}^2$.

The Signal to Noise Ratio (SNR) experienced at the l -th transmission on the n -th subcarrier during the i -th OFDM symbol ($\dot{\gamma}_{n,l}[i]$) is given by:

$$\dot{\gamma}_{n,l}[i] = \frac{|\Omega_{n,l}[i]|^2 p_n}{\sigma_{\mathcal{N}}^2}. \quad (4.2)$$

Furthermore, we assume that MRC is performed at the receiver, so that after L transmissions, the SNR experienced at the receiver, using CC, is given by:

$$\gamma_n[i] = \sum_{l=1}^L \dot{\gamma}_{n,l}[i] = \frac{p_n}{\sigma_{\mathcal{N}}^2} \sum_{l=1}^L |\Omega_{n,l}[i]|^2. \quad (4.3)$$

4.2.2 Rayleigh Fading Channel

Fading and multipath occur in many radio communication systems. In wireless communications, there could be more than one path, over which the signal can travel between the transmitter and receiver antennas; this is due to atmospheric scattering and refraction, as well as reflections from buildings and other objects. As the result of multipath reception, the mobile antenna receives a large number of reflected and scattered waves, arriving along different paths and having different attenuations and delays, and they might add at the receiving antenna either constructively or destructively. Moreover, if the receiver moves over a distance in the order of wave length or more, the multipath received signals will incur rapid fluctuations in their amplitudes and phases. Depending on the nature of the propagation environment, there are different models describing the statistical behavior of the multipath fading: Rayleigh, Rician or Nakagami- m models. In our evaluation, we focus on Rayleigh channel. Further, we consider a discrete multipath channel, where

the multipath signal paths are made up of a relatively small and identifiable number of components reflected by obstacles encountered in open areas, which results in a channel model with a finite number of multipath components.

One characteristic of a multipath medium is the dispersion, or time spreading, introduced in the signal that is transmitted through the channel. A second characteristic is due to the time variations in the structure of the medium. As a result of such time variations, the nature of the multipath varies with time.

Moreover, in addition to multipath (or small-scale fading), wireless communications are affected by another type of fading, referred to as shadowing (or large-scale fading). Shadow fading reveals itself as an attenuation of the signal power, induced by prominent terrain contours between transmitter and receiver. The shadow fading is modeled by a zero-mean log-normal Gaussian distribution with a standard deviation σ .

Power delay profile

In a scattered environment, the received signals arrive along different paths with different power attenuation and delays. The term delay refers to excess delay, which represents the delay measured from the first perceptible signal that arrives at the receiver. Furthermore, the maximum excess delay (T_m), also termed maximum delay spread, is the delay between the first and the last component of the signal, during which the received power falls below some threshold level, e.g., 20 dB below the strongest component. Thus, the relationship between T_m and the symbol time (T_{sym}) leads to two different fading schemes:

- When $T_m > T_{sym}$, the channel exhibits a frequency selective fading, where the multipath components extend beyond the symbol duration, which leads to significant Inter-Symbol Interference (ISI) experienced at the receiver.
- When $T_m \ll T_{sym}$, the channel exhibits a flat fading, or frequency non-selective fading. In this case, there is a very little ISI, but the system distortion still appears because the multipath signal can add destructively, reducing considerably the SNR.

However, the maximum excess delay (T_m) is not necessarily the best indicator of the system performance on the channel, because some channels with the same value of T_m can have very different delay power profiles. Thus, a more useful measurement is the Root Mean Square (RMS) delay spread (δ_t) defined as [72]:

$$\delta_t = \sqrt{\frac{\sum_{k=1}^K P_k (\tau_k - \bar{\tau})^2}{\sum_{k=1}^K P_k}}, \quad (4.4)$$

where P_k is the power in path k , τ_k is the path delay, and $\bar{\tau}$ is the mean excess delay given by:

$$\bar{\tau} = \frac{\sum_{k=1}^K P_k \tau_k}{\sum_{k=1}^K P_k}. \quad (4.5)$$

Coherence Bandwidth

While the delay spread is a natural phenomenon caused by reflected and scattered propagation paths in the radio channel, the coherence bandwidth (B_c) is a defined relation derived from the RMS delay spread. It is a statistical measure of the range of frequencies over which the channel can be considered flat, i.e. a channel which passes all spectral components with approximately equal gain and linear phase.

Two sinusoids with frequency separation greater than B_c are affected quite differently by the channel. If the coherence bandwidth is defined as the bandwidth over which the frequency correlation function is above 0.5, then the coherence bandwidth is approximately [72, 73]:

$$B_c \approx \frac{1}{5\delta_t}. \quad (4.6)$$

The two fading schemes mentioned above for frequency selective and flat fading can also be described in terms of the coherence and channel bandwidth (W):

- When $B_c < W$, the channel is referred to as frequency selective.
- Whenever $B_c \gg W$, the flat fading degradation occurs. As noted before, flat fading does not introduce ISI.

Doppler Spread and Coherence Time

Delay spread and coherence bandwidth are parameters which describe the time dispersive nature of the channel in a local area. However, they do not offer information about the time varying nature of the channel caused by either relative motion between the transmitter and the receiver, or by movement of objects in the channel. Doppler spread and coherence time (T_c) are parameters which describe the time varying nature of the channel in a small-scale region.

The coherence time (T_c) is a statistical measure of the time duration over which the channel impulse response is invariant, and quantifies the similarity of the channel response at different times. In other words, coherence time is the duration over which two received signals have a strong potential for amplitude correlation.

Coherence time and Doppler spread (f_D) are inversely proportional to each other [72, 73]:

$$T_c \approx \frac{1}{f_D}, \quad (4.7)$$

where $f_D = \frac{v f_c}{c}$, v is the vehicular speed, f_c refers to the carrier frequency and c the speed of light.

If the coherence time is defined as the time over which the time correlation is above 0.5, then the coherence time is approximately [74]:

$$T_c \approx \frac{9}{16\pi f_D}. \quad (4.8)$$

In practice, the first approximation (Equation (4.7)) suggests a time duration during which a Rayleigh fading signal may fluctuate wildly, while the second (Equation (4.8)) is too restrictive. Henceforth, we use Equation (4.7) to evaluate the coherence time.

4.2.3 Rayleigh Fading Simulation Model

Some characteristics of the wireless channels have been introduced in the previous section. In this section, we introduce some recognized models to simulate the Rayleigh flat fading channels.

The statistical characteristics of the fields and signals in the reception of radio frequencies by a moving vehicle are deduced from a scattering propagation model. It is worthwhile to note that a such model is termed scattered and incoherent field, since the energy arrives at the receiver by way of a number of indirect paths, with random phases.

A close approximation of attenuation due to multipath fading in wireless channels can be done by Rayleigh fading. Rayleigh fading is a reasonable model when there are many objects in the environment that scatter the radio signal before it reaches the receiver. One of the first Rayleigh fading models was introduced by Clarke [75]. This model has been considered as a reference model in the literature that mainly proposed extensions of this model. In the following, we briefly describe Clarke [75], Jakes [76] and Pätzold [77] models.

Reference model

Clarke's reference model [75] assumes that, at any point, the received field is made up of K waves, with the same amplitude E_0 , and that the corresponding angles of arrival (α_k) occur at random for different positions of the receiver, and whose phases (ϕ_k) are completely

random throughout 0 to 2π . The phase and angle of arrival of each wave are assumed to be statistically independent.

Assuming that the total received field $\mu(t)$, at any receiving point, is composed of the superposition of the K received waves, it can be expressed as [75]:

$$\mu(t) = E_0 \sum_{k=1}^K \Gamma_k \exp[j(\omega_d t \cos \alpha_k + \phi_k)], \quad (4.9)$$

where Γ_k is the random path gain of the k -th wave, and $\omega_d = 2\pi f_D$ is the maximum radian Doppler frequency (occurring when $\alpha_k = 0$).

Therefore, assuming that Γ_k is real valued, Equation (4.9) can be written as a sum of in-phase ($\mu_I(t)$) and quadrature phase ($\mu_Q(t)$) components:

$$\begin{aligned} \mu(t) &= \mu_I(t) + j\mu_Q(t), \\ \mu_I(t) &= E_0 \sum_{k=1}^K \Gamma_k \cos(\omega_d t \cos \alpha_k + \phi_k), \\ \mu_Q(t) &= E_0 \sum_{k=1}^K \Gamma_k \sin(\omega_d t \cos \alpha_k + \phi_k). \end{aligned} \quad (4.10)$$

Jakes model

One of the most famous fading channel models was proposed by Jakes [76]. Based on Clarke's model, Jakes derived his well-known simulation model for Rayleigh fading channels by assuming that the K waves, emerging from scatterers, arrive at a moving receiver with uniformly distributed arrival angles (see Figure 4.1), and with the same phase. Thus, Jakes model assumes for k -th wave ($k = 1, 2, \dots, K$):

$$\begin{aligned} \Gamma_k &= \frac{1}{\sqrt{K}}, \\ \alpha_k &= \frac{2\pi k}{K}, \\ \phi_k &= 0. \end{aligned} \quad (4.11)$$

Furthermore, Jakes chooses K of the form $K = 4M + 2$, so that the number of distinct Doppler frequency shifts is reduced from K to $M + 1$. Thus, the fading waveform may be generated through the use of $M + 1$ complex low-frequency oscillators. Hence, Equation 4.10

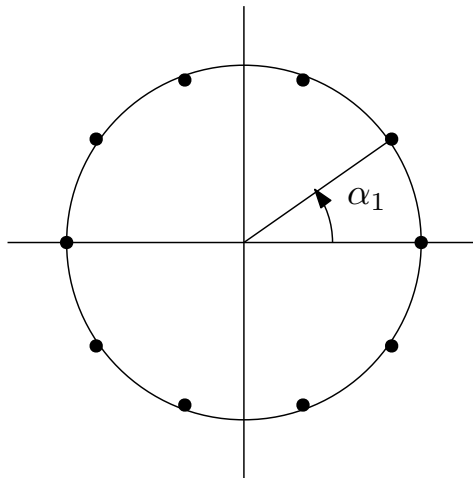


Figure 4.1 Wave's arrival angles in Jakes model.

is written, for Jakes model, as follows:

$$\begin{aligned}
 \tilde{\mu}(t) &= \tilde{\mu}_I(t) + j\tilde{\mu}_Q(t), \\
 \tilde{\mu}_I(t) &= \frac{2}{\sqrt{K}} \sum_{m=0}^M a_m \cos(\omega_m t), \\
 \tilde{\mu}_Q(t) &= \frac{2}{\sqrt{K}} \sum_{m=0}^M b_m \cos(\omega_m t),
 \end{aligned} \tag{4.12}$$

where:

$$\begin{aligned}
 a_m &= \begin{cases} \sqrt{2} \cos \beta_0, & m=0 \\ 2 \cos \beta_m, & m=1, \dots, M \end{cases} \\
 b_m &= \begin{cases} \sqrt{2} \sin \beta_0, & m=0 \\ 2 \sin \beta_m, & m=1, \dots, M \end{cases} \\
 \beta_m &= \begin{cases} \frac{\pi}{4}, & m=0 \\ \frac{\pi m}{M}, & m=1, \dots, M \end{cases} \\
 \omega_m &= \begin{cases} \omega_d, & m=0 \\ \omega_d \cos \frac{2\pi m}{K}, & m=1, \dots, M \end{cases}
 \end{aligned}$$

Pätzold model

Although Jakes channel simulator is widely used, it has some undesirable properties, e.g., the simplified relationships forced in Jakes model make this simulation model deterministic and stationary. Thus, various modifications of Jakes simulator have been proposed [78–81]. In [77], Pätzold et al. proposed a generalized method of exact Doppler spread, and introduced a closed form of the model parameters, which fulfills the main requirements imposed by the reference model.

In this model, the received field over a path at the receiver is made of the superposition of several sinusoids, each with an amplitude, a phase and an angle of arrival. Compared to Jakes model, Pätzold's model ignored the problem of non-zero cross-correlation function of the inphase and quadrature components of the generated complex waveforms. Moreover, each path k is modeled using multiple sinusoids. More specifically, the received field from the k -th path ($k = 1, 2, \dots, K$), in Pätzold model, is expressed as:

$$\begin{aligned}\mu_k(t) &= \mu_{I,k}(t) + j\mu_{Q,k}(t) \\ \mu_{I,k}(t) &= \sqrt{\frac{2}{M_k}} \sum_{m=1}^{M_k} \cos(2\pi f_{I,m,k}t + \phi_{I,m,k}), \\ \mu_{Q,k}(t) &= \sqrt{\frac{2}{M_k}} \sum_{m=1}^{M_k} \cos(2\pi f_{Q,m,k}t + \phi_{Q,m,k}),\end{aligned}\quad (4.13)$$

where M_k specifies the number of sinusoids used to model the k -th path; $\phi_{I,m,k}$ and $\phi_{Q,m,k}$ refer to the phase of the m -th components of $\mu_{I,k}(t)$ and $\mu_{Q,k}(t)$ respectively and are independently and identically distributed random variables having a uniform distribution over $[0; 2\pi]$; $f_{I,m,k}$ and $f_{Q,m,k}$ are the discrete Doppler frequencies of the in-phase and quadrature components respectively, calculated for each component within a single path, and are given by:

$$\begin{aligned}f_{I,m,k} &= f_D \cos\left[\frac{\pi}{2M_k}\left(m - \frac{1}{2}\right) + \frac{\pi}{4M_k} \cdot \frac{k}{K+2}\right], \\ f_{Q,m,k} &= f_D \cos\left[\frac{\pi}{2M_k}\left(m - \frac{1}{2}\right) - \frac{\pi}{4M_k} \cdot \frac{k}{K+2}\right].\end{aligned}\quad (4.14)$$

Simulation Model

In order to simulate the Rayleigh channel, we use the function `rayleighchan` from Matlab. This function implements the methodology described in [72] for discrete multi-path. In a nutshell, a discrete multi-path channel model is used, in which the input $\{s_i\}$ is supposed

to be band limited and the output can be written as:

$$y_i = \sum_{n=-N}^N s_{i-n} h_n, \quad (4.15)$$

where

$$h_n = \sum_{k=1}^K \check{\Omega}_k \text{sinc} \left[\frac{\tau_k}{T_S} - n \right] \quad (4.16)$$

is the tap weight, $\check{\Omega}_k$ and τ_k are the path-gain and the delay of the k -th path respectively, and T_S is the sampling period.

Now path-gains $\check{\Omega}_k$ are obtained using Pätzold model. From this process, the path-gain is obtained by scaling the result with the average path-gain:

$$\check{\Omega}_k = \sqrt{E(|\check{\Omega}_k|^2)} \mu_k. \quad (4.17)$$

4.2.4 System Level Model

For system level simulations, we adopt the model introduced in Section 2.2. Recall that we consider the downlink of a cellular network with omnidirectional Base Stations (BSs) implementing either MBSFN or SC-PTM transmissions. Moreover, the SINR with SC-PTM is computed as for a unicast transmission. With MBSFN all stations from the MBSFN area emit useful signal, whereas all stations outside this area contribute to interference. The ISI caused by delays exceeding the Cyclic Prefix (CP) is taken into account. Channel model includes distance dependent path-loss and log-normal shadowing.

4.3 Link Level Abstraction

At link level, we adopt a simplified methodology to allow us obtaining very quick results for various scenarios compared to the simulation of a complete transmitter-receiver chain.

4.3.1 Overall Architecture

The overall architecture is shown in Figure 4.2. On the left hand side, we use an existing link level simulator, e.g., the Matlab LTE Toolbox [82] or the Vienna LTE Simulator [83]. We generate a BLER vs. SNR curve in Additive White Gaussian Noise (AWGN) for a given set of input parameters including e.g. the Modulation and Coding Scheme (MCS), number of antennas, bandwidth, etc. This curve is an input of our simulator (right hand side of

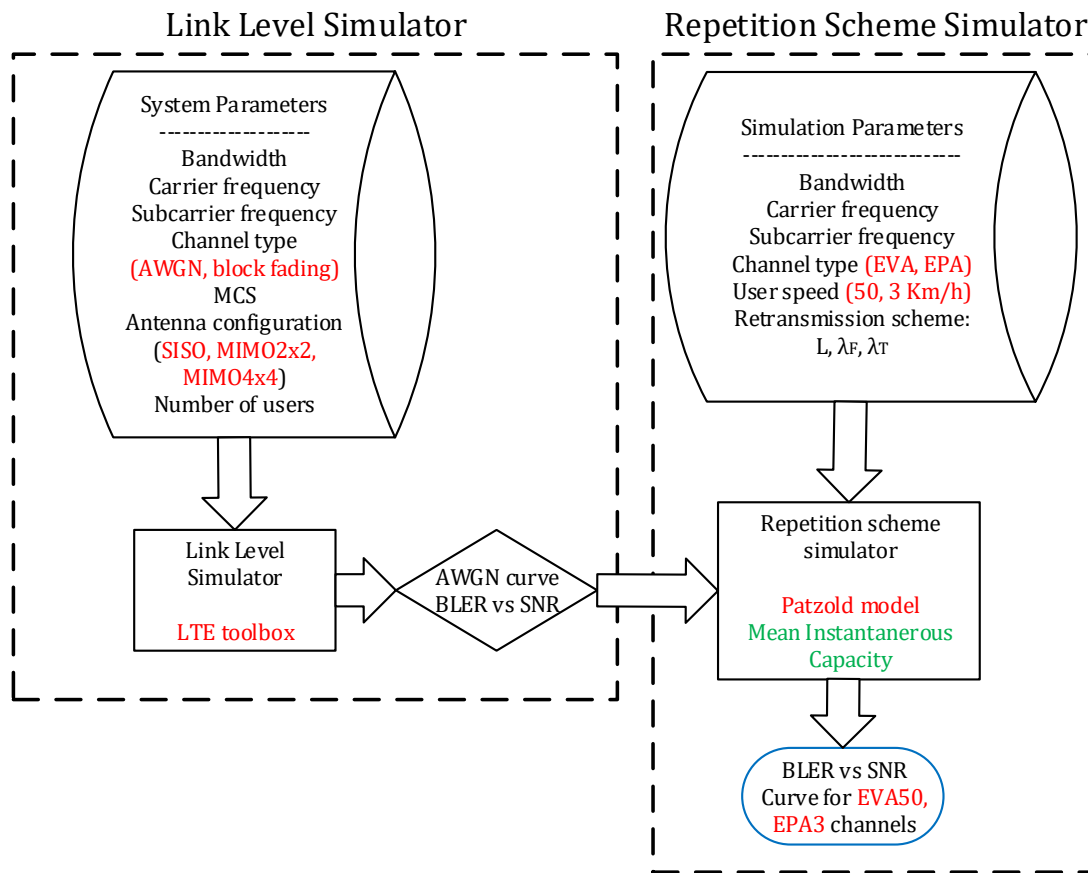


Figure 4.2 Link Level Methodology.

the figure) together with the Rayleigh fading channel to be simulated and the repetition scheme we aim to evaluate.

The repetition scheme simulator generates a fading channel according to the method described in Section 4.2.3, computes the effective SNR and evaluate the BLER for every RB thanks to the BLER vs. SNR curve in AWGN. This approach allows to quickly test various repetition schemes on various channels and speeds. One point on the BLER vs. SNR curve is obtained in few minutes compared to possibly several hours with a complete link level simulator (on a Mac Book Pro 2.6GHz Intel Core i5).

4.3.2 Effective SNR

In order to evaluate the radio link quality over a RB j of N_{sc} subcarriers and N_{sym} OFDM symbols, we adopt the Mean Instantaneous Capacity (MIC) approach. Other similar link layer abstractions exist, such as Exponential Effective SNR Mapping (EESM) (see e.g. [84]), but MIC has the advantage to be simple, to have an information theoretical interpretation and still provide good results [85].

Exponential Effective SNR Mapping (EESM)

The EESM technique is used for performance evaluation of multi-carrier systems, in order to map the instantaneous channel state, such as the instantaneous SNR (γ_n) of each subcarrier in OFDM, to an instantaneous effective SNR (γ_{eff}), as follows [86, 87]:

$$\gamma_{eff} = -\beta \ln \left(\frac{1}{N_{sc}} \sum_{n=1}^{N_{sc}} e^{-\frac{\gamma_n}{\beta}} \right) \quad (4.18)$$

where β is a parameter that must be optimized from link-level simulation results based on MCS. β is independent of the channel type.

Mean Instantaneous Capacity (MIC)

The first step in this method is to determine the instantaneous capacity of the n -th subcarrier at the i -th OFDM symbol over the j -th RB using Shannon's formula:

$$C_n^{(j)}[i] = \log_2(1 + \gamma_n^{(j)}[i]), \quad (4.19)$$

where $\gamma_n^{(j)}[i]$ is the SNR experienced on subcarrier n , at symbol i of RB j . The MIC is then computed by averaging over the $N_{sc} \times N_{sym}$ Resource Elements:

$$MIC_j = \frac{1}{N_{sc} \times N_{sym}} \sum_{n=1}^{N_{sc}} \sum_{i=1}^{N_{sym}} C_n^{(j)}[i]. \quad (4.20)$$

The effective SNR is then given in terms of MIC value by [85]:

$$\gamma_{eff}^{(j)} = 2^{MIC_j} - 1. \quad (4.21)$$

4.3.3 BLER Evaluation

The effective SNR is now mapped to BLER versus SNR curves in AWGN to estimate the BLER of the transmitted block, i.e., the probability that this block is erroneous. More specifically, a $BLER_j$ is associated to RB j as follows:

$$BLER_j = BLER_{AWGN}(\gamma_{eff}^{(j)}), \quad (4.22)$$

where $BLER_{AWGN}$ represents the BLER vs. SNR curve for the AWGN channel, obtained by link level simulator.

4.4 Repetition Scheme

In this section, we present our repetition scheme justified by design principles.

4.4.1 Design Principles

The way repetitions are performed depends on the channel characteristics introduced in Section 4.2.2 and video constraints.

Coherence Bandwidth

In order to achieve a maximum diversity, it is desirable that repetitions occur in frequency at a distance greater than the coherence bandwidth. PMR mission-critical networks are expected to be operated in 5 MHz bandwidth, which gives an upper limit for frequency separation between two repetitions. In Table 4.1, we provide some examples of coherence bandwidths for some typical multi-path fading environments, deduced from the corresponding power delay profile [88]. We note that the evaluated coherence bandwidth, in terms of number of Resource Blocks (RBs), assumes a RB bandwidth of 180 kHz.

Multi-path propagation channel	Coherence Bandwidth (B_C)	
Extended Pedestrian A (EPA)	4.6 MHz	≈ 23 RBs
Extended Vehicular A (EVA)	540 kHz	3 RBs
Extended Typical Urban (ETU)	200 kHz	≈ 1 RB

Table 4.1 Coherence Bandwidth of typical multi-path fading channels.

Coherence Time

It is desirable to perform repetitions beyond the coherence time of the channel. However, as the number of repetitions increases, delay increases as well. In video traffic, there is an upper limit beyond which this delay becomes unacceptable. PMR networks operate at 700 MHz, thus, we can deduce the coherence time for typical User Equipment (UE) speeds, see Table 4.2.

UE speed	3 km/h	50 km/h	120 km/h
Coherence Time (T_c)	514 ms	31 ms	1.3 ms

Table 4.2 Coherence time of typical PMR UE speed.

Video Quality Constraints

Group calls for mission-critical communications are subject to video quality constraints. Several approaches have been proposed to predict the video Quality of Experience (QoE) through objective video quality metrics with the goal of not relying on human evaluations. Peak Signal to Noise Ratio (PSNR) of the decoder luminance reconstruction [89] and the Structural SIMilarity (SSIM) [90] are such examples.

However, to keep things simple, we retain in this chapter only the constraints on the BLER and the average delay between two frames. A more accurate evaluation of the video quality is left for further work. In [91], Solera et al. use an emulator to evaluate video services over Long Term Evolution (LTE) networks and assume a fixed target BLER of 10%. Moreover, in [92], the PSNR is evaluated in terms of BLER, and the system performance is studied for a target BLER of 10%. Based on these references, we adopt this constraint for the BLER.

A typical video codec over wireless is H264 Level 1.2 with 320x240 resolution, maximum transmission rate of 384 kbps, and frame rate of 20 fps. In order to receive all retransmitted copies of a given frame before the transmission of the next one, the maximum transmission time of each frame shouldn't thus exceed 50 ms. The maximum intra-frame period allowed is then $50/(L - 1)$ ms when L transmissions are performed. This gives us an upper bound on the delay between two repetitions, e.g., 16 ms when $L = 4$.

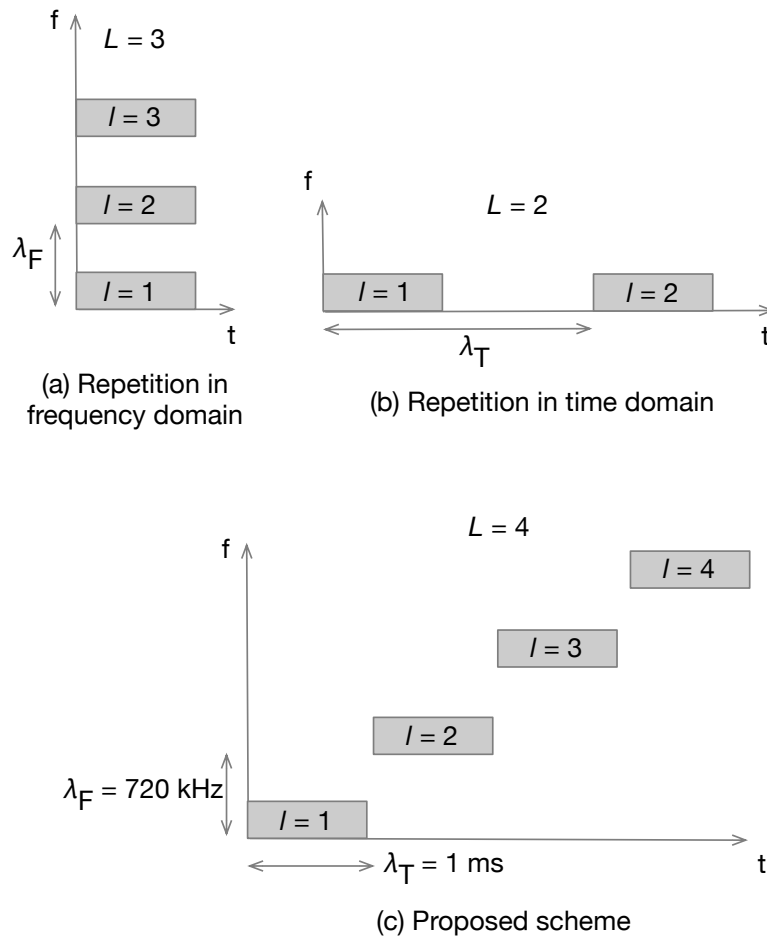


Figure 4.3 Repetition Schemes.

4.4.2 Proposed Scheme

A repetition scheme is characterized by the triplet $(L, \lambda_F, \lambda_T)$, where L is the number of repetitions, λ_T is the time delay and λ_F the frequency hopping step between two consecutive repetitions. Figures 4.3a and 4.3b show two such schemes where only the frequency or the time degrees of freedom are exploited respectively.

Owing to the design principles described above and the simulation results, the proposed scheme adopt $L = 4$, $\lambda_F = 720 \text{ kHz}$ (4 RBs) and $\lambda_T = 1 \text{ ms}$ (1 TTI) for EVA50 channel and Single Input Single Output (SISO), see Figure 4.3c. As shown in the simulation results, $L = 4$ offers a good trade-off between coverage and capacity. The choice of λ_F (1 RB above the coherence bandwidth) provides significant diversity gains with the channel EVA50, i.e., for mission-critical communications deployed in an urban environment. It also allows an easy multiplexing of the group calls within the 25 RBs by cyclically shifting in frequency

the next transmission while never violating the 4 RBs distance. The choice of λ_T ensures that the delay constraint is met. It doesn't provide much more gain compared to $\lambda_T = 0$ but allows the application of the scheme on the uplink as well. Indeed, a UE can then concentrate its transmit power on every transmissions, while with $\lambda_T = 0$ it would have shared its power between transmitted RBs. Higher uplink coverage is thus expected with the proposed delay.

We note that for a 5 MHz OFDM channel, we can say that 10 RBs is an upper limit for λ_F . Indeed, going beyond this value may leads to an inefficient scheme in terms of frequency diversity. As an example, let consider a repetition scheme with $L = 4$ and $\lambda_F = 13$ RBs; in such scheme, third and fourth transmissions will be performed on similar RBs with those used in first and second transmissions, in terms of channel gains.

Figure 4.3c shows the block grid for a repetition scheme with time delay $\lambda_T = 1$ ms and a frequency hopping step $\lambda_F = 720$ kHz (4 RBs). Each RB consists of 12 subcarriers and 12 symbols. For each subcarrier, the mean path gain is computed over the samples of the i -th OFDM symbol, and the values are stored in an array $\Omega_{n,l}[i]$ at the l -th transmission over the n -th subcarrier (step 9 of Algorithm 1).

After L transmissions and for the average SNR (snr) in range $[SNR_{min}; SNR_{max}]$, the SNR at the receiver ($\gamma_n[i]$) is given by the following:

$$\gamma_n[i] = \sum_{l=1}^L \Omega_{n,l}[i] \times snr. \quad (4.23)$$

The proposed scheme is summarized in Algorithm 1, and the parameters are defined in Table 4.3.

Variables	Description
L	Number of transmissions
N_{RB}	Number of simulated RBs
N_{sc}	Number of subcarriers in a RB
N_{sym}	Number of symbols per scheduled block
N_{sam}	Number of samples in a symbol
λ_T	Time interval between consecutive blocks
λ_F	Frequency hopping between consecutive retransmitted blocks

Table 4.3 Repetition algorithm variables.

Algorithm 1: Repetition Scheme Algorithm.

```

1: Input: BLER vs. SNR AWGN curve ( $BLE_{AWGN}$ ), channel type,  $\lambda_F, \lambda_T, L, W, f_c$ ,
   subcarrier frequency  $\Delta f, N_{sc}, N_{sym}, N_{sam}, \nu$ , SNR range ( $[SNR_{min}; SNR_{max}]$ ).
2: Output: Estimated BLER for each SNR value.
3:  $\Omega \leftarrow \text{rayleighchan}(W, f_c, \Delta f, \nu)$ : generate channel path-gains  $\Omega(N_{sc}; N_{sam} \times N_{sym})$ 
   using rayleighchan Matlab function.
4: for  $snr \in [SNR_{min}; SNR_{max}]$  do
5:   for  $j = 1$  to  $N_{RB}$  do
6:     for  $n = 1$  to  $N_{sc}$  do
7:       for  $i = 1$  to  $N_{sym}$  do
8:         for  $l = 1$  to  $L$  do
9:            $\Omega_{n,l}[i] \leftarrow \text{mean}(\Omega(n + \lambda_F(l-1); 1 + [i + \lambda_T(l-1) - 1]N_{sam} : [i + \lambda_T(l-1)]N_{sam} - 1))$ 
10:        end for
11:        $\gamma_n[i] \leftarrow \sum_{l=1}^L \Omega_{n,l}[i] \times snr$ 
12:        $C_n[i] \leftarrow \log_2(1 + \gamma_n[i])$ 
13:     end for
14:   end for
15:    $C \leftarrow \text{mean}_{n,i}(C_n[i])$ 
16:    $MIC \leftarrow \text{mean}(\log_2(1 + C))$ 
17:    $\gamma_{eff} \leftarrow 2^{MIC} - 1$ 
18:    $BLE_j(snr) \leftarrow BLE_{AWGN}(\gamma_{eff})$ 
19: end for
20:  $BLE(snr) \leftarrow \text{mean}(BLE_j(snr))$ 
21: end for

```

4.5 Simulation Results

In this section, we present the evaluation results of the proposed repetition scheme.

4.5.1 Simulation Parameters

Simulation parameters are summarized in Table 4.4. We use typical parameters for PMR networks, e.g., a carrier frequency of 700 MHz, a bandwidth of 5 MHz, and for MBSFN, e.g., a fixed robust MCS and extended cyclic prefix. We use typical parameters for PMR networks shown in Table 4.4.

Parameter	Assumption
Carrier frequency (f_c)	700 MHz
Duplex mode	Frequency Division Duplex (FDD)
Channel Bandwidth (W)	5 MHz
Sampling frequency	7.68 MHz
Nb. of subcarriers per RB (N_{sc})	12 subcarriers
Nb. of OFDM symbols (N_{sym})	12 symbols
Number of simulated frames	1000 frames
Modulation and coding scheme	MCS 2 [55, Table 7.1.7.1-1A]
Fast Fourier Transform size	512
Subcarrier bandwidth (Δf)	15 kHz

Table 4.4 Link Level simulation parameters.

In a first stage, the repetition scheme is evaluated for an EVA multipath channel for a group of users moving at 50 km/h (EVA50 channel), assuming SISO antenna configuration. Then, we validate the evaluated gains for another channel type (EPA3), as well as different Multiple Input Multiple Output (MIMO) antenna configurations².

4.5.2 Validation of the Link Level Abstraction

Figure 4.4 shows the comparison between the link level abstraction and link level simulations for SISO and EVA50. Link level simulations have been obtained with the Matlab LTE toolbox and with the LTE Vienna simulator assuming EVA50 channel. Link level abstraction curves have been obtained using the methodology presented in Section 4.3 that relies on AWGN curves and MIC. We see that curves deviates for BLERs lower than 10^{-2} but match well at the target BLER of 10^{-1} we are studying.

Matlab LTE Toolbox is used to generate other AWGN curves (BLER vs. SNR). Figure 4.5a shows a comparison between the AWGN performance using SISO, MIMO 2x2, MIMO 4x2 and MIMO 4x4.

An increased gain is observed by using MIMO 2x2 and MIMO 4x4 respectively, while a similar gain is observed for MIMO 2x2 and MIMO 4x2. Figure 4.5b shows the comparison between the link level performance obtained with Matlab LTE Toolbox for SISO, MIMO 2x2 and MIMO 4x2 assuming EVA50 channel. A gain of 2 dB is observed for MIMO 2x2 compared to SISO, while a similar performance is observed for both 2x2 and 4x2 MIMO configurations at the target BLER of 10^{-1} . As a consequence, we ignore MIMO 4x2 configuration in our evaluations.

²I would like to thank Dima Al Tabbal for her help in simulating the proposed scheme in MIMO and EPA environments.

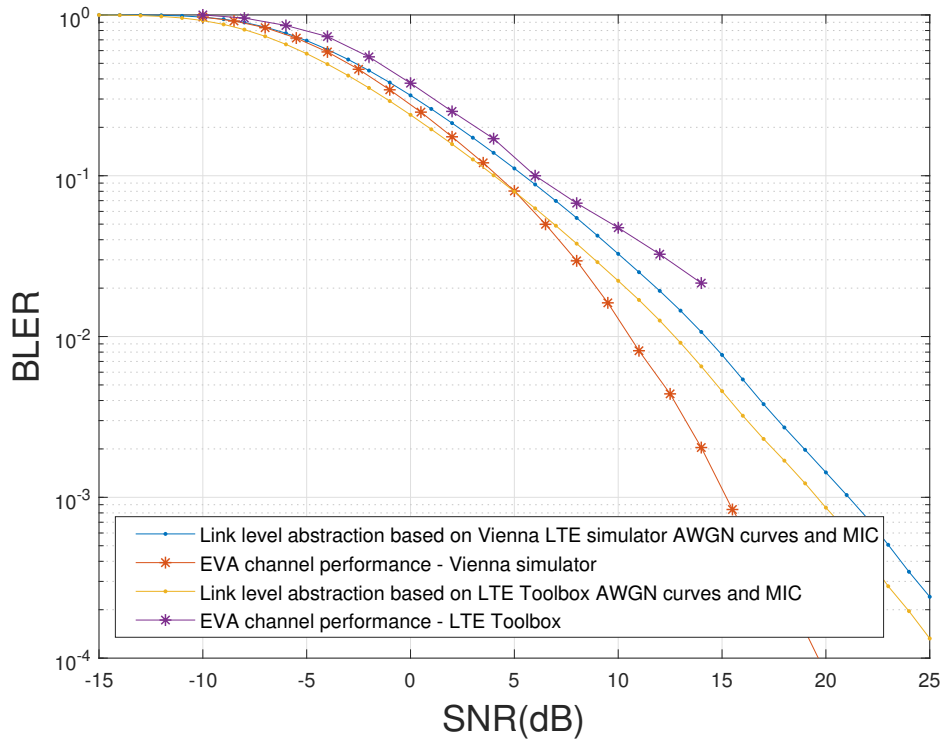


Figure 4.4 Comparison between link level abstraction and link level simulations using Matlab LTE Toolbox or Vienna LTE simulator.

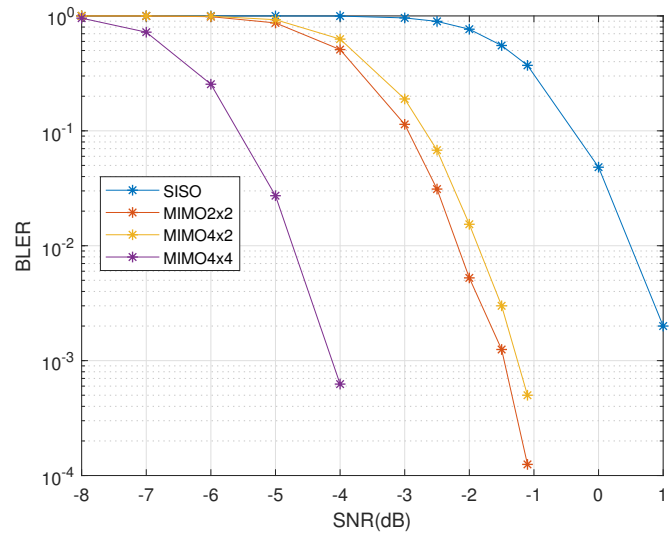
4.5.3 Repetition Scheme Results for EVA50 channel

In this section, we focus on the EVA50 channel. We start with a reference scenario, which is SISO, and then compare it to MIMO transmit diversity schemes.

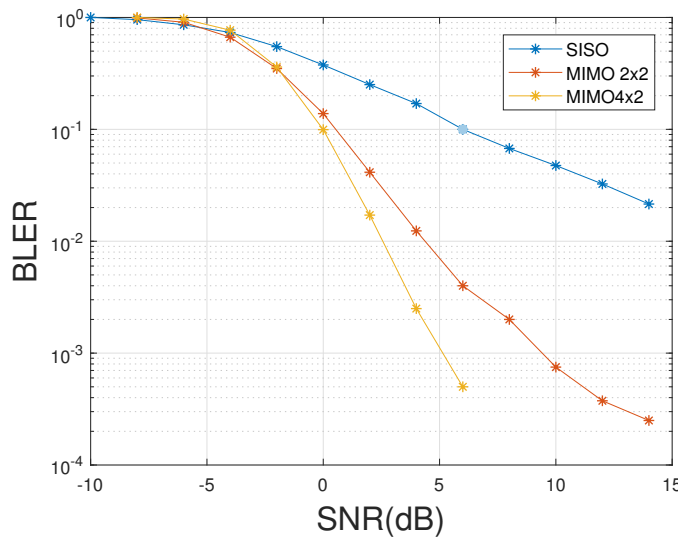
SISO case

In Figure 4.6, we show the performance of different repetition schemes characterized by different number of repetitions (L), time delays (λ_T) and frequency hopping steps (λ_F). In Figure 4.6a, when $\lambda_F = 0$ and $\lambda_T = 1$ ms, a constant gain is observed for every L when the SNR increases. Gains of 3, 5 and 6 dB are observed for $L = 2, 3$, and 4 respectively over $L = 1$. This is due to the increase of received power at the receiver.

When either λ_F or λ_T are increased, a diversity gain is also observed, especially when these parameters are larger than the coherence bandwidth and time, respectively. As expected, best performances are achieved when $\lambda_F = 720$ kHz and $\lambda_T = 16$ ms. By comparing the left and right sides of Figure 4.6, we however see that frequency diversity has more impact than time diversity with the chosen values.



(a) AWGN



(b) EVA50

Figure 4.5 Link Level Simulations using Matlab LTE Toolbox.

This is confirmed by Figure 4.7, which shows the SNR threshold required to reach the BLER target of 10^{-1} as a function of the number of repetitions L for different repetition schemes. It is clear that increasing the frequency distance between repetitions is much more effective than increasing the delay. Moreover, when $\lambda_F = 720 \text{ kHz}$ is chosen, increasing the delay has a negligible impact. The reason lies in the delay constraint that prevents us to fully benefit from time diversity. Considering higher values of L would lead to small SNR gains at the cost of a loss of capacity. With the proposed scheme ($L = 4, \lambda_F = 720 \text{ kHz}$

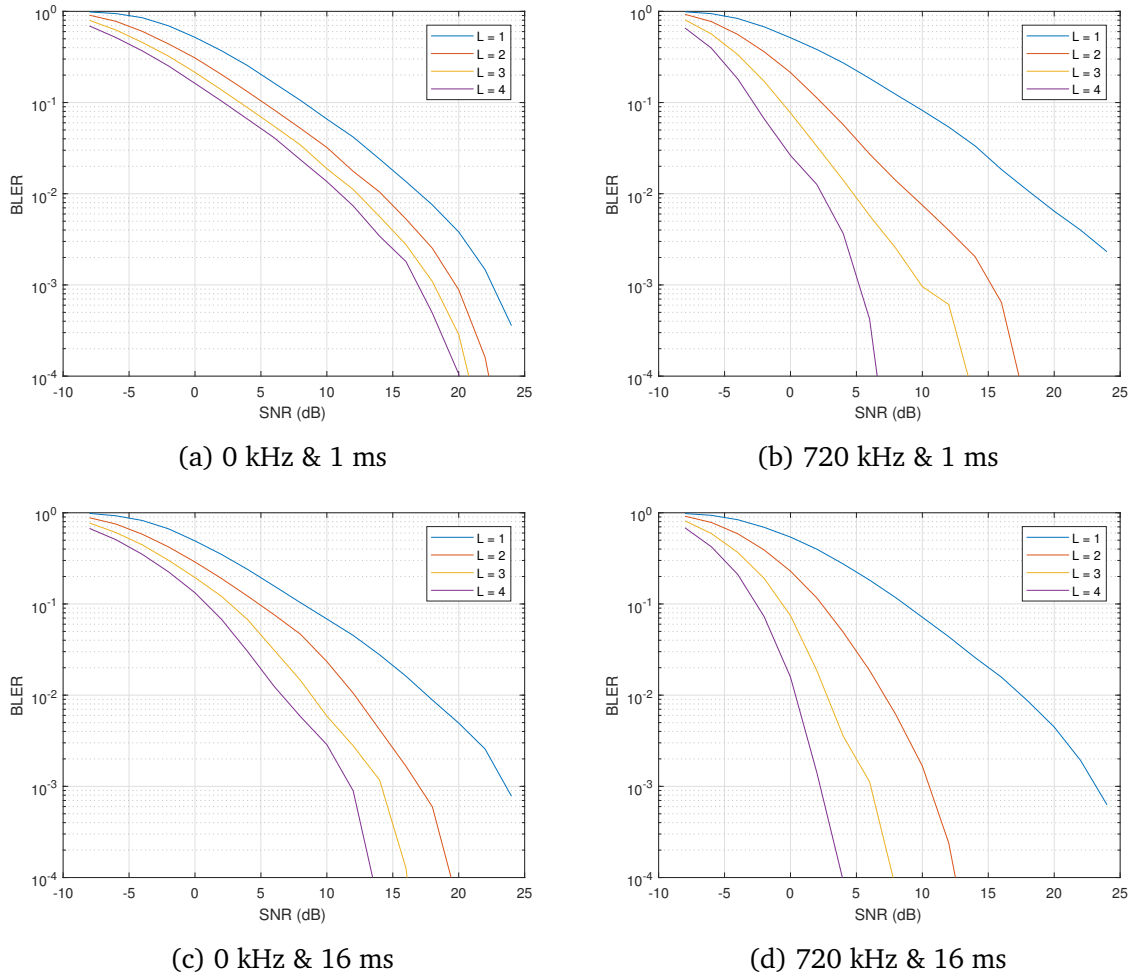


Figure 4.6 BLER vs. SNR for various frequency hopping steps and time delays and for $L = 1, 2, 3,$ and 4 repetitions for EVA50 channel, SISO case.

and $\lambda_T = 1$ ms), we have a 11 dB gain compared to $L = 1$ (today's scheme in MBSFN), 4.5 dB gain over consecutive repetitions ($L = 4, \lambda_F = 0$ and $\lambda_T = 1$ ms) and 3 dB gain over repetitions solely in time ($L = 4, \lambda_F = 0$ and $\lambda_T = 16$ ms, the maximum delay allowed by the video codec).

MIMO Case

The performance of the proposed repetition scheme is evaluated under various MIMO antenna configurations, assuming EVA50 channel. We compare the performance of different repetition schemes assuming similar parameters to those used in SISO case.

Figure 4.8 shows the performance of different repetition schemes characterized by the triplet $(L, \lambda_F, \lambda_T)$ for MIMO 2x2 configuration. The simulations of MIMO 2x2 and

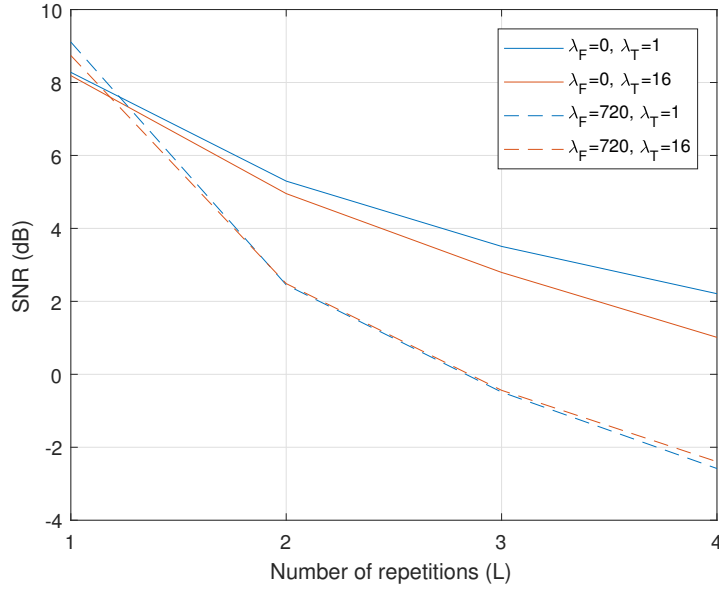


Figure 4.7 SNR thresholds for different repetition schemes at target $BLER = 10^{-1}$ for SISO case and EVA50 channel (λ_F in kHz and λ_T in ms).

4x4 configuration show similar gains with those obtained in SISO case, when comparing the different schemes with the reference one ($L = 1$). Also, frequency diversity provides significant gains compared to time diversity.

We note that our tests for different values of frequency hopping between repetitions, e.g. $\lambda_F = 1080$ kHz, 1440 kHz and 1800 kHz, show that similar gains are achieved over the scheme assuming $\lambda_F = 720$ kHz (see Figure 4.9). Moreover, the simulations show that increasing the number of repetitions to $L = 6$ improves the SNR threshold by 2 dB, at the cost of a 50% loss in the system capacity, compared to a scheme with $L = 4$.

Figure 4.10 summarizes the SNR thresholds required to reach the BLER target of 10^{-1} for SISO, MIMO 2x2 and MIMO 4x4 configurations. Compared to a scheme without repetitions ($L = 1$), we show that an approximately 11 dB gain can be achieved with the proposed scheme for each antenna configuration.

4.5.4 Validation of Repetition Scheme Results for EPA3 channel

As aforementioned, in video traffic, there is an upper bound on the delay between consecutive repetitions, which is 16 ms for $L = 4$ (see Section 4.4.1). However, in contrary to EVA50 channel case, the preferable scheme of performing repetitions beyond the coherence time and coherence bandwidth, is not possible for EPA3. Indeed, the coherence time of

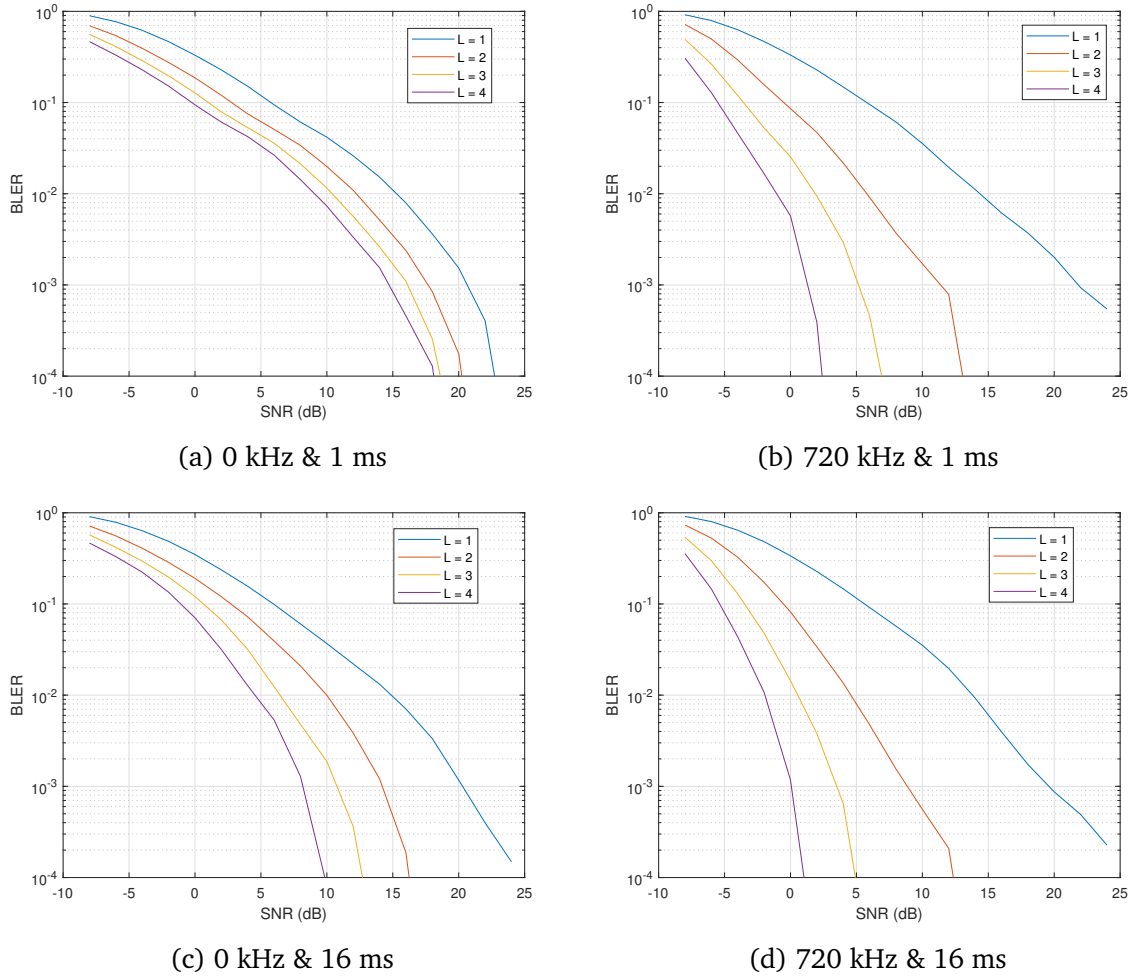
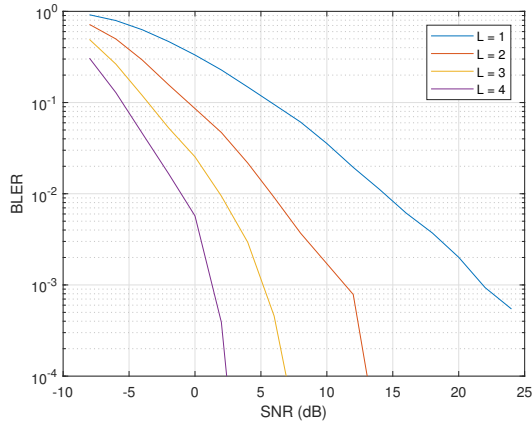


Figure 4.8 BLER vs. SNR for MIMO 2x2 with various λ_T and λ_F , and $L = 1, 2, 3$ and 4 repetitions, for EVA50 channel.

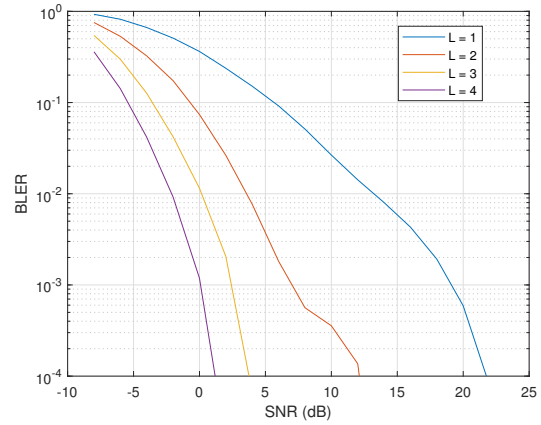
EPA3 channel is 514 ms, and its coherence bandwidth is 4.6 MHz, while the channel bandwidth for PMR networks is 5 MHz. As a consequence, we set the transmission time interval between repetitions to 16 ms, and the frequency hopping step to 1800 kHz.

Figure 4.11 shows the SNR gains of different repetition schemes with frequency diversity in case of SISO, MIMO 2x2 and MIMO 4x4 configurations. Compared to a scheme without repetitions ($L = 1$), 10 dB SNR gain is achieved with the proposed scheme ($L = 1$, $\lambda_F = 1800$ kHz and $\lambda_T = 16$ ms) in different configurations.

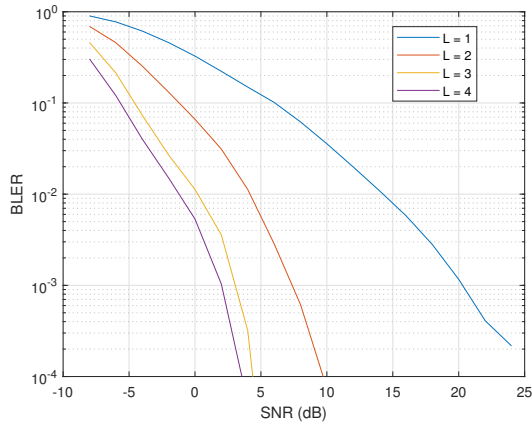
Although the EPA3 channel is much less favorable than EVA50 for repetitions, there is only a 1 dB difference between the models at the target BLER of 10^{-1} . Moreover, similarly to EVA50 case, only 2 dB gain is achieved with $L = 6$ repetitions compared to $L = 4$ in EPA3 case (see curves $\lambda_F = 1800$ kHz and $\lambda_T = 16$ ms for SISO and MIMO 2x2 configurations



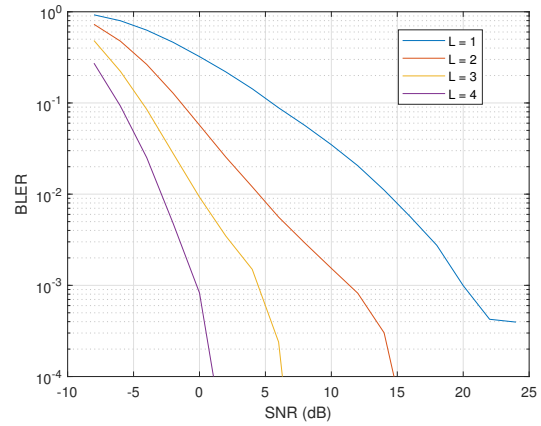
(a) 720 KHz & 1 ms



(b) 1080 KHz & 1 ms



(c) 1440 KHz & 1 ms



(d) 1800 KHz & 1 ms

Figure 4.9 BLER vs. SNR for EVA50 and MIMO 2x2 channel, with various λ_F , $\lambda_T = 1$ ms and $L = 1, 2, 3$ and 4 repetitions.

in Figure 4.11), thus, increasing the number of repetitions beyond $L = 4$ is not practical, since it provides a low coverage gain at the cost of resources waste.

4.5.5 Cell Radius Gain

In order to evaluate the cell coverage gains, we adopt the model described in Chapter 2 to estimate the achievable cell range in an urban environment for a SFN120 configuration (group members are in 1 cell, there are 2 rings of transmitting cells and there is no reserved cell), based on SNR thresholds presented in Figure 4.10 and Figure 4.11, for EVA50 and EPA3 channels, and for an outage probability of 2%. The results are summarized in Figure 4.12 and Figure 4.13 respectively. With the proposed scheme, cell radius increases

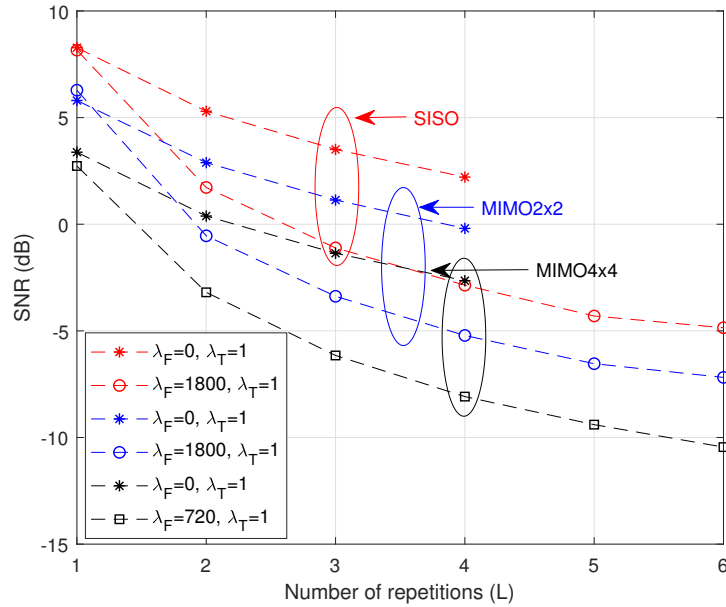


Figure 4.10 SNR thresholds for different repetition schemes at target BLER= 10^{-1} (λ_F in KHz and λ_T in ms), assuming different antenna configurations for EVA50.

significantly compared to a network without repetitions on one hand, and compared to successive repetitions ($L = 4$, $\lambda_F = 0$ and $\lambda_T = 1$ ms) on the other hand.

We note that the SISO configuration provides low performance in case of a scheme without repetitions. This is due to the low SNR levels of the reception chain obtained by Matlab LTE Toolbox.

It's worthwhile to note that the proposed scheme can be adopted for SC-PTM transmissions, since it reduces transmission delays and signalling overhead over the uplink channel for group communications, with respect to the currently adopted HARQ scheme. In Figure 4.12 and Figure 4.13, we show that SC-PTM in conjunction with our scheme can provide higher cell range than traditional MBSFN without repetition.

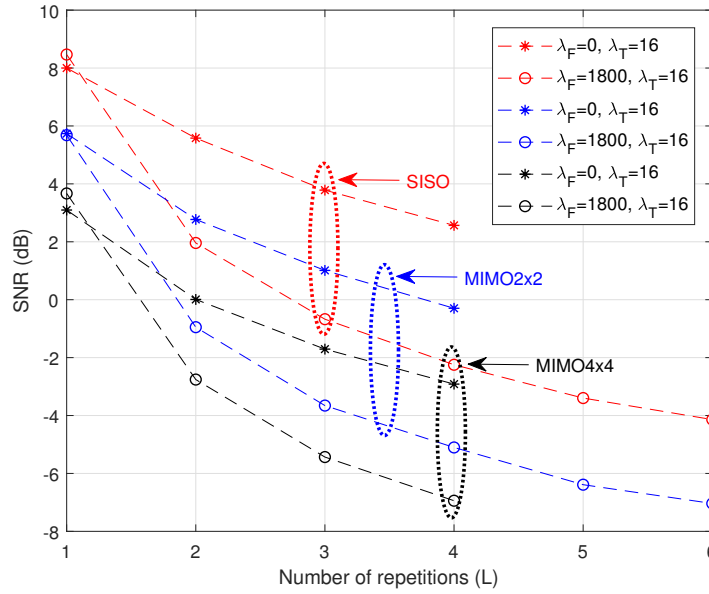


Figure 4.11 SNR thresholds for different repetition schemes at target BLER= 10^{-1} (λ_F in kHz and λ_T in ms), assuming different antenna configurations for EPA3.

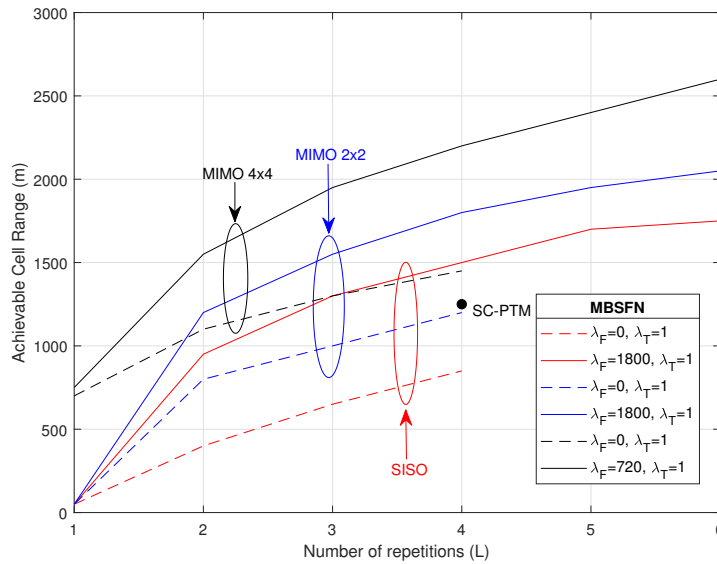


Figure 4.12 Cell range in MBSFN and SC-PTM urban networks for a target BLER= 10^{-1} and outage probability of 2% (λ_F in kHz and λ_T in ms) for EVA50 and SFN120. SC-PTM is with MIMO 4x4 and $\lambda_F = 720$ kHz.

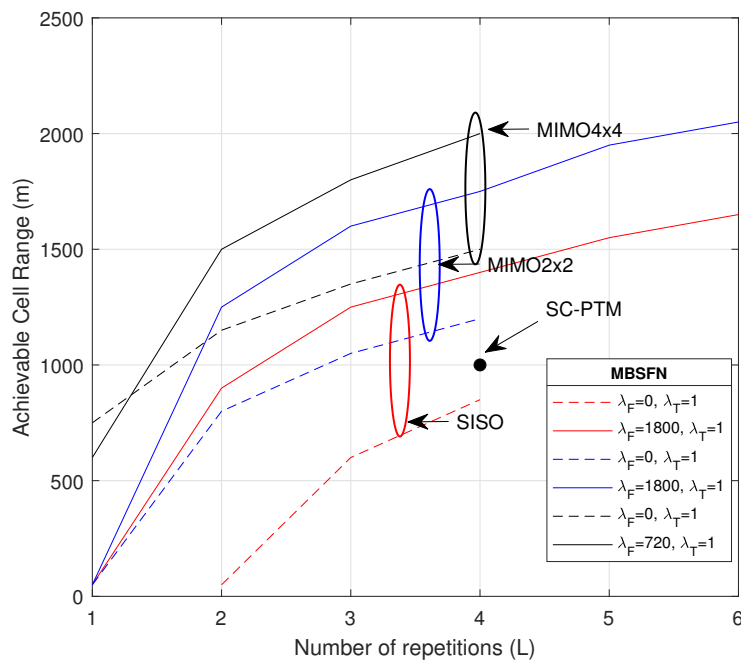


Figure 4.13 Cell range in MBSFN and SC-PTM urban networks for a target BLER= 10^{-1} and outage probability of 2% (λ_F in kHz and λ_T in ms) for EPA3 and SFN120. SC-PTM is with MIMO 4x4 and $\lambda_F = 720$ kHz.

4.6 Conclusion

In this chapter, a repetition scheme adopted for Professional Mobile Radio (PMR) networks using Multicast/Broadcast Single Frequency Network (MBSFN) and Single-Cell Point-To-Multipoint (SC-PTM) to convey group communications is proposed and evaluated in terms of Signal to Noise Ratio (SNR) and cell coverage gains. The proposed scheme takes into account the coherence bandwidth and the coherence time of the multipath fading channel together with service delay constraints. The comparison between different schemes show that frequency shifts between repetitions significantly improves the network performance, while time diversity increases transmission delay without bringing important gains for EVA50. In a less dynamic channel like EPA3, it is not possible to retransmit beyond the the coherence bandwidth and the coherence time. Nevertheless, important gains can be still achieved with the same repetition scheme as for EVA50. Multiple Input Multiple Output (MIMO) with transmit diversity brings new gains at the cost of more deployed antennas. The MIMO scheme 4x2 doesn't bring any added value compared to MIMO 2x2. Simulation results show that significant SNR gains can be achieved over classical MBSFN transmissions without repetitions. This translates in a cell range improvements in an urban environment when compared to a scheme without repetition. The proposed scheme could be adopted for next MBSFN and SC-PTM standard releases as an attractive option to increase cell coverage for mission-critical communications.

Chapter 5

A Dynamic Clustering Algorithm for Multi-Point Transmissions

Contents

5.1	Introduction	86
5.2	Model and Problem Formulation	89
5.2.1	System Model	89
5.2.2	Traffic Model and Preliminary Results	90
5.2.3	Problem Formulation	94
5.3	A Dynamic Clustering Algorithm	95
5.3.1	Main Routine	95
5.3.2	Group Call Clustering	95
5.3.3	Cell Weights Optimization	100
5.3.4	Complexity Analysis	104
5.4	Simulation Results	104
5.4.1	Simulations Settings	104
5.4.2	Group Call Multi-point Transmission	105
5.4.3	Objective Function and Blocking Probabilities	106
5.4.4	SINR Improvements	107
5.4.5	Performance Evaluation Based Minimum Group SINR	108
5.4.6	Impact of Traffic Intensity	108
5.5	Conclusion	115

5.1 Introduction

As introduced in Chapter 1, group communication based on Multimedia Broadcast/Multicast Service (MBMS) is the main service allowed by Professional Mobile Radio (PMR) networks, and thus point-to-multi-point transmission schemes are natural solutions for this service. In Chapter 2, we show that cooperation between several Base Stations (BSs) to serve a group of users helps mitigating Inter-Cell Interference (ICI), improving system throughput and cell edge performance. The New Radio Fifth Generation (5G) standard facilitates this functionality by allowing a split of the radio protocol stack of the next generation Node-B (gNB) between a central unit able to coordinate several distributed units dedicated to lower layers [93].

If all BSs of an area cooperate, we have a Multicast/Broadcast Single Frequency Network (MBSFN) transmission. As aforementioned in Chapter 1 and Chapter 2, all the BSs in an MBSFN area are synchronized and transmit the same signal over the same radio resources to all users of a group, so that the Signal to Interference plus Noise Ratio (SINR) of the users is maximized. However, radio resources can be wasted due to the transmission of data in cells where there is no group user.

Another multi-point approach, the Single-Cell Point-To-Multipoint (SC-PTM), consists in transmitting the signal only in cells that cover the group users. If several group users are located in a given cell, the Base Station (BS) uses multicast transmission to serve them. Recall that, from Chapter 2, this technique has the advantage of maximizing the capacity of the network at the price of a degraded SINR for the group users, especially those at cell edge owing to the higher ICI compared to MBSFN.

In general, there is a coverage-capacity trade-off between the full MBSFN cooperation and SC-PTM and it may be advantageous to consider *clusters* of cells cooperating using Coordinated MultiPoint (CoMP). In this chapter, we formulate a problem to capture this coverage-capacity trade-off in mission-critical networks using multi-point transmissions and we propose a dynamic clustering algorithm to solve this problem.

Related Work

Dynamic clustering in cooperative transmissions can be classified into network-centric and user-centric clustering. In the former, a set of BSs forms a cluster, and all the users attached to them are served by the cluster. While in the latter, each user may have its own cluster of coordinated BSs. Both approaches have been well studied subjects in the literature.

Greedy algorithms based approaches have been widely used in network-centric clustering algorithms, e.g. [94–98]. One of the first papers on BS clustering is presented in [94];

a greedy algorithm based on sum-rate maximization is developed. Yoon et al. focused in [95] on cell-edge users performance, and developed a greedy clustering algorithm to maximize the cooperation gain, along with an interference weight calculation algorithm to reduce complexity. A resource allocation method to improve spectral efficiency is proposed in [96], for non-overlapping dynamic clusters, derived using a greedy algorithm to distribute the users over groups served by a BS cluster. In [97], a dynamic BS clustering algorithm has been proposed based on maximizing the weighted sum rate, using a greedy iterative algorithm. This algorithm has been combined with the scheduling process and evaluated with some traffic models in [98]. However, greedy search method based clustering algorithms may not provide the optimal cluster for group communications, since the cluster must be designed based on all group users performance. We note that, for computational complexity reasons, only non-overlapping clusters are considered in these studies, in order to reduce computational complexity, which may be sub-optimal for some users.

Furthermore, dynamic user-centric clustering schemes have been investigated. In [99], the authors designed a user-centric clustering scheme which aimed at maximizing the average throughput of the network, subject to the limitations on the synchronization and backhaul capacity constraints, as well as limited number of served users per cell, using an exhaustive-search based method. Such algorithms are of exponential complexity. Garcia et al. presented in [100] a criterion to balance the cost of resource utilization and the radio quality induced by BS cooperation; this criterion penalizes in a simple way higher cluster sizes without being related to traffic characteristics. In [101], a user-centric joint clustering and scheduling for CoMP in heterogeneous networks has been modeled using game theoretic approaches, combined with graph-coloring algorithms. To account for the large number of cells in a dense network, the authors proposed a scalable algorithm and assumed a maximum cluster size. Bassoy et al. evaluated in [102] the trade-off in CoMP clustering in the aim of improving heterogeneous network load balancing. The proposed algorithm employs a user-centric clustering approach assuming a limited cluster size to maximize CoMP gains in a first stage; then, a new clustering algorithm is used to distribute traffic gradually from macro loaded cells into relatively less-loaded small cells. Such scheme increases drastically model complexity when applied to MBMS traffic. In [103], the authors study the trade-off between cooperative gain and cost in a CoMP system; a user-centric cluster size minimization problem subject to rate constraints is formulated, and a sub-gradient method is employed to solve a relaxed version of the problem, using a Lagrangian approach. This paper consider a fixed number of users and thus does not take into account traffic dynamics.

Although user-centric approaches proposed in the literature offer more flexibility compared to network-centric schemes, they are not adapted to group calls. Moreover, existing clustering algorithms mainly focus on the physical data rate improvement, without investigating traffic dynamics constraints to address the trade-off involved by the cluster size, e.g. [94–100]. Besides, many proposed models, such that [94–97, 101, 102], are limited by a fixed or maximal cluster size, which may not be optimal for some groups, especially in case group members are distributed in many different cells.

In the literature related to MBMS, Rong et al. presented in [104] a comparison between different MBMS transmission schemes; they evaluated a dynamic MBSFN scheme which only utilizes a subset of the cells for adaptively broadcasting the signal, depending on the presence of users in the cells. An algorithm to optimize the scheduling and resource allocation for unicast User Equipments (UEs) and MBMS in a MBSFN environment has been proposed in [105]; the authors show the trade-off between improving user data rates through unicast, and improving spectrum efficiency through multicast. However, the trade-off involved by clustering is not assessed in both studies.

To the best of our knowledge, dynamic clustering of cooperative cells has thus not been studied in the literature in the context of mission-critical communications with the objective of optimizing dynamic traffic and coverage performance metrics.

Contributions

In this chapter, our contributions are the following:

- We formulate a problem to capture the coverage-capacity trade-off in mission-critical communications, where group calls are served by multiple cells using coordinated multi-point transmissions.
- We derive a Kaufman-Roberts-like formula for computing the blocking probability in every cell of a cooperative multi-point transmission scheme.
- For every group, we formulate a submodular minimization problem, in which the average SINR in the group and weights related to every selected cell are taken into account and that results in an optimal cluster of serving BSs. The traffic weight of a cell represents a cost for using the radio resources in this cell. This problem is solved using the minimum-norm algorithm. We evaluate the performance of the latter compared to a Greedy based approach, and we show that it provides accurate results.

- As group calls arrive in the system, are served and leave the system in a dynamic fashion, every cell experiences a blocking probability that depends on its traffic weight. We formulate a minimization problem, in which traffic weights are optimized in order to maintain blocking probabilities close to a target value. As the objective function involves the resolution of a Markov process, we rely in derivative-free optimization and the Nelder-Mead simplex method to solve this problem.
- We provide simulation results showing how the proposed framework outperforms the MBSFN full cooperation scheme in terms of blocking probabilities and SC-PTM in terms of coverage.

The rest of this chapter is organized as follows: in Section 5.2, we present our system model and we introduce the problem. Our dynamic clustering algorithm is presented in Section 5.3. Section 5.4 presents and discusses the simulation results and conclusions are summarized in Section 5.5.

Notations: For a finite set $V = \{1, \dots, n\}$ of n elements, we denote 2^V the set of all its subsets. Every subset S of V can be represented by a vector in $\{0, 1\}^n$ denoted $\mathbb{1}_S$, which has 1 at the positions of the elements of S and 0 elsewhere. Take now $x \in \mathbb{R}^n$, a vector of n real components. We denote x_i the component of x corresponding to the element $i \in V$. We denote also $x(S) = \sum_{i \in S} x_i = \mathbb{1}_S^T x$. A set function F is a function from 2^V to \mathbb{R} . Equivalently, we can write: $F : \{0, 1\}^V \mapsto \mathbb{R}$. We denote $\{x \geq \alpha\}$ the set $\{i \in V | x_i \geq \alpha\}$. For a collection of points of \mathbb{R}^n $S = \{q_1, \dots, q_m\}$, we denote $aff(S) = \{y \in \mathbb{R}^n | y = \sum_{i=1}^m \alpha_i q_i, \alpha_i \in \mathbb{R}\}$ the affine hull of S and $conv(S) = \{y \in \mathbb{R}^n | y = \sum_{i=1}^m \alpha_i q_i, \alpha_i \in \mathbb{R}_+\}$ the convex hull of S .

5.2 Model and Problem Formulation

In this section, we present our system model, and we introduce the clustering problem.

5.2.1 System Model

We consider the downlink of a cellular network with omni-directional BSs serving groups of UEs. We focus on a specific subset $V = \{1, \dots, n\}$ of n cells forming an MBSFN synchronization area and thus able to perform multi-point transmissions to serve group of users located in this area.

When a subset $S \subseteq V$ of BSs serves a group \mathcal{U} of users using multi-point transmissions, a time-synchronized common waveform is transmitted simultaneously from S using the same resources, to convey the common service data requested by the group of users. User

Equipment (UE) receives copies of the signal with different delays, amplitudes and phases and treat the multi-cell transmissions in the same way as multi-path components of a single-cell transmission without incurring any additional complexity. It can thus benefit from spatial diversity, increased useful signal power and reduced inter-cell interference.

The signal received from a BS $b \in S$ is part of the useful received signal, provided that the propagation delay does not exceed the cyclic prefix duration [49]. Hence, the SINR experienced by the UE u can be expressed as (see Equation (2.4)):

$$\gamma_u(S) = \frac{\sum_{b \in S} \omega_{bu} g_{bu} P_T}{\sum_{b \in S} (1 - \omega_{bu}) g_{bu} P_T + \sum_{b \notin S} P_T g_{bu} + \mathcal{N}}. \quad (5.1)$$

For a multicast group \mathcal{U} of N users served by cells in S , we define the average SINR of the group as:

$$\bar{\gamma}_{\mathcal{U}}(S) = \frac{1}{N} \sum_{u \in \mathcal{U}} \gamma_u(S). \quad (5.2)$$

If $S = V$, we say that we have a full MBSFN transmission or full cooperation of the synchronization area, this is the best choice of S for a group in terms of average SINR. If S is made of the set of best servers without cooperation, we have a SC-PTM transmission.

Figure 5.1 shows an example of such a network, where BS locations have been drawn according to a Poisson process. The set V is shown in white, while gray cells are outside the MBSFN synchronization area. A group of users is shown that is served by a subset of the cells in this area.

5.2.2 Traffic Model and Preliminary Results

We consider a dynamic traffic model, in which group of users arrive in the synchronization area, use a resource for a group call for a certain duration and leave the system. Group calls are usually video calls in mission-critical communications. We assume random Poisson arrivals with rate λ and random exponential service duration with rate μ . There are R resources available in every BS. Let $\rho = \lambda/\mu$.

When a group arrives in the system, it is served by a subset S of BSs with probability p_S and one resource is consumed in every BS in S . The way S is chosen will be detailed later on. To fix ideas, S can be the set of best servers, i.e., the BSs providing the highest power to every user in the group; or we can choose $S = V$ if we want to maximize the average SINR of the group. In general, S is chosen according to some policy balancing the radio quality and the usage of resources.

The cardinality of 2^V is $P = 2^n$. To every element of S of 2^V , we associate a unique index $s \in \{1, \dots, P\}$. For $b \in \{1, \dots, n\}$, let $\mathcal{P}_V(b) = \{s \in 2^V | b \in S\}$ be the elements of 2^V

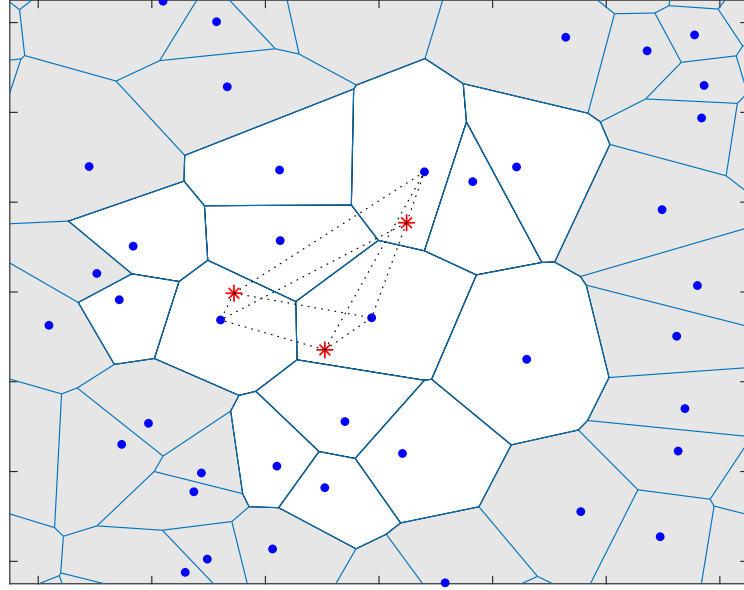


Figure 5.1 Network model: White cells are part of a MBSFN synchronization area. Cell borders are represented using Voronoi tessellation. Red stars represent UEs of a group. A (multicast) group of users is served by a cluster of cells of the synchronization area.

that contain b . The traffic model induces a continuous-time Markov chain with state space:

$$\mathcal{E} = \{(n_1, \dots, n_s, \dots, n_p) \in \mathbb{N}^P, \text{ s.t.} \\ \sum_{s \in \mathcal{P}_V(b)} n_s \leq R, b \in \{1, \dots, n\}, s \in \{1, \dots, P\}\} \quad (5.3)$$

where n_s is the number of group calls served by S . The constraint states that in any cell b , no more than R resources can be allocated. The transition rate between states x and $y \in \mathcal{E}$ is given by:

$$q(x, y) = \begin{cases} p_s \lambda & \text{if } y = x + e_s \\ x_s \mu & \text{if } y = x - e_s \\ 0 & \text{otherwise} \end{cases} \quad (5.4)$$

where $e_s = (0, \dots, 1, \dots, 0)$ with 1 at the s -th coordinate. Define $q(x, x) = -\sum_{y \neq x} q(x, y)$. Let $Q = (q(x, y))_{x, y \in \mathcal{E}}$ be the infinitesimal generator of the Markov process and $\pi(x)$ the stationary probability of being in state x , we have $\pi Q = 0$. Let $\mathcal{B}_s = \{(n_1, \dots, n_p) | \exists b \in$

s s.t. $\sum_{t \in \mathcal{O}_V(b)} n_t = R$, these are the states that are blocking for calls requiring the activation of the BSs in s because at least one station in s has already R resources occupied.

Proposition 1. *The stationary probabilities of the continuous-time Markov chain (\mathcal{E}, Q) are given by:*

$$\pi(x) = \pi(0) \frac{(p_1 \rho)^{n_1}}{n_1!} \dots \frac{(p_P \rho)^{n_P}}{n_P!}, \quad \forall x \in \mathcal{E} \quad (5.5)$$

where $\pi(0)$ is obtained by normalization.

Proof. Setting $R = \infty$, the random process is equivalent to P independent birth-and-death processes. It is thus reversible and its stationary probabilities are the product of the stationary probabilities of the independent processes. When $R < \infty$, the process is a truncation of a reversible process. Hence the result. \square

Corollary 1. *The blocking probability for a group call requiring the activation of the BSs in s is:*

$$\Pi(s) = \sum_{x \in \mathcal{B}_s} \pi(x). \quad (5.6)$$

The overall blocking probability is:

$$\Pi = \sum_{s=1}^P p_s \Pi(s). \quad (5.7)$$

We now focus on every individual cell $b \in V$ and compute the probability that this cell has R resources occupied. For $i = 1, \dots, n$, let $v_i = [v_{i1} \dots v_{iP}]^T$ be the vector such that $v_{is} = 1$ if $i \in s$ and 0 otherwise. Let $\zeta(m_1, \dots, m_n)$, $0 \leq m_i \leq R$, $\forall i$, be the function defined as follows:

$$\zeta(m_1, \dots, m_n) = \sum_{x \in \mathcal{E} | \forall i, x^T v_i = m_i} \frac{(p_1 \rho)^{n_1}}{n_1!} \dots \frac{(p_P \rho)^{n_P}}{n_P!}. \quad (5.8)$$

This is a quantity that is proportional to the joint probability that cell 1 serves m_1 calls, cell 2 serves m_2 call, ..., cell n serves m_n calls.

Lemma 1. *We have for any $m_i \neq 0$:*

$$\zeta(m_1, \dots, m_n) = \frac{1}{m_i} \sum_{j=1}^P p_j \rho v_{ij} \zeta(m_1 - v_{1j}, \dots, m_n - v_{nj}), \quad (5.9)$$

with $\zeta(0, \dots, 0) = 1$ and $\zeta(m_1, \dots, m_n) = 0$ whenever $\exists i$ s.t. $m_i < 0$.

Proposition 2. For a BS b , the probability that this station has R resources occupied is given by:

$$\tilde{\Pi}(b) = \frac{\sum_{\forall k \neq b, m_k=0, \dots, R} \zeta(m_1, \dots, m_b = R, \dots, m_n)}{\sum_{\forall k, m_k=0, \dots, R} \zeta(m_1, \dots, m_n)}, \quad (5.10)$$

where at the numerator, R is the value taken by the variable m_b .

Proof. The proofs of Lemma 1 and Proposition 2 are similar to the derivation of the Kaufman-Roberts formula for multi-Erlang-B systems [106]:

$$\begin{aligned} \zeta(m_1, \dots, m_n) &= \sum_{x \in \mathcal{E} | \forall i, x^T v_i = m_i} \frac{(p_1 \rho)^{n_1}}{n_1!} \dots \frac{(p_P \rho)^{n_P}}{n_P!} \\ &= \sum_{x \in \mathcal{E} | \forall i, x^T v_i = m_i} \frac{x^T v_i (p_1 \rho)^{n_1}}{m_i n_1!} \dots \frac{(p_P \rho)^{n_P}}{n_P!} \\ &= \frac{1}{m_i} \sum_{x \in \mathcal{E} | \forall i, x^T v_i = m_i} \sum_{j=1}^P n_j v_{ij} \frac{(p_1 \rho)^{n_1}}{n_1!} \dots \frac{(p_P \rho)^{n_P}}{n_P!} \\ &= \frac{1}{m_i} \sum_{x \in \mathcal{E} | \forall i, x^T v_i = m_i} \sum_{j=1}^P p_j \rho v_{ij} \frac{(p_1 \rho)^{n_1}}{n_1!} \dots \frac{(p_j \rho)^{n_j-1}}{(n_j-1)!} \dots \frac{(p_P \rho)^{n_P}}{n_P!} \\ &= \frac{1}{m_i} \sum_{j=1}^P p_j \rho v_{ij} \sum_{x \in \mathcal{E} | \forall i, x^T v_i = m_i} \frac{(p_1 \rho)^{n_1}}{n_1!} \dots \frac{(p_j \rho)^{n_j-1}}{(n_j-1)!} \dots \frac{(p_P \rho)^{n_P}}{n_P!} \\ &= \frac{1}{m_i} \sum_{j=1}^P p_j \rho v_{ij} \zeta(m_1 - v_{1j}, \dots, m_n - v_{nj}). \end{aligned}$$

□

With a slight abuse of vocabulary, we call this probability, *the blocking probability in station b* . It is clear that the policy for choosing S plays an important role in terms of traffic: the higher the probability for a BS b to be chosen, the higher the traffic load in this cell and the higher the probability $\tilde{\Pi}(b)$ to have no resource available for a new call.

Despite its accuracy in modeling group call performance, the blocking probability of a BS b provided in Proposition 2 has an exponential complexity, which is detrimental in large networks. Therefore, we can approximate this probability by using the Erlang-B law as follows:

$$\tilde{\Pi}(b) \approx \frac{\frac{\rho_b^R}{R!}}{\sum_{r=0}^R \frac{\rho_b^r}{r!}}, \quad (5.11)$$

where $\rho_b = \rho \sum_{s=1}^P p_s v_{bs}$ is the traffic load in cell b . Although this sum has still 2^n terms, in practice, ρ_b can be in practice measured by BS b so that the load is obtained at very low cost.

Moreover, in order to reduce complexity, the blocking probability given in Equation (5.11) can be evaluated in $O(R)$, provided that ρ_b is evaluated in $O(1)$, using the following recursive classical formula:

$$\tilde{\Pi}(b, R) \approx \frac{\rho_b \tilde{\Pi}(b, R-1)}{R + \rho_b \tilde{\Pi}(b, R-1)}, \quad (5.12)$$

and $\tilde{\Pi}(b, 0) = 1$. This equation is an approximation of (5.10) in the sense that it ignores the correlation between loads in different cells induced by group calls.

5.2.3 Problem Formulation

The clustering policy to select the set S for a given group is based on a minimization problem. Our aim is to strike a balance between the radio quality of the group, measured by its average SINR and the amount of resources used in the network to serve this group. For this, we define the weight w_b of a BS b , a free parameter that represents the cost of using resources in station b in a multi-point transmission. Our policy consists in choosing for the group \mathcal{U} a set S^* that solves the following set function minimization problem:

$$\min_{S \in \mathcal{P}_V} \Psi_{\mathcal{U}}(S) \triangleq w(S) - \bar{\gamma}_{\mathcal{U}}(S), \quad (5.13)$$

where $\Psi_{\mathcal{U}} : \mathcal{P}_V \mapsto \mathbb{R}$ is a set function balancing the cost and the radio quality, S is the set of serving BSs, $w(S) = \sum_{b \in S} w_b$ is the sum of the weights of the stations in S , and $\bar{\gamma}_{\mathcal{U}}(S)$ is the mean SINR of UEs $u \in \mathcal{U}$ when the group is served by S . By convention, we set $\Psi_{\mathcal{U}}(\emptyset) = 0$.

Clusters are formed dynamically for every group call according to the above clustering policy. For a fixed vector of weights $w \in \mathbb{R}^n$, the traffic demand together with the clustering policy induces a blocking probability $\tilde{\Pi}(b; w)$ in every cell b that we make now explicitly dependent on the weights vector. If $\tilde{\Pi}(b; w)$ is high, it is natural to increase the weight w_b because the quality of service in this cell is poor. On the contrary, if $\tilde{\Pi}(b; w)$ is very small, we can decrease its weight so that this cell is chosen with higher probability and allows to increase the SINR of the users. We thus define target blocking probabilities $\bar{\Pi}(b)$ that every cell should attain. We now formulate a second minimization problem:

$$\min_{w \in \mathbb{R}^n} G(w) \triangleq \sum_{b=1}^n \|\tilde{\Pi}(b; w) - \bar{\Pi}(b)\|^2, \quad (5.14)$$

where $G : \mathbb{R}^n \mapsto \mathbb{R}^+$ is a real valued function representing the quadratic error with respect to the targets, $\tilde{\Pi}(b; w)$ is the blocking probability of cell b when the clustering policy is applied with weights w and $\bar{\Pi}(b)$ is the target blocking probability for cell b . Therefore, our problem is resolved by finding w^* , a minimizer of G :

$$G(w^*) = \min_{w \in \mathbb{R}^n} G(w). \quad (5.15)$$

5.3 A Dynamic Clustering Algorithm

In this section, we show how the above problems are solved.

5.3.1 Main Routine

The main routine of the algorithm is shown in Algorithm 2. It is executed in a central entity for the whole synchronization area (e.g. in a Software Defined Network controller of the cellular network, e.g. the Multi-cell/multicast Coordination Entity (MCE), see Section 1.2.3) and selects a set of serving cells for every new group arrival. The algorithm proceeds by periods of duration T . During a period, the weights are fixed and T is sufficiently long in order that the Markov process of group call arrivals and departures has reached the stationary regime.

When a group call arrives at a certain time instant τ (step 5), the set of serving cells is determined by solving the optimization problem (5.13). Time is updated (step 6) and we record the number of calls during the period with the variable M (step 6). The number of group calls served by the same set of cells S is incremented (step 8). The group of users is served with S (step 9). The duration of the call is recorded with variable D (step 10).

At the end of a period (step 12), the probabilities of every subset are computed (step 14) and the load ρ is estimated (step 15). New weights are computed by solving the optimization problem (5.14) (step 16). Variables M , D , and $n_{S'}$ are reinitialized before the next period starts (step 17).

5.3.2 Group Call Clustering

In this section, we focus on the first minimization problem (5.13).

Algorithm 2: Dynamic Clustering Algorithm (executed in a central entity for the entire synchronization area)

```

1: Input:  $T, \bar{\Pi}(b) \forall b$ .
2: Output: For every group of users, a set  $S$  of cooperative serving cells.
3: Init:  $t \leftarrow 0; t' \leftarrow 0; w \leftarrow 0; \forall S' \subseteq V, n_{S'} \leftarrow 0; M \leftarrow 0; D \leftarrow 0$ 
4: while true do
5:   if a new group  $\mathcal{U}$  arrives at  $\tau$  then
6:      $t \leftarrow \tau; M \leftarrow M + 1$ 
7:      $S \leftarrow \text{Min-Norm}(\mathcal{U}, w)$ , see Algorithm 4
8:      $n_S \leftarrow n_S + 1$ 
9:     Serve group  $\mathcal{U}$  with  $S$ .
10:     $D \leftarrow D + \text{duration of this call}$ 
11:   end if
12:   if  $|t - t'| \geq T$  then
13:      $t' \leftarrow t$ 
14:      $\forall S' \subseteq V, p_{S'} \leftarrow \frac{1}{M} n_S$ 
15:      $\lambda \leftarrow \frac{M}{|t - t'|}; \mu \leftarrow \frac{M}{D}; \rho \leftarrow \frac{\lambda}{\mu}$ 
16:      $w \leftarrow \text{Nelder-Mead}(\rho, p_{S'} \forall S' \subseteq V, \bar{\Pi}(b) \forall b)$ , see Algorithm 6
17:      $M \leftarrow 0; D \leftarrow 0; \forall S' \subseteq V, n_{S'} \leftarrow 0$ 
18:   end if
19: end while

```

Optimal Clustering using Submodular Optimization

We show that, for a given group of users \mathcal{U} and a given set of weights $w \in \mathbb{R}^n$, problem (5.13) is a submodular minimization problem. Thus, we use the submodular properties and the minimum-norm algorithm to minimize the Ψ function (a detailed study on submodular functions minimization is presented in Appendix A).

Definition 1 (Submodular Function [107]). *A set function $F : 2^V \mapsto \mathbb{R}$ is submodular if and only if, for all subsets $A, B \subseteq V$ and $e \in V$ such that $A \subseteq B$ and $e \notin B$, we have: $F(A \cup e) - F(A) \geq F(B \cup e) - F(B)$.*

Moreover, a function F is *supermodular* if $-F$ is submodular and a function F that is both submodular and supermodular is called *modular*. A function F is modular if and only if there exists $w \in \mathbb{R}^n$ such that $F(A) = \sum_{e \in A} w_e$ for all $A \subseteq V$. Besides, the linear combination of submodular functions is submodular, and submodularity is preserved under taking nonnegative linear combinations [107].

Proposition 3. *For a given group \mathcal{U} and a given weight vector $w \in \mathbb{R}^n$, the objective function $\Psi_{\mathcal{U}}$ defined in (5.13) is submodular.*

Proof. For a user $u \in \mathcal{U}$, we first show that γ_u is supermodular. Take $A \subseteq B \subseteq V$, $e \in V \setminus B$ and denote: $\gamma_u(A) = \frac{a_1}{a_2}$, $\gamma_u(B) = \frac{b_1}{b_2}$ and $c \geq 0$ the useful power received by u from e , so that $\gamma_u(A \cup e) = \frac{a_1+c}{a_2-c}$ and $\gamma_u(B \cup e) = \frac{b_1+c}{b_2-c}$. From the inclusions of sets and the conservation of the system energy, we have $a_1 \leq b_1$, $a_2 \geq b_2$, $a_1 + a_2 = b_1 + b_2$, $a_2 - c \geq 0$ and $b_2 - c \geq 0$. From the two last inequalities, we deduce that $a_2 + b_2 \geq 2c$. Now the inequality $\gamma_u(A \cup e) - \gamma_u(A) \leq \gamma_u(B \cup e) - \gamma_u(B)$ is equivalent to $a_2 + b_2 \geq c$, which is always verified whatever $A \subseteq B \subseteq V$, $e \in V \setminus B$ and $u \in \mathcal{U}$. We have indeed:

$$\begin{aligned}\gamma_u(A \cup e) - \gamma_u(A) &= \frac{c(a_1 + a_2)}{a_2(a_2 - c)} \\ \gamma_u(B \cup e) - \gamma_u(B) &= \frac{c(b_1 + b_2)}{b_2(b_2 - c)}\end{aligned}$$

so that the inequality is successively equivalent to:

$$\begin{aligned}b_2(a_1 + a_2)(b_2 - c) &\leq a_2(b_1 + b_2)(a_2 - c) \\ b_2^2 a_1 + b_2^2 a_2 - b_2 a_1 c - b_2 a_2 c &\leq a_2^2 b_1 + a_2^2 b_2 - a_2 b_1 c - a_2 b_2 c \\ b_2^2(a_1 + a_2) - a_2^2(b_1 + b_2) &\leq c(b_2(a_1 + a_2) - a_2(b_1 + b_2)) \\ a_2 + b_2 &\geq c\end{aligned}$$

By non negative linear combination, we deduce that $\bar{\gamma}_{\mathcal{U}}$ is also supermodular and $-\bar{\gamma}_{\mathcal{U}}$ is submodular. The function $\Psi_{\mathcal{U}}$ is the sum of a submodular function and a modular function, so it is submodular. \square

Two important sets play a role in submodular function minimization.

Definition 2 (Submodular and Base Polyhedron [107]). *Let F be a submodular function such that $F(\emptyset) = 0$. The submodular polyhedron \mathcal{P}_F and the base polyhedron \mathcal{B}_F are defined as:*

$$\begin{aligned}\mathcal{P}_F &= \{w \in \mathbb{R}^n : w(A) \leq F(A) \text{ for all } A \subseteq V\}, \\ \mathcal{B}_F &= \{w \in \mathcal{P}_F : w(V) = F(V)\}.\end{aligned}$$

The connection between submodular function minimization problem and the base polytope is given in the following lemma deduced from the seminal work of Fujishige in [108].

Lemma 2 ([107]). *The linear optimization over the base polyhedron, shown in Algorithm 3 solves linear minimization over \mathcal{B}_F . Moreover, all extreme points of \mathcal{B}_F can be obtained using this algorithm using all possible ordering of x coordinates.*

Algorithm 3: Linear optimization over the base polyhedron.

- 1: **Input:** $x \in \mathbb{R}^n$
- 2: **Output:** $q = \arg \min_{p \in \mathcal{B}_F} x^T p$
- 3: Sort the coordinates of x in increasing order :

$$x_{j_1} \leq x_{j_2} \leq \dots \leq x_{j_n},$$

where $\{j_1, \dots, j_n\}$ is a permutation of the elements of $V = \{1 \dots n\}$.

- 4: Define for $q = \{q_{j_k}\}_{k=1, \dots, n}$ such that :

$$q_{j_k} = F(\{j_1, \dots, j_k\}) - F(\{j_1, \dots, j_{k-1}\}),$$

with $F(\{j_1, \dots, j_{k-1}\}) = F(\emptyset) = 0$ for $k = 1$.

- 5: **return** q
-

Lemma 3 ([107, 108]). *Let F be a submodular function such that $F(\emptyset) = 0$. Let s^* be the point of \mathcal{B}_F with minimum-norm, i.e., $s^* = \arg \min_{s \in \mathcal{B}_F} \frac{1}{2} \|s\|_2^2$. The minimal minimizer of F is $\{j \in V | s_j^* < 0\}$.*

Wolfe has described in [109] an iterative procedure to find minimum norm points in polytopes. Although the base polytope has exponentially many constraints, a simple linear optimization method can minimize any linear function over it. Therefore, Fujishige has suggested in [110] to use Wolfe's procedure on the base polytope coupled with Algorithm 3 as a natural approach to submodular function minimization. Algorithm 4 shows the procedure to solve (5.13).

We provide in the following a brief explanation of the different steps of the algorithm. Following [109], let's call a *corral*, a set of points whose affine minimizer is also in its convex hull. Along the algorithm, a set S is populated with vertices of \mathcal{B}_F . If this set of vertices is sufficient to find the minimum norm point of \mathcal{B}_F , the algorithm stops. Otherwise, a new vertex is added to S and some vertices are removed so that S becomes a corral. The algorithm thus proceeds by major cycles (steps 4-19) and every major cycles possibly involves several minor cycles (steps 8-17).

At the beginning of a major cycle (step 5), we have a corral S together with its affine minimizer $x \in \text{conv}(S)$. If this x verifies the optimality condition, the algorithm stops (step 6). Note that the optimality check is a simple condition resulting from the convexity of \mathcal{B}_F . Otherwise, a new point from the vertices of \mathcal{B}_F (step 5) is added to S (step 7) and minor cycles start. A vertex of \mathcal{B}_F is obtained by means of Algorithm 3, as explained in Lemma 2.

In the minor cycle, the new affine minimizer y of S is computed (step 9). This operation is a standard quadratic minimization problem with linear constraints. If by chance $y \in$

$\text{conv}(S)$ (step 10), then S is a corral and a new major cycle starts with S and $x \leftarrow y$. Otherwise (steps 12-16), x is moved in the direction of y (step 14) up to the boundary of $\text{conv}(S)$ (steps 13 and 14). As we are on the boundary of $\text{conv}(S)$, at least one point of S is not necessary any more to describe x . Such points are removed from S (step 15). Minor cycles continue until a corral is found (step 11). In this case, x and y can coincide (step 18) and a new major cycle starts with this corral and x .

Further explanations about these steps are presented in Section A.5.

Algorithm 4: Min-norm Algorithm (inspired by [111]).

- 1: **Input:** A group \mathcal{U} . A weight vector $w \in \mathbb{R}^n$.
 - 2: **Output:** A set S of serving cells solving (5.13) and the value F of the objective function.
 - 3: **Init:** $F \leftarrow \Psi_{\mathcal{U}}$. Let q be a vertex of \mathcal{B}_F (see Algorithm 3 and Lemma 2); $x \leftarrow q$; $S \leftarrow \{q\}$; let λ_i s.t. $x = \sum_i \lambda_i q_i$; $\lambda_1 \leftarrow 1$
 - 4: **while** true (**major cycle**) **do**
 - 5: $q \leftarrow \arg \min_{p \in \mathcal{B}_F} x^T p$, (see Algorithm 3 and Lemma 2)
 - 6: **if** $\|x\|^2 = x^T q$ **then** Return $S^* \leftarrow \{i | x_i < 0\}$ **end if**
 - 7: $S \leftarrow S \cup \{q\}$
 - 8: **while** true (**minor cycle**) **do**
 - 9: $y \leftarrow \arg \min_{z \in \text{aff}(S)} \|z\|$; let α_i s.t. $y = \sum_i \alpha_i q_i$
 - 10: **if** $\alpha_i \geq 0$ for all i % y is in $\text{conv}(S)$ **then**
 - 11: break.
 - 12: **else**
 - 13: $\theta \leftarrow \min_{i: \alpha_i < \lambda_i} \lambda_i / (\lambda_i - \alpha_i)$
 - 14: $x \leftarrow \theta y + (1 - \theta)x$; $\lambda \leftarrow \theta \alpha + (1 - \theta)\lambda$
 - 15: $S \leftarrow \{q_i : \lambda_i > 0\}$
 - 16: **end if**
 - 17: **end while**
 - 18: $x \leftarrow y$; $\lambda \leftarrow \alpha$
 - 19: **end while**
-

Lemma 4. Every iteration of Algorithm 4 has a $O(n^2)$ complexity.

Proof. Algorithm 3 complexity is dominated by the sorting of the coordinates of x and is thus in $O(n \log n)$. The minimization over the affine hull in step 9 has a complexity in $O(n^2)$. All other steps are in $O(n)$. \square

It is however not known how many iterations are required for the termination. Our simulation results show that very few iterations are in practice required in our case.

Greedy Clustering

The greedy algorithm has been widely used in the literature on clustering for multi-point transmissions, see e.g. [94–98]. For comparison with the minimum-norm algorithm, we thus introduce a greedy approach to find an approximate minimizer of the function $\Psi_{\mathcal{U}}$ for a given group of users \mathcal{U} and a set of weights $w \in \mathbb{R}^n$.

The greedy approach, summarized in Algorithm 5, consists in initializing the cluster of BSs as the set of best server cells of group users (step 3). Then, at every iteration and if possible, we add to the cluster the BS that decreases at most the objective function (5.13) (steps 5-12). If there is no such BS (step 4) or if we have reached the whole set of cells (step 17), we return the current cluster.

Algorithm 5: Greedy Group Call Clustering.

- 1: **Input:** A group \mathcal{U} . A weight vector $w \in \mathbb{R}^n$.
 - 2: **Output:** A set S of serving cells solving (5.13) and the value F of the objective function.
 - 3: **Init:** Let S the set of best server BSs of \mathcal{U} members; $\bar{S} \leftarrow V \setminus S$; $F \leftarrow \Psi_{\mathcal{U}}(S)$.
 - 4: **while** $\bar{S} \neq \emptyset$ **do**
 - 5: **for** $j \in \bar{S}$ **do**
 - 6: $\Psi_{\mathcal{U},j} \leftarrow \Psi_{\mathcal{U}}(S \cup \{j\})$
 - 7: **end for**
 - 8: **if** $\Psi_{\mathcal{U}}(S) > \min_{j \in \bar{S}}(\Psi_{\mathcal{U},j})$ **then**
 - 9: $b \leftarrow \arg \min_{j \in \bar{S}}(\Psi_{\mathcal{U},j})$
 - 10: $S \leftarrow S \cup \{b\}$
 - 11: $\bar{S} \leftarrow \bar{S} \setminus \{b\}$
 - 12: $F \leftarrow \min_{j \in \bar{S}}(\Psi_{\mathcal{U},j})$
 - 13: **else**
 - 14: **return** S, F
 - 15: **end if**
 - 16: **end while**
 - 17: **return** S, F
-

We note that the Algorithm 5 requires $n - 1$ iterations in the worst case and has thus a complexity in $O(n)$.

5.3.3 Cell Weights Optimization

In this section, we consider the problem of finding an unconstrained minimum of the real-valued function G (see Equation (5.15)). The difficulty lies in the fact that a closed-form of G is not available as its evaluation requires to solve a Markov process. An interesting

class of methods for solving derivative-free (or black box) functions are the direct search methods, which update iteratively an initial assumption of a solution using a few function evaluations along linearly independent directions [112], in contrast to other optimization techniques, which require derivatives of the objective function to determine a search direction. Therefore, direct-search methods provide simpler calculations and relatively low storage requirements over derivative-based methods. Direct-search methods have been classified into two classes: heuristic techniques and theoretically-based techniques [113]. A set of the proposed methods, e.g. [114–116], are based on the idea of simplicial search, in which an n -dimensional simplex is iteratively "improved" through certain reflection, expansion and contraction steps, possibly interspersed with shrink steps (see Figure 5.2). The most popular is the Nelder-Mead simplex method [114].

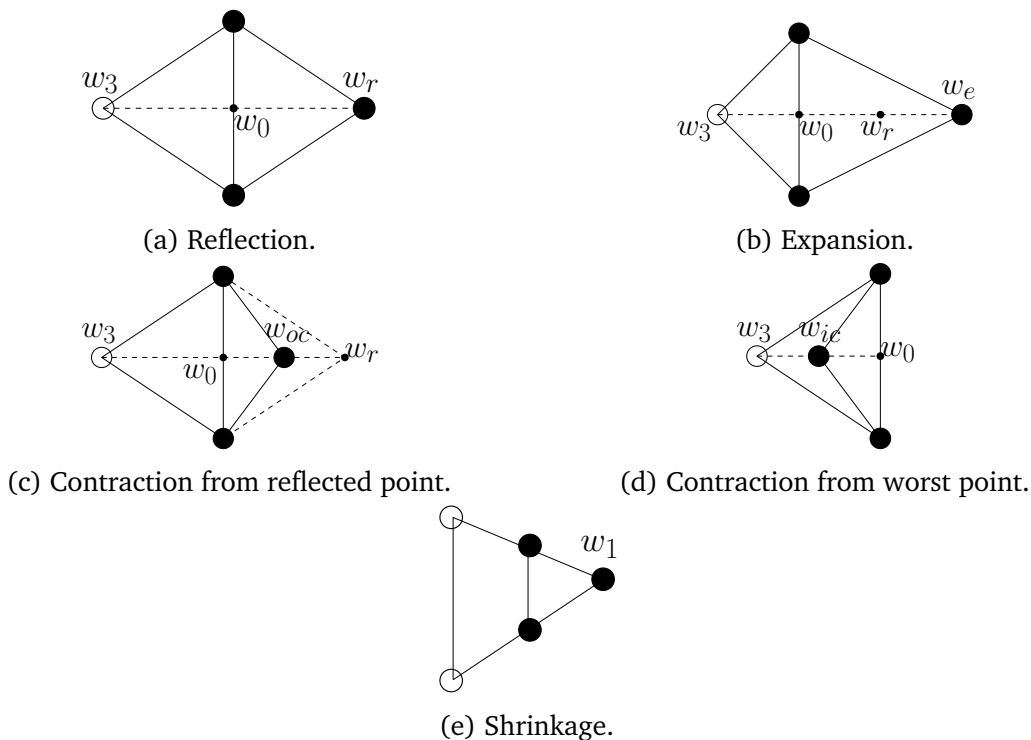


Figure 5.2 Simplex operations in \mathbb{R}^2 (white dots indicate the worst vertices before operations; solid dots indicate new simplex).

The Nelder-Mead (NM) algorithm is an heuristic that operates on an n -dimensional simplex of $n + 1$ vertices, and aims to improve the "worst" vertex (i.e., with highest objective function value), through certain transformations of the simplex. These transformations are done with respect to a centroid vector (step 20), which is nothing else than the average vector of the simplex.

We thus start with $n + 1$ random vectors w (step 3) that are sorted according to the objective function (step 6). With period I (step 7), we check if the standard deviation of the blocking probability around their target values is small and if it is the case, we return the best weight vector (step 8-10). Otherwise, we perform a random oriented restart, i.e., we randomly generate new weights for the cells, which are far from their target (steps 11-18).

The possible transformations of the simplex are shown in Figure 5.2. In a Reflection (steps 21-23), the worst vector (w_{n+1}) is reflected with respect to the centroid and the reflected point replaces the worst vector if the objective function is decreased at this point. Expansion (steps 24-26) and contraction (steps 28-30, 35-37) are two other possible transformations. The simplex is shrunk (steps 32 and 39), towards the best vertex, whenever it is not improved by the preceding transformations, and new iteration is then started. A restatement of the original Nelder-Mead (NM) algorithm [114] has been presented in [117], and is the basis of Algorithm 6.

However, despite its generally good performance, the NM algorithm can stagnate, fail to converge or converge to a non-optimal vertex, even for simple and convex objective functions. Then, numerous variants of this algorithm have been developed and analyzed, aiming to improve its performance and converge to a stationary vertex under mild conditions on the objective function.

A possible improvement of the original algorithm is to impose restarts of the algorithm during the optimization run at certain iterations, by applying a fresh simplex. A restart is global when it is completely independent of previous results. It is local when a new simplex is initialized using the best known solution and a projection of the most recent simplex. However, such schemes, e.g. the globalized bounded NM [118], increase significantly the number of iterations of the algorithm, and don't provide good solutions to our problem, as observed in our simulations.

Therefore, we propose an oriented restart of the NM algorithm adapted to our model (steps 8-19). The idea is to reinitialize the simplex by modifying the weights of the cells having blocking probabilities far from their target. At every restart, the weight of cells having the lowest blocking probability are decreased, while the weight of cells having blocking probabilities higher than their targets are increased. A random perturbation is applied to every modification. The proposed restart scheme is applied periodically at the beginning of the NM algorithm major cycle. The period is controlled by the integer parameter I in Algorithm 6.

Algorithm 6: Nelder-Mead Simplex with Oriented Restart

```

1: Input: A set of parameters  $-1 < \delta_{ic} < 0 < \delta_{oc} < \delta_r < \delta_e$  and  $0 < \delta_s < 1, \epsilon_1 > 0, \epsilon_2 > 0, I \in \mathbb{N} \setminus \{0\}, \rho, p_S, \forall S' \subseteq V, \bar{\Pi}(b) \forall b \in V$ .
2: Output: A weight vector  $w^* \in \mathbb{R}^n$  solving (5.14).
3: Init:  $f \leftarrow G$ . Generate  $n + 1$  vertices  $w \in \mathbb{R}^n$ .  $It \leftarrow 0$ .
4: while true do
5:    $It \leftarrow It + 1$ 
6:   Sort the vertices according to the objective function values:  $f(w_1) \leq \dots \leq f(w_{n+1})$ 
7:   if  $f(w_{n+1}) - f(w_1) > \epsilon_1$  or  $\text{mod}(It, I) = 0$  then
8:     if  $\text{stddev}(\bar{\Pi}(b; w_1), b \in V) < \epsilon_2$  then
9:       Return  $w^* \leftarrow w_1$ 
10:    end if
11:     $b \leftarrow \arg \min_{j \in V} \bar{\Pi}(j; w_1); \theta \leftarrow \text{rand}(1, n + 1)$ 
12:     $\forall i \in \{1, \dots, n + 1\}, (w_i)_b \leftarrow (w_i)_b \theta_i$ 
13:     $\theta \leftarrow \text{rand}(1, n + 1)$ 
14:    for  $b \in V$  do
15:      if  $\bar{\Pi}(b; w_1) > \bar{\Pi}(b)$  then
16:         $\forall i \in \{1, \dots, n + 1\}, (w_i)_b \leftarrow (w_i)_b / \theta_i$ 
17:      end if
18:    end for
19:  end if
20:  % Compute the centroid ( $w_0$ ) of all vertices except  $w_{n+1}$ :  $w_0 \leftarrow \frac{1}{n} \sum_{i=1}^n w_i$ 
21:  % Reflection: Compute reflected point:  $w_r \leftarrow w_0 + \delta_r(w_0 - w_{n+1})$ 
22:  if  $f(w_1) \leq f(w_r) < f(w_n)$  then
23:     $w_{n+1} \leftarrow w_r$ 
24:  else if  $f(w_r) < f(w_1)$  then
25:    % Expansion: Compute the expanded point:  $w_e \leftarrow w_0 + \delta_e(w_r - w_0)$ 
26:    if  $f(w_e) < f(w_r)$  then  $w_{n+1} \leftarrow w_e$  else  $w_{n+1} \leftarrow w_r$  end if
27:  else if  $f(w_n) \leq f(w_r) < f(w_{n+1})$  then
28:    % Outside contraction: Compute the contracted point:  $w_{oc} \leftarrow w_0 + \delta_{oc}(w_r - w_0)$ 
29:    if  $f(w_{oc}) \leq f(w_r)$  then
30:       $w_{n+1} \leftarrow w_{oc}$ 
31:    else
32:      Shrink:  $w_i \leftarrow w_1 + \delta_s(w_i - w_1); \forall i \in \{2, \dots, n + 1\}$ 
33:    end if
34:  else
35:    % Inside contraction: Compute the contracted point:  $w_{ic} \leftarrow w_0 - \delta_{ic}(w_{n+1} - w_0)$ 
36:    if  $f(w_{ic}) \leq f(w_{n+1})$  then
37:       $w_{n+1} \leftarrow w_{ic}$ 
38:    else
39:      Shrink:  $w_i \leftarrow w_1 + \delta_s(w_i - w_1); \forall i \in \{2, \dots, n + 1\}$ 
40:    end if
41:  end if
42: end while

```

5.3.4 Complexity Analysis

The general complexity of the Nelder-Mead algorithm has not been assessed in the literature [119]. However, the complexity of a single iteration of Nelder-Mead algorithm has been introduced in [119].

Lemma 5. *If the simplex is updated without shrink, the iteration has a $\Theta(n)+\Theta(T_G)$ complexity, where T_G is the complexity of evaluating the objective function G . If shrink is needed, the complexity increases to $\Theta(n^2) + \Theta(nT_G)$.*

Proof. Based on [119], each iteration consists in 3 steps: sort the simplex, evaluate its centroid (besides worst vertex) and its transformation. Sorting requires $\Theta(n \log n)$ complexity at the very first iteration. Then, the elements between 2 and $n - 1$ are already sorted, so that at every subsequent iteration, sorting has only $\Theta(n)$ complexity.

The computation of the first centroid is in $\Theta(n^2)$ as it involves a sum of n elements from \mathbb{R}^n . In subsequent iterations, if there is no shrink, only w_1 , w_n and w_{n+1} may change, so that the centroid computation is updated with $\Theta(n)$ complexity. If there is a shrink, a constant value is added to every w_i so that the complexity is still $\Theta(n)$ for the centroid computation.

For the last step, there are two cases. If there is no shrink, from 1 to 4 new points are computed in $\Theta(n)$ depending on the transformation and from 1 to 4 function evaluations are required, i.e., with complexity $\Theta(T_G)$. If there is a shrink, all points are updated in $\Theta(n^2)$ and n function evaluations are required with $\Theta(nT_G)$ complexity. \square

Lemma 6. *Each iteration has a complexity in $\Theta(n+R)$ (when shrink is not needed) or $\Theta(n^2+R)$ (shrink is used) when the Erlang-B approximation (5.12) is adopted for the evaluation of G . Each iteration has an exponential complexity when (5.9) is adopted for the evaluation of G .*

5.4 Simulation Results

In this section, we compare the proposed dynamic clustering scheme to SC-PTM and full MBSFN cooperation schemes and we compare minimum-norm algorithm to the greedy algorithm.

5.4.1 Simulations Settings

We evaluate the performance of the proposed scheme in a MBSFN synchronization area of 14 BSs, while all other cells are interfering (see Figure 5.1). In the simulations, for

simplicity reasons, we ignore the correlation between blocking probabilities in different cells and adopt the Erlang-B approximation. In order to assess the traffic dynamics in our evaluations, we assume the following users and group distributions:

- 25% of arriving UEs are served by a given cell (overloaded cell), 3% of them are dropped in another cell (underloaded cell), while other UEs are uniformly distributed in the other cells of the synchronization area;
- 50% of arriving groups are centralized, i.e., all the users are distributed in the closest area (of radius 1.5 km) of a team leader UE (a typical use case for mission-critical communications). In the remaining groups, the UEs are randomly distributed in the target network.

The other system simulation parameters that were taken into account for our simulations are summarized in Table 5.1. They are typical for mission-critical communications.

Parameter	Value
Carrier frequency	700 MHz
Channel Bandwidth (W)	5 MHz
Groups arrival rate (λ)	$1/55 \text{ s}^{-1}$
Mean service duration ($1/\mu$)	180 s
Available resources per BS (R)	5 resources
Number of users per group (N)	10 UEs/group
Clustering algorithm period (T)	30 minutes
Target blocking probability $\bar{\Pi}(b)$	2%
NM parameters $\{\delta_r, \delta_e, \delta_{oc}, \delta_{ic}, \delta_s\}$	$\{1, 2, 1/2, -1/2, 1/2\}$

Table 5.1 Simulation parameters.

5.4.2 Group Call Multi-point Transmission

We focus here on the results provided by Algorithm 4. Figure 5.3 shows the evolution of function Ψ_{oz} along algorithm's iterations for the proposed scheme, evaluated with the weight vector provided by NM algorithm at the end of the simulation. The values of the objective function for SC-PTM and full MBSFN cooperation are provided for comparison. Results show that these schemes are outperformed by the proposed algorithm and that the submodular minimization problem is solved in very few iterations.

Furthermore, in Figure 5.4, we compare for a specific group the Greedy clustering with the minimum-norm algorithm and show the objective function along the iterations of the

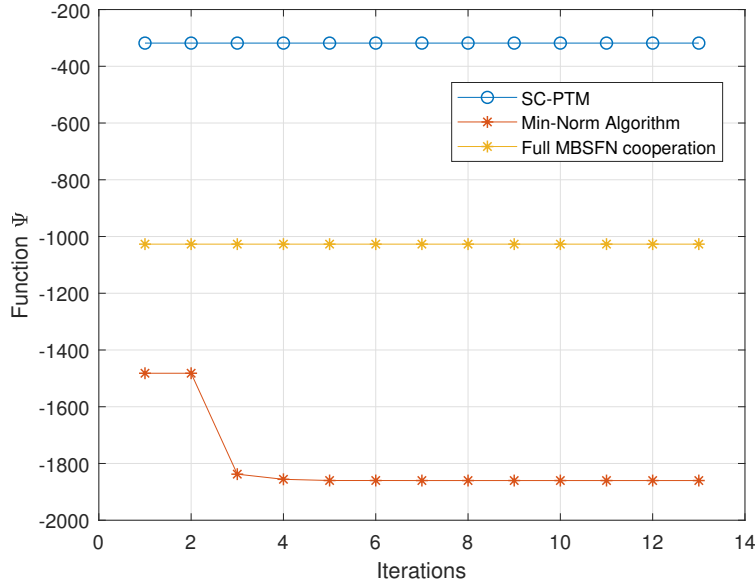


Figure 5.3 Evolution of function Ψ_{α} along the iterations of Algorithm 4.

two algorithms. The min-norm algorithm stops after two iterations, while greedy requires five iterations. We see that greedy, a widely used algorithm for multi-point transmission clustering, may not provide the optimal solution.

5.4.3 Objective Function and Blocking Probabilities

Figure 5.5 shows the evolution of the objective function G , of cell weights and of blocking probabilities for each cell along the iterations of Algorithm 6. We see that the function G decreases until it converges in few tens of iterations to a value close to 0 when blocking probabilities of all cells are close to corresponding targets. Moreover, along the algorithm, the cell weights and blocking probabilities fluctuate, especially at the iterations corresponding to random restarts, until the probabilities reach their fixed targets (2%). Note that the weight of BS1 is very high compared to other weights because this cell is overloaded.

The first iterations of the NM algorithm reveals that the blocking probabilities are very high in all cells. This means that with initial weights the proposed scheme provides almost a full cooperation scheme for all arriving groups. Gradually, the cluster sizes are decreased so that blocking probabilities decrease up to their target value. The coverage-capacity trade-off is thus well handled by the proposed scheme. This fact is illustrated in Figure 5.6, where we show the clusters evolution provided by the proposed scheme along Algorithm 6 iterations for a given group.

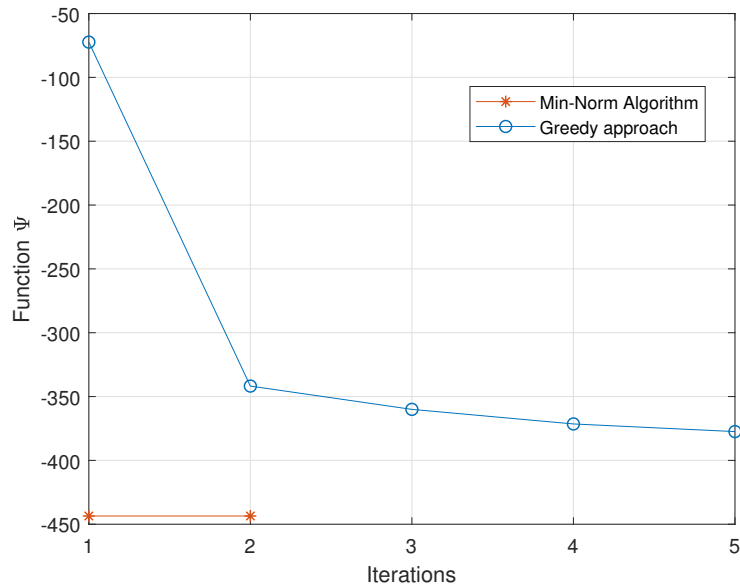


Figure 5.4 Comparison of min-norm algorithm with greedy clustering to minimize function Ψ .

Moreover, for the simulated scenario, the blocking probability of all cells in full cooperation scheme is 13.4%, while in SC-PTM, it is 3% and 0.01% in the overloaded and underloaded cells respectively, and falls below 0.8% in all other cells. Thus, SC-PTM provides the best performance in terms of blocking, however at the cost of lower coverage as we will see.

In Figure 5.7, we test the globalized bounded NM on the same simulated scenario and show the evolution of G with this scheme. We see that with the globalized bounded NM, the function G and the cell weights are still fluctuating after 2000 iterations, whereas with our oriented random restart, few tens of iterations were sufficient to obtain convergence (see Figure 5.5a).

5.4.4 SINR Improvements

In order to compare the performance of different transmission schemes in terms of coverage gain, we show in Figure 5.8 the corresponding mean SINR and minimum group SINR, as well as UEs SINR Cumulative Distribution Function (CDF) curves. The mean SINR is obtained by averaging group user SINRs and the minimum group SINR is the worst SINR in every group.

The SINR gain depends of course on clusters size. Thus, full MBSFN cooperation scheme provides the best SINR results, since all BSs inside the synchronization area contribute to the transmission. On the other hand, in SC-PTM, there is no cooperation between BSs and only the UEs best server cells contribute independently to the transmission, therefore, the SINR values are the lowest in such a scheme. Since in dynamic clustering the cluster size is intermediate between those schemes, it leads to moderate SINR gains. As a conclusion, in the proposed scheme, the target blocking probabilities allows to trade capacity against coverage.

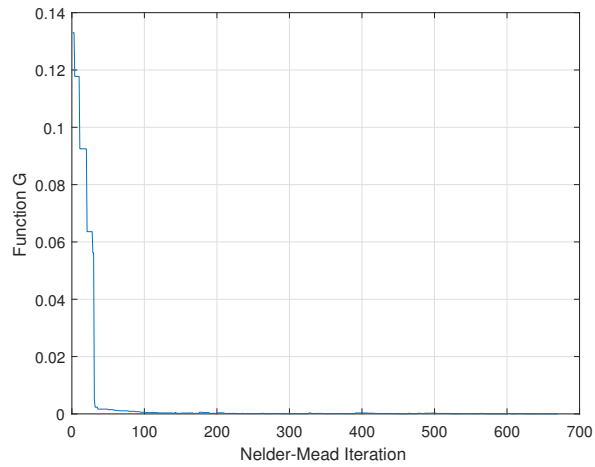
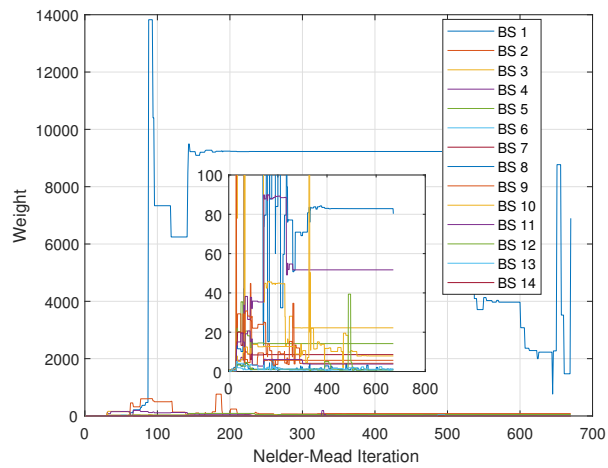
5.4.5 Performance Evaluation Based Minimum Group SINR

In mission-critical communications, the group performance may be evaluated based on the minimum SINR experienced by its members, instead of its mean SINR. In such case, the function Ψ_{gk} is not necessarily submodular and the minimum-norm algorithm may not solve the minimization problem in Equation (5.13). We thus perform an exhaustive search and compare the results to our scheme.

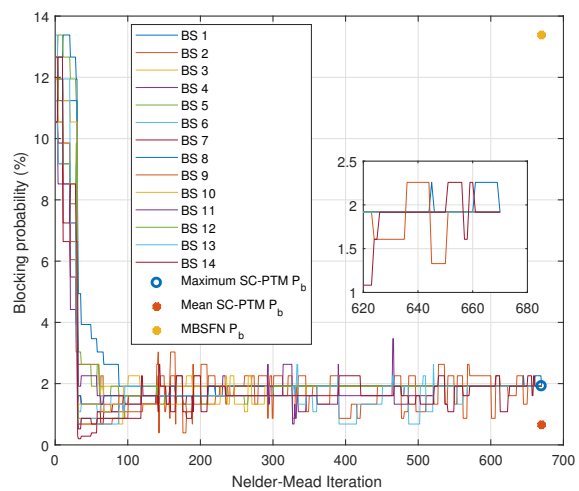
In Figure 5.9, we compare the CDF distributions of group minimum SINR and UEs SINR for both approaches. We see that our approach offers slightly lower SINRs than the exhaustive search and is thus near-optimal even when group minimum SINR is considered.

5.4.6 Impact of Traffic Intensity

We now show how in extreme cases of traffic our scheme tends to full cooperation MBSFN or SC-PTM. In Figure 5.10a a very low traffic is considered, so that all cells can cooperate to serve groups without violating the blocking probability constraint. In Figure 5.10b, a high traffic is assumed. Cells are selected as in SC-PTM. The SINR is however improved because we assume that serving cells cooperate to serve the groups whereas SC-PTM serving BSs interfere each others. This shows our approach self-adapts to traffic conditions and includes MBSFN and SC-PTM as special cases.

(a) Function G .

(b) Cell weights.



(c) Cells blocking probabilities.

Figure 5.5 Evolution of the objective function G , cell weights and blocking probabilities along the iterations of Algorithm 6.

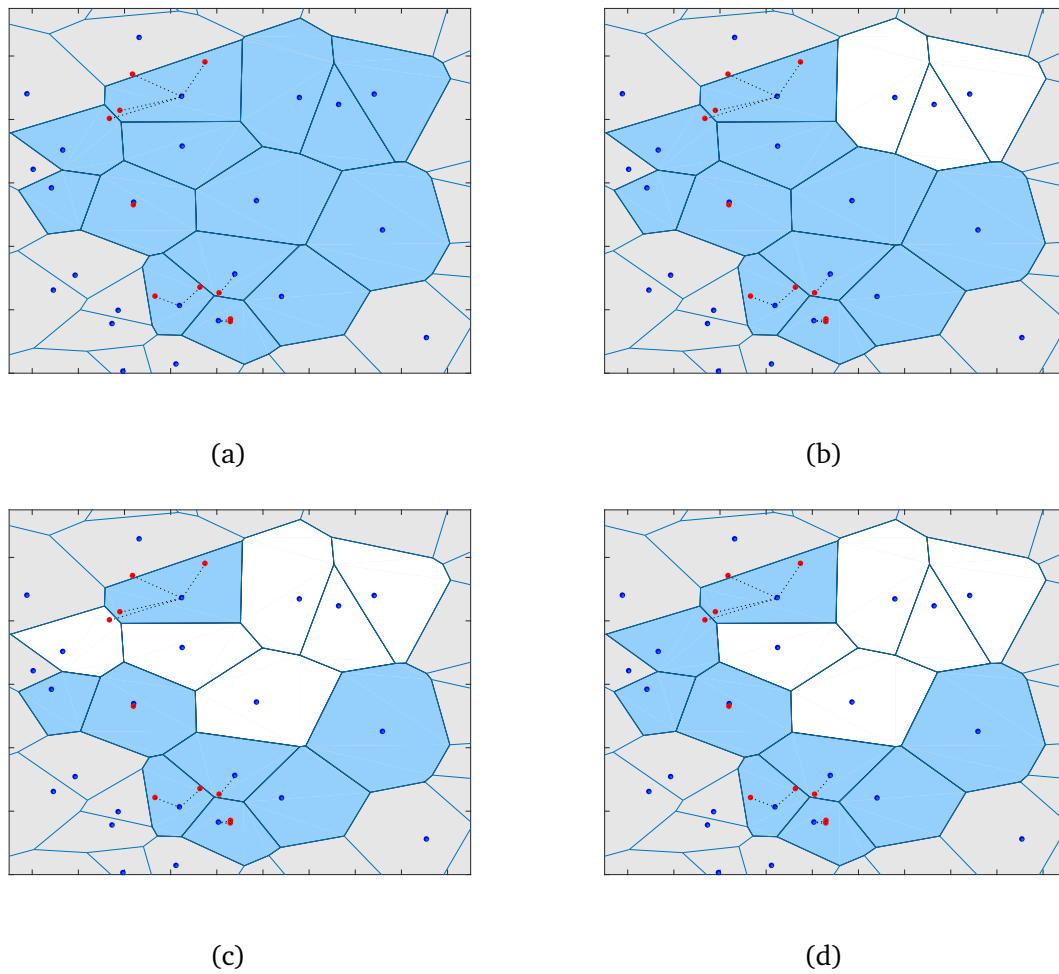
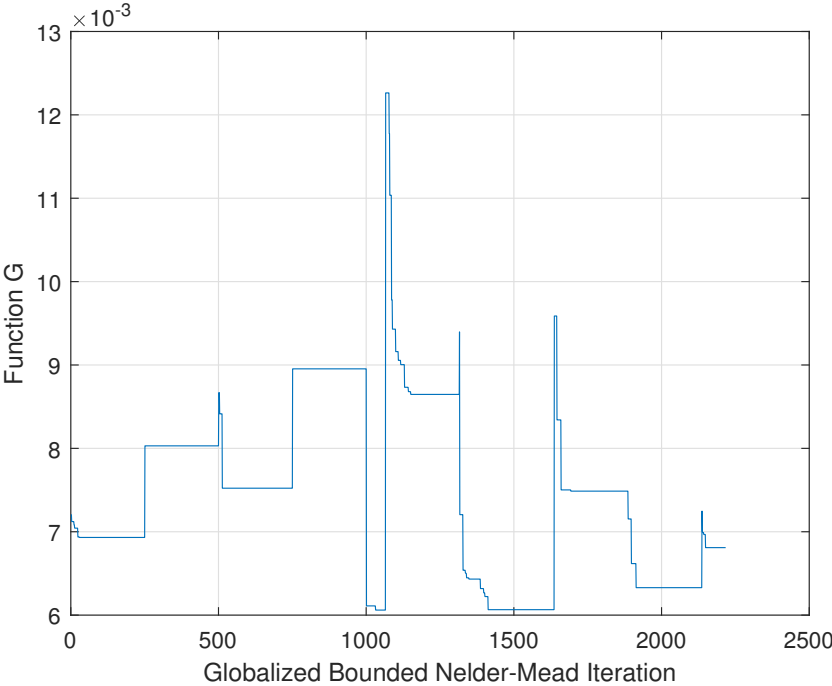
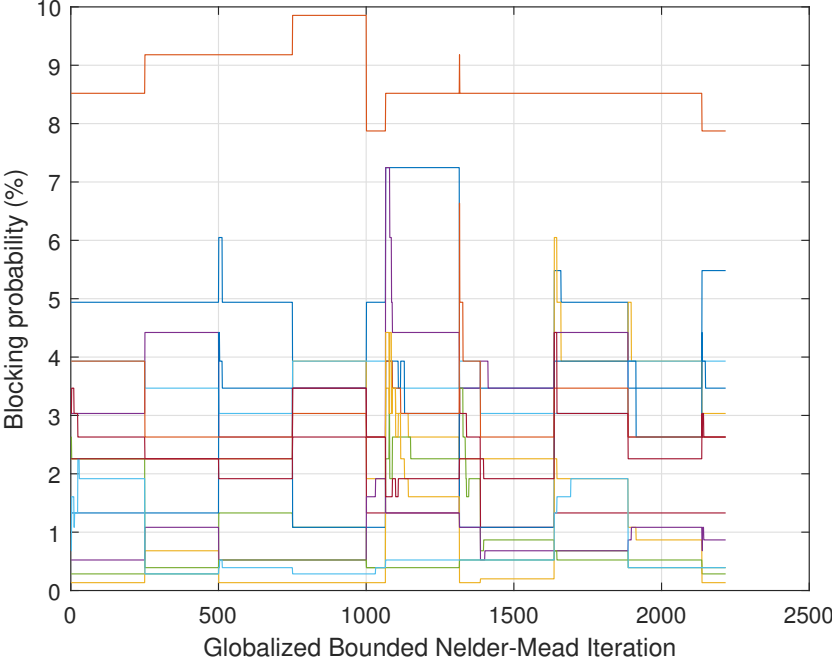


Figure 5.6 Clustering evolution along Algorithm 6 iterations for a given group. The cluster serving the group is formed by the blue cells, while the white cells are interfering. The links show the best server of each UE.

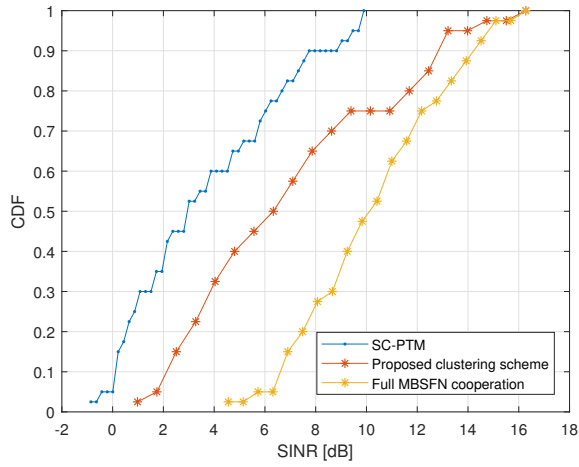


(a) Function G.

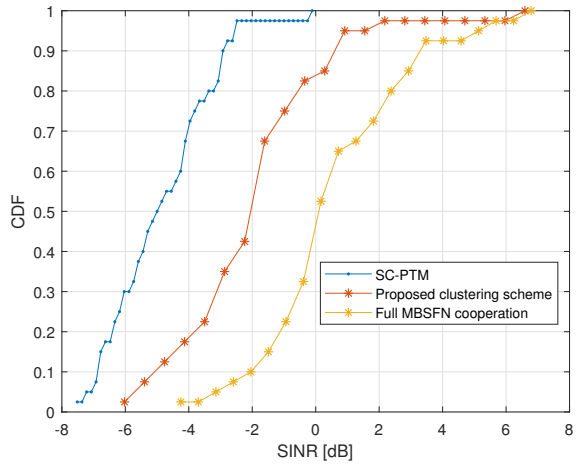


(b) Cells blocking probabilities.

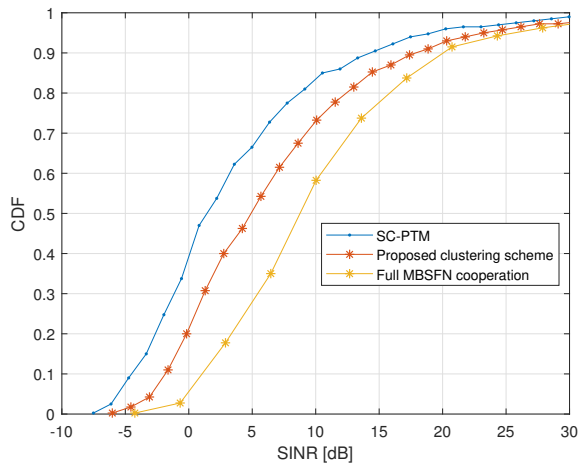
Figure 5.7 Evolution of the objective function G and blocking probabilities along the iterations of globalized bounded NM algorithm.



(a) CDF distributions of group mean SINR.

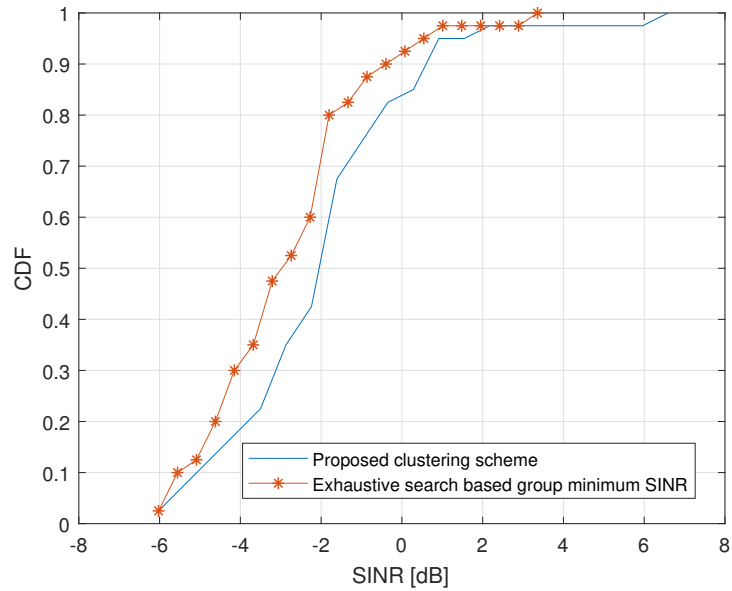


(b) CDF distributions of group minimum SINR.

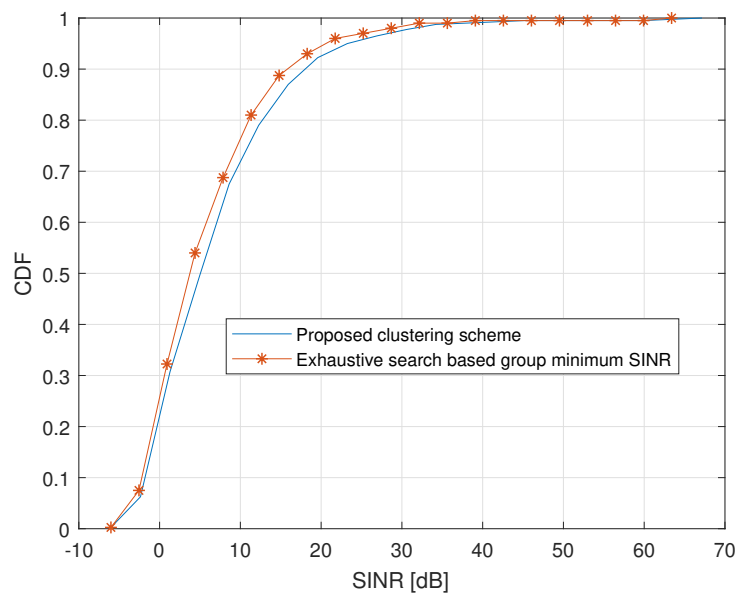


(c) CDF distributions of UEs SINR.

Figure 5.8 Comparison of group mean, minimum and UEs SINR CDF of SC-PTM, full MBSFN cooperation transmissions with proposed clustering scheme obtained at the end of Algorithm 6.



(a) CDF distributions of group minimum SINR.



(b) CDF distributions of UEs SINR.

Figure 5.9 Evaluation of the group minimum and UEs SINR using the proposed scheme, compared to a modified scheme based on exhaustive approach to evaluate function $\Psi_{\mathcal{U}}$ upon to minimum group SINR.

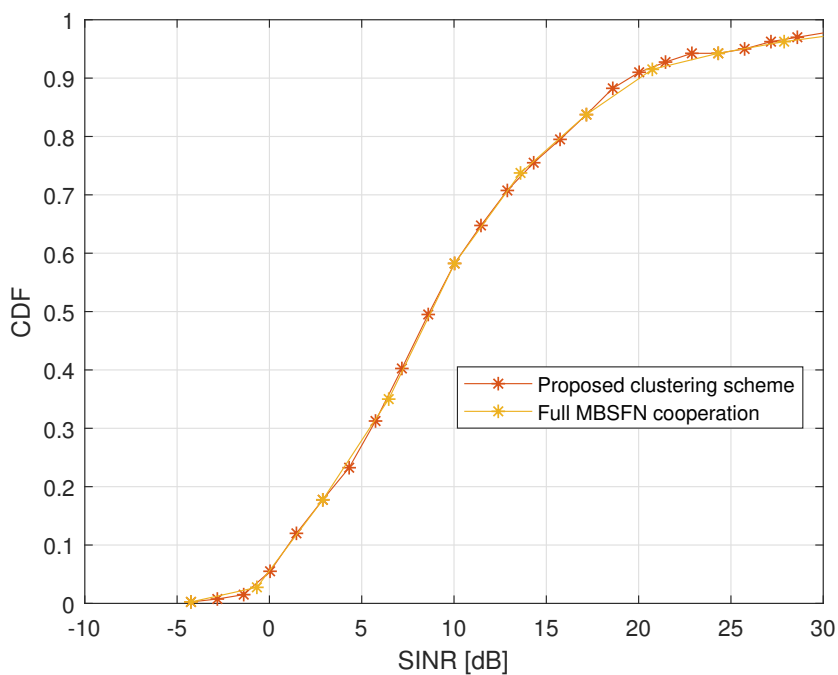
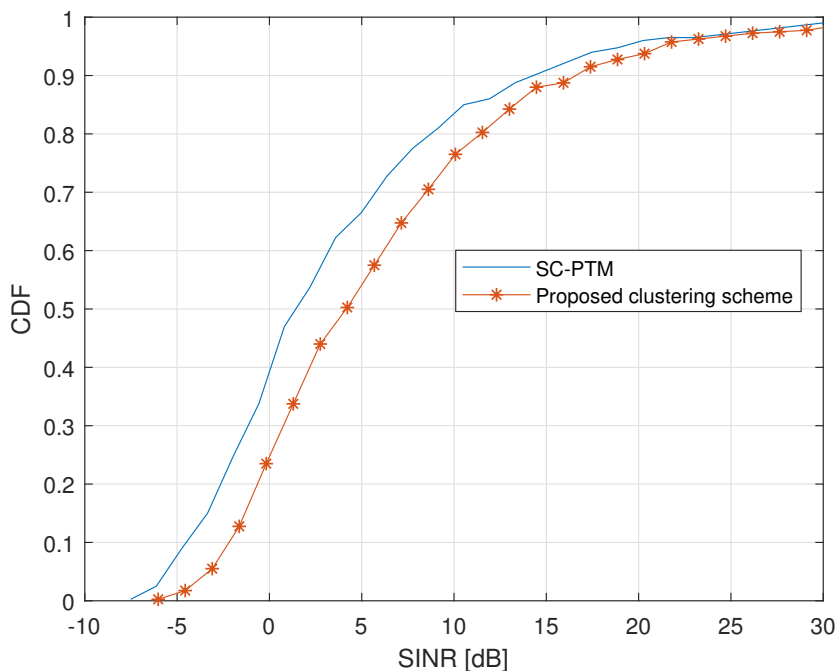
(a) Low traffic load ($\lambda = 1/100 \text{ s}^{-1}$).(b) High traffic load ($\lambda = 1/25 \text{ s}^{-1}$).

Figure 5.10 Impact of the traffic load on network performance.

5.5 Conclusion

In this chapter, we formulate a problem to capture the coverage-capacity trade-off arising in mission-critical networks serving group of users by means of cooperative multi-point transmissions. A dynamic clustering algorithm is proposed to solve this problem. We consider a dynamic traffic in which group calls arrive, are served by a cluster of cells and leave the system. For every group, a submodular minimization problem is formulated to find the best subset of cells in terms of average Signal to Interference plus Noise Ratio (SINR) and cell costs of using radio resources. At a larger time scale, cell costs are optimized in order that the blocking probability in every cell is close to a target. We rely here on derivative-free optimization and more specifically on the Nelder-Mead simplex method. The comparison of the proposed scheme with Single-Cell Point-To-Multipoint (SC-PTM) and full cooperation schemes show that it outperforms them in terms of coverage and system capacity respectively.

Conclusion and Further Work

In this thesis, an evaluation of mobile networks physical layer transmission modes has been introduced, from Professional Mobile Radio (PMR) networks requirements perspective. Thus, we focused on the transmission of Multimedia Broadcast/Multicast Service (MBMS), the main service allowed by these networks.

In Chapter 2, the performance of Multicast/Broadcast Single Frequency Network (MBSFN), Single-Cell Point-To-Multipoint (SC-PTM) and unicast transmissions has been evaluated in terms of Signal to Interference plus Noise Ratio (SINR) distribution, System Spectral Efficiency (SSE), outage probability and cell range, assuming different User Equipments (UEs) distribution scenarios and network configurations. Moreover, we introduced the coverage gain provided by Transmission Time Interval (TTI) bundling, allowed by SC-PTM and unicast transmissions, and we presented the trade-off between coverage and capacity by varying the number of TTI bundling retransmissions.

In Chapter 3, we introduced an analytical model, that allows quick calculations of the SINR for MBSFN based mission-critical communications, in terms of the distance to the nearest serving Base Station (BS). We show that our model matches well Monte Carlo simulations when shadowing standard deviation is low. When shadowing standard deviation increases, our model becomes less accurate but outperforms the Fenton-Wilkinson approach.

In Chapter 4, a repetition scheme adopted for PMR networks using MBSFN and SC-PTM to convey group communications is proposed and evaluated in terms of Signal to Noise Ratio (SNR) and cell coverage gains. The proposed scheme takes into account the coherence bandwidth and the coherence time of the multi-path fading channel together with service delay constraints. We show that the former improves significantly the network performance, while the latter increases transmission delay without bringing important gains. We show that up to 11 dB gain in SNR is achieved over classical MBSFN transmissions without repetitions. System level simulations show that cell radius is significantly improved in a MBSFN. The proposed scheme could be adopted for next MBSFN and SC-PTM standard releases as an attractive option to increase cell coverage for mission-critical communications.

Dynamic clustering has been assessed in Chapter 5. We formulate a problem to capture the coverage-capacity trade-off arising in mission-critical networks serving group of users by means of cooperative multi-point transmissions, and we propose a dynamic clustering algorithm to solve this problem. The proposed algorithm consists on a submodular minimization problem formulated to find the best subset of serving cells in terms of average SINR and cell costs of using radio resources, along with a derivative-free optimization method, the Nelder-Mead, to minimize these costs in the objective of maintaining the blocking probability in every cell close to a target value. The proposed submodular minimization problem is compared to a Greedy search based method, and we show that our method ensures finding the optimal solution. The comparison of the proposed scheme with SC-PTM and full cooperation schemes show that it outperforms them in terms of coverage and system capacity respectively.

Furthermore, enhancing some of the proposed models in this thesis is of high importance. The work on the analytical model of SINR in MBSFN networks, proposed in Chapter 3, will continue in the aim of improving its performance with higher shadowing standard-deviations. In this context, there is some helpful studies to approximate the sum of log-normal random variables (e.g. [120]).

Moreover, the proposed solution for the evaluation of the traffic model in MBSFN networks, in Section 5.2.2, needs further improvements to reduce its complexity. On the other hand, the proposed submodular minimization problem in Chapter 5 may be enhanced, from the network performance perspective, by adding a condition on the minimal acceptable SINR inside a group; this condition is crucial in mission-critical communications, since the network must ensure coverage for all its users.

Further work will assess also the impact of some technologies, such that millimeter wave and massive MIMO, on the performance of PMR networks. These technologies have been introduced in next generation mobile networks to improve system performance, thus, we aim to evaluate their potential impact on network coverage. Moreover, using drones equipped with Base Stations (BSs), acting as a flying BSs, is a promising solution for wide coverage networks, owing to their ability to move to any uncovered area. Further evaluations of the performance impact of such a solution are required before implementation.

Publications

- Alaa Daher, Marceau Coupechoux, Philippe Godlewski, Pierre Ngouat and Pierre Minot, [SC-PTM or MBSFN for Mission Critical Communications?](#), 2017 IEEE 85th Vehicular Technology Conference (VTC2017-Spring), June 2017.
- Alaa Daher, Marceau Coupechoux, Philippe Godlewski, Jean-Marc Kelif, Pierre Ngouat and Pierre Minot, [SINR Model for MBSFN Based Mission Critical Communications](#), 2017 IEEE 86th Vehicular Technology Conference (VTC2017-Fall), September 2017.
- Alaa Daher, M. Shabbir Ali, Marceau Coupechoux, Philippe Godlewski, Pierre Ngouat and Pierre Minot, [A Repetition Scheme for MBSFN Based Mission-Critical Communications](#), 2018 IEEE 88th Vehicular Technology Conference (VTC2018-Fall), August 2018.
- Alaa Daher, Marceau Coupechoux, Philippe Godlewski, Pierre Ngouat and Pierre Minot, A Dynamic Clustering Algorithm for Multi-Point Transmissions in Mission-Critical Communications, submitted.

Bibliography

- [1] 3GPP, “Study on physical layer enhancements for NR ultra-reliable and low latency case (URLLC),” TR 38.824, 3rd Generation Partnership Project (3GPP), Nov. 2018.
- [2] 3GPP, “Public safety broadband high power User Equipment (UE) for band 14,” TR 36.837, 3rd Generation Partnership Project (3GPP), Dec. 2012.
- [3] 3GPP, “Updates to the WID on Feasibility Study on Study on Isolated (was "Resilient") E-UTRAN Operation for Public Safety,” TSG SP-130596, 3rd Generation Partnership Project (3GPP), Dec. 2013.
- [4] 3GPP, “Group Communication System Enablers (GCSE),” TS 22.468, 3rd Generation Partnership Project (3GPP), June 2018.
- [5] 3GPP, “Mission Critical Push To Talk (MCPTT),” TS 22.179, 3rd Generation Partnership Project (3GPP), Sept. 2018.
- [6] 3GPP, “Mission Critical Video services,” TS 22.281, 3rd Generation Partnership Project (3GPP), Sept. 2018.
- [7] 3GPP, “Mission Critical Data services,” TS 22.282, 3rd Generation Partnership Project (3GPP), Sept. 2018.
- [8] 3GPP, “Mobile Communication System for Railways,” TS 22.289, 3rd Generation Partnership Project (3GPP), Dec. 2018.
- [9] 3GPP, “Feasibility Study on Maritime Communication Services over 3GPP system,” TS 22.289, 3rd Generation Partnership Project (3GPP), Sept. 2018.
- [10] J. Kim, S. W. Choi, Y. S. Song, Y. K. Yoon, and Y. K. Kim, “Automatic train control over LTE: Design and performance evaluation,” *IEEE Communications Magazine*, vol. 53, no. 10, pp. 102–109, 2015.
- [11] T. Doumi, M. F. Dolan, S. Tatesh, A. Casati, G. Tsirtsis, K. Anchan, and D. Flore, “LTE for public safety networks,” *IEEE Communications Magazine*, vol. 51, no. 2, pp. 106–112, 2013.
- [12] R. Ferrús, O. Sallent, G. Baldini, and L. Goratti, “LTE: The technology driver for future public safety communications,” *IEEE Communications Magazine*, vol. 51, no. 10, pp. 154–161, 2013.
- [13] P. Stavroulakis, *TERrestrial Trunked Radio - TETRA: A Global Security Tool*. Signals and Communication Technology, Springer Berlin Heidelberg, 2007.

- [14] R. Ferrús and O. Sallent, "Extending the LTE / LTE-A Business Case to Professional Mobile Radio," *IEEE vehicular technology magazine*, vol. 9, no. 3, pp. 1–7, 2014.
- [15] L. Carlà, R. Fantacci, F. Gei, D. Marabissi, and L. Micciullo, "LTE enhancements for public safety and security communications to support group multimedia communications," *IEEE Network*, vol. 30, no. 1, pp. 80–85, 2016.
- [16] A. Raza, "LTE network strategy for Smart City Public Safety," *2016 IEEE International Conference on Emerging Technologies and Innovative Business Practices for the Transformation of Societies (EmergiTech)*, pp. 34–37, 2016.
- [17] A. Gorcin and H. Arslan, "Public safety and emergency case communications: Opportunities from the aspect of cognitive radio," *2008 IEEE Symposium on New Frontiers in Dynamic Spectrum Access Networks, DySPAN 2008*, pp. 591–600, 2008.
- [18] 3GPP, "Group Communication System Enablers for LTE (GCSE_LTE)," TS 23.468, 3rd Generation Partnership Project (3GPP), Dec. 2017.
- [19] 3GPP, "Proximity-based services (ProSe)," TS 23.303, 3rd Generation Partnership Project (3GPP), June 2018.
- [20] 3GPP, "Study on LTE Device to Device Proximity Services," TS 36.843, 3rd Generation Partnership Project (3GPP), Mar. 2014.
- [21] 3GPP, "Study on RAN sharing enhancements," TS 36.856, 3rd Generation Partnership Project (3GPP), June 2014.
- [22] 3GPP, "Study on isolated Evolved Universal Terrestrial Radio Access Network (E-UTRAN) operation for public safety," TR 33.897, 3rd Generation Partnership Project (3GPP), Mar. 2016.
- [23] ITU-R, "IMT Vision – Framework and overall objectives of the future development of IMT for 2020 and beyond," Tech. Rep. M.2083-0, International Telecommunication Union (ITU), Sept. 2015.
- [24] 3GPP, "Feasibility Study on New Services and Markets Technology Enablers for Critical Communications," TS 22.862, 3rd Generation Partnership Project (3GPP), Sept. 2016.
- [25] ITU-T, "The Tactile Internet," tech. rep., International Telecommunication Union (ITU), Aug. 2014.
- [26] SOFTIL Innovative Communications, "5G Technologies, Key for more Effective Mission Critical Communications." <https://www.softil.com/articles/5g-technologies-key-for-more-effective-mission-critical-communications/>.
- [27] 3GPP, "Multimedia Broadcast/Multicast Service (MBMS): Architecture and functional description," TS 23.246, 3rd Generation Partnership Project (3GPP), Dec. 2017.
- [28] L. Zhang, Y. Cai, Z. He, C. Wang, and P. Skov, "Performance evaluation of LTE MBMS baseline," in *Proceedings - 5th International Conference on Wireless Communications, Networking and Mobile Computing, WiCOM 2009*, 2009.

- [29] H. Jenkač, G. Liebl, T. Stockhammer, and W. Xu, "Retransmission Strategies for MBMS over GERAN," pp. 1773–1779, 2005.
- [30] A. Soares, A. Correia, J. C. Silva, and N. Souto, "UE counting mechanism for MBMS considering PtM macro diversity combining support in UMTS networks," *IEEE International Symposium on Spread Spectrum Techniques and Applications*, pp. 361–365, 2006.
- [31] F. Khan, *LTE for 4G mobile broadband: air interface technologies and performance*, vol. 00. 2009.
- [32] J. F. Monserrat, J. Calabuig, A. Fernández-Aguilella, and D. Gómez-Barquero, "Joint delivery of unicast and e-MBMS services in LTE networks," in *IEEE Transactions on Broadcasting*, vol. 58, pp. 157–167, 2012.
- [33] A. Alexiou, C. Bouras, V. Kokkinos, A. Papazois, and G. Tschritzis, "Efficient MCS selection for MBSFN transmissions over LTE networks," in *2010 IFIP Wireless Days, WD 2010*, 2010.
- [34] 3GPP, "Evolved Universal Terrestrial Radio Access (E-UTRA) and Evolved Universal Terrestrial Radio Access Network (E-UTRAN): Overall description," TS 36.300, 3rd Generation Partnership Project (3GPP), Sept. 2018.
- [35] E. Dahlman, S. Parkvall, and J. Skold, "4G LTE/ LTE-Advanced for Mobile Broadband," pp. 403–411, 2011.
- [36] MCC Work Plan Manager (Alain Sultan), "Release 13 analytical view version Sept. 9th 2015," TSG RP-151569, 3rd Generation Partnership Project (3GPP), Sept. 2015.
- [37] Huawei, HiSilicon, TD-Tech, SouthernLINC, Potevio, China Unicom, MediaTek Inc., CATT, "Comparison of SC-PTM and MBSFN use for Public Safety," TSG R2-151516, 3rd Generation Partnership Project (3GPP), Apr. 2015.
- [38] Nokia Networks, "Performance evaluation of UL feedback schemes for SC-PTM," TSG R2-151592, 3rd Generation Partnership Project (3GPP), Apr. 2015.
- [39] Huawei, HiSilicon, "Motivation of Rel-13 new study item proposal for support of Single-Cell Point-To-Multipoint transmission in LTE," TSG RP-141920, 3rd Generation Partnership Project (3GPP), 2011.
- [40] 3GPP, "Radio Resource Control (RRC); Protocol specification ," TS 36.331, 3rd Generation Partnership Project (3GPP), Sept. 2018.
- [41] J. Kim, S. W. Choi, W. Y. Shin, Y. S. Song, and Y. K. Kim, "Group communication over LTE: A radio access perspective," *IEEE Communications Magazine*, vol. 54, no. 4, pp. 16–23, 2016.
- [42] Ericsson, "Initial radio resource efficiency evaluation of Single-Cell PTM," TSG R2-151684, 3rd Generation Partnership Project (3GPP), Apr. 2015.

- [43] A. Alexiou, C. Bouras, V. Kokkinos, A. Papazois, and G. Tschirzits, "Spectral Efficiency Performance of MBSFN-enabled LTE Networks," in *IEEE 6th International Conference on Wireless and Mobile Computing, Networking and Communications*, pp. 361–367, 2010.
- [44] Huawei, HiSilicon, TD-Tech, "SC-PTM configuration," TSG R2-151407, 3rd Generation Partnership Project (3GPP), Apr. 2015.
- [45] A. Alexiou, C. Bouras, V. Kokkinos, and G. Tschirzits, "Communication cost analysis of MBSFN in LTE," in *IEEE International Symposium on Personal, Indoor and Mobile Radio Communications, PIMRC*, pp. 1366–1371, 2010.
- [46] N. D. Nguyen, R. Knopp, N. Nikaein, and C. Bonnet, "Implementation and validation of Multimedia Broadcast Multicast Service for LTE/LTE-advanced in OpenAirInterface platform," in *Proceedings - Conference on Local Computer Networks, LCN*, pp. 70–76, 2013.
- [47] J. S. M. Kottkamp, A. Rössler, "LTE Release 9 technology introduction," in *White Paper*, 2011.
- [48] 3GPP, "Introduction of the Multimedia Broadcast/Multicast Service (MBMS) in the Radio Access Network (RAN)," TS 25.346, 3rd Generation Partnership Project (3GPP), Mar. 2017.
- [49] L. Rong, O. B. Haddada, and S. E. Elayoubi, "Analytical analysis of the coverage of a MBSFN OFDMA network," *GLOBECOM - IEEE Global Telecommunications Conference*, pp. 2388–2392, 2008.
- [50] A. Alexiou and C. Bouras, "Forward error correction for reliable e-MBMS transmissions in LTE networks," in *Cellular Networks— Positioning, Performance Analysis, Reliability*, pp. 353–374, 2011.
- [51] 3GPP, "Study on Single-Cell Point-To-Multipoint transmission for E-UTRA," TR 36.890, 3rd Generation Partnership Project (3GPP), June 2015.
- [52] Public Safety Communications Research Program, "Extended cell testing." http://www.pscr.gov/projects/testing_evaluation/extended_cell/pscr_extended_cell_coverage.pdf, 2016.
- [53] 3GPP, "Physical layer measurements," TS 36.214, 3rd Generation Partnership Project (3GPP), Mar. 2016.
- [54] C. Ball, T. Hindelang, I. Kambourov, and S. Eder, "Spectral efficiency assessment and radio performance comparison between LTE and WiMAX," *IEEE International Symposium on Personal, Indoor and Mobile Radio Communications, PIMRC*, 2008.
- [55] 3GPP, "Physical Layer Procedures," TS 36.213, 3rd Generation Partnership Project (3GPP), Sept. 2018.
- [56] J. Fan, Q. Yin, G. Y. Li, B. Peng, and X. Zhu, "MCS selection for throughput improvement in downlink LTE systems," *Proceedings - International Conference on Computer Communications and Networks, ICCCN*, 2011.

- [57] J. C. Ikuno, M. Wrulich, and M. Rupp, "Performance and modeling of LTE H-ARQ," *Wsa 2009*, p. 6, 2009.
- [58] Y. Singh, "Comparison of Okumura , Hata and COST-231 models on the basis of path loss and signal strength," *International Journal Computer Applications (0975-8887)*, vol. 59, no. 11, pp. 37–41, 2012.
- [59] D. Ohmann, A. Awada, I. Viering, M. Simsek, and G. P. Fettweis, "Best server SINR models for single-and multi-point transmission in wireless networks," in *2015 IEEE Global Communications Conference, GLOBECOM 2015*, 2016.
- [60] S. Talarico and M. C. Valenti, "An Accurate and Efficient Analysis of a MBSFN Network," in *2014 IEEE International Conference on Acoustics, Speech and Signal Processing (ICASSP)*,, 2014.
- [61] J. M. Kelif, M. Coupechoux, and P. Godlewski, "Spatial outage probability for cellular networks," *GLOBECOM - IEEE Global Telecommunications Conference*, pp. 4445–4450, 2007.
- [62] D. Ben Cheikh, J.-M. Kelif, M. Coupechoux, and P. Godlewski, "SIR distribution analysis in cellular networks considering the joint impact of path-loss, shadowing and fast fading," *EURASIP Journal on Wireless Communications and Networking*, vol. 2011, no. 1, p. 137, 2011.
- [63] L. F. Fenton, "The Sum of Log-Normal Probability Distributions in Scatter Transmission Systems," *IRE Transactions on Communications Systems*, vol. 8, no. 1, pp. 57–67, 1960.
- [64] S. C. Schwartz and Y.-S. Yeh, "On the distribution function and moments of power sums with log-normal components," *Bell System Technical Journal*, vol. 61, no. 7, pp. 1441–1462, 1982.
- [65] A. Abu-Dayya and N. Beaulieu, "Comparison of Methods of Computing Log-normal Sum Distributions and Outages for Digital Wireless Applications," in *ICC/SUPERCOMM'94 - 1994 International Conference on Communications*, pp. 175–179, 1994.
- [66] K. C. Beh, A. Doufexi, and S. Armour, "Performance Evaluation of Hybrid ARQ Schemes of 3GPP LTE OFDMA System," in *2007 IEEE 18th International Symposium on Personal, Indoor and Mobile Radio Communications*, pp. 1–5, IEEE, 2007.
- [67] M. Gidlund and P. Ahag, "Enhanced HARQ scheme based on rearrangement of signal constellations and frequency diversity for OFDM systems," in *Vehicular Technology Conference, 2004. VTC 2004-Spring. 2004 IEEE 59th*, vol. 1, pp. 500–504, 2004.
- [68] T. Kumagai, M. Mizoguchi, T. Onizawa, H. Takanashi, and M. Morikura, "A maximal ratio combining frequency diversity ARQ scheme for OFDM signals," in *1998 IEEE 9th International Symposium on Personal, Indoor and Mobile Radio Communications*, pp. 528–532, IEEE, 1999.

- [69] A. Pokhariyal, T. Kolding, and P. Mogensen, "Performance of Downlink Frequency Domain Packet Scheduling for the UTRAN Long Term Evolution," in *2006 IEEE 17th International Symposium on Personal, Indoor and Mobile Radio Communications*, pp. 1–5, IEEE, 2006.
- [70] C. Wengerter, J. Ohlhorst, and A. Golitschek Edler von Elbwart, "Fairness and Throughput Analysis for Generalized Proportional Fair Frequency Scheduling in OFDMA," *2005 IEEE 61st Vehicular Technology Conference*, vol. 3, no. 2, pp. 1903–1907, 2005.
- [71] H. Wang and A. O. Fapojuwo, "A Survey of Enabling Technologies of Low Power and Long Range Machine-to-Machine Communications," *IEEE Communications Surveys & Tutorials*, vol. 19, no. 4, pp. 2621–2639, 2017.
- [72] M. Jeruchim, P. Balaban, and K. Shanmugan, *Simulation of communication systems: modeling, methodology, and techniques*. Springer Science & Business Media, 2000.
- [73] J. G. Proakis and M. Salehi, *Digital Communications*. McGraw-Hill Higher Education, 2001.
- [74] D. Greenwood and L. Hanzo, *Characterization of Mobile Radio Channels*. Pentech Press, London, 1994.
- [75] R. H. Clarke, "A Statistical Theory of Mobile-Radio Reception," *Bell System Technical Journal*, vol. 47, no. 6, pp. 957–1000, 1968.
- [76] W. Jakes, *Microwave Mobile Communications*. Wiley-IEEE Press, 1974.
- [77] M. Patzold, Cheng-Xiang Wang, and B. Hogstad, "Two New Sum-of-Sinusoids-Based Methods for the Efficient Generation of Multiple Uncorrelated Rayleigh Fading Waveforms," *IEEE Transactions on Wireless Communications*, vol. 8, pp. 3122–3131, 2009.
- [78] M. F. Pop and N. C. Beaulieu, "Limitations of sum-of-sinusoids fading channel simulators," *IEEE Transactions on Communications*, vol. 49, no. 4, pp. 699–708, 2001.
- [79] M. Pätzold, R. Garcia, and F. Laue, "Design of high-speed simulation models for mobile fading channels by using table look-up techniques," *IEEE Transactions on Vehicular Technology*, vol. 49, no. 4, pp. 1178–1190, 2000.
- [80] P. Dent, G. Bottomley, and T. Croft, "Jakes fading model revisited," *Electronics Letters*, vol. 29, no. 13, p. 1162, 1993.
- [81] Y. R. Zheng and C. Xiao, "Simulation models with correct statistical properties for Rayleigh fading channels," *IEEE Transactions on Communications*, vol. 51, no. 6, pp. 920–928, 2003.
- [82] "Simulate, analyze, and test the physical layer of LTE and LTE-Advanced wireless communications systems," 2017. The MathWorks, Natick, MA, USA. Available on mathworks.com.

- [83] C. Mehlhruer, M. Wrulich, J. C. Ikuno, D. Bosanska, and M. Rupp, "Simulating the long term evolution physical layer," *17th European Signal Processing Conference (EUSIPCO 2009)*, Glasgow, Scotland, vol. 27, no. Eusipco, p. 124, 2009.
- [84] X. He, K. Niu, Z. He, and J. Lin, "Link layer abstraction in MIMO-OFDM system," *2007 International Workshop on Cross Layer Design, IWCLD 2007*, pp. 41–44, 2007.
- [85] K. Ramadas and R. Jain, "WiMAX system evaluation methodology," in *Wimax Forum*, Jan, 2007.
- [86] Ericsson, "System-level evaluation of OFDM - further considerations," TSG R1-031303, 3rd Generation Partnership Project (3GPP), Nov. 2003.
- [87] M. Pauli, U. Wachsmann, and S.-H. S. Tsai, "Quality determination for a wireless communications link," June 12 2007. US Patent 7,231,183.
- [88] 3GPP, "Base Station (BS) radio transmission and reception," TS 36.104, 3rd Generation Partnership Project (3GPP), Sept. 2017.
- [89] Q. Huynh-Thu and M. Ghanbari, "Scope of validity of PSNR in image/video quality assessment," *Electronics Letters*, vol. 44, no. 13, p. 800, 2008.
- [90] Z. Wang, A. Bovik, H. Sheikh, and E. Simoncelli, "Image Quality Assessment: From Error Visibility to Structural Similarity," *IEEE Transactions on Image Processing*, vol. 13, pp. 600–612, 4 2004.
- [91] M. Solera, M. Toril, I. Palomo, G. Gomez, and J. Poncela, "A Testbed for Evaluating Video Streaming Services in LTE," *Wireless Personal Communications*, vol. 98, no. 3, pp. 1–21, 2017.
- [92] R. Zhang, S. L. Regunathan, and K. Rose, "Video coding with optimal inter/intra-mode switching for packet loss resilience," *IEEE Journal on Selected Areas in Communications*, vol. 18, no. 6, pp. 966–976, 2000.
- [93] 3GPP, "NR; Base Station Radio Transmission and Reception," TS 38.104, 3rd Generation Partnership Project (3GPP), Sept. 2018.
- [94] A. Papadogiannis, D. Gesbert, and E. Hardouin, "A Dynamic Clustering Approach in Wireless Networks with Multi-Cell Cooperative Processing," in *2008 IEEE International Conference on Communications*, pp. 4033–4037, 2008.
- [95] M. Yoon, M.-S. Kim, and C. Lee, "A Dynamic Cell Clustering Algorithm for Maximization of Coordination Gain in Uplink Coordinated System," *IEEE Transactions on Vehicular Technology*, vol. 65, pp. 1752–1760, 2016.
- [96] Y. Du and G. de Veciana, "'Wireless networks without edges': Dynamic radio resource clustering and user scheduling," in *2014 IEEE Conference on Computer Communications (INFOCOM)*, pp. 1321–1329, 2014.
- [97] P. Baracca, F. Boccardi, and N. Benvenuto, "A dynamic clustering algorithm for downlink CoMP systems with multiple antenna UEs," *EURASIP Journal on Wireless Communications and Networking*, pp. 1–14, 2014.

- [98] S. Scholz, "Combining dynamic clustering and scheduling for coordinated multipoint transmission in LTE," in *2017 IEEE 28th Annual International Symposium on Personal, Indoor, and Mobile Radio Communications (PIMRC)*, pp. 1–7, 2017.
- [99] D. Liu, S. Han, C. Yang, and Q. Zhang, "Semi-dynamic User-Specific Clustering for Downlink Cloud Radio Access Network," *IEEE Transactions on Vehicular Technology*, vol. 65, pp. 2063–2077, 2016.
- [100] V. Garcia, Y. Zhou, and J. Shi, "Coordinated multipoint transmission in dense cellular networks with user-centric adaptive clustering," *IEEE Transactions on Wireless Communications*, vol. 13, no. 8, pp. 4297–4308, 2014.
- [101] L. Liu, Y. Zhou, V. Garcia, L. Tian, and J. Shi, "Load Aware Joint CoMP Clustering and Inter-Cell Resource Scheduling in Heterogeneous Ultra Dense Cellular Networks," *IEEE Transactions on Vehicular Technology*, vol. 67, pp. 2741–2755, 2018.
- [102] S. Basso, M. Jaber, M. A. Imran, and P. Xiao, "Load Aware Self-Organising User-Centric Dynamic CoMP Clustering for 5G Networks," *IEEE Access*, vol. 4, pp. 2895–2906, 2016.
- [103] Z. Zhang, N. Wang, J. Zhang, X. Mu, and K. M. Wong, "Cooperation resource efficient user-centric clustering for QoS provisioning in uplink CoMP," in *2017 IEEE 18th International Workshop on Signal Processing Advances in Wireless Communications (SPAWC)*, pp. 1–5, 2017.
- [104] L. Rong, S. E. Elayoubi, and O. B. Haddada, "Performance evaluation of cellular networks offering TV services," *IEEE Transactions on Vehicular Technology*, vol. 60, no. 2, pp. 644–655, 2011.
- [105] J. Chen, M. Chiang, J. Erman, G. Li, K. Ramakrishnan, and R. K. Sinha, "Fair and optimal resource allocation for LTE multicast (eMBMS): Group partitioning and dynamics," in *2015 IEEE Conference on Computer Communications (INFOCOM)*, pp. 1266–1274, 2015.
- [106] J. W. Roberts, "A service system with heterogeneous user requirements," in *Performance of Data Communications systems and their applications*, vol. 29, pp. 423–431, 1981.
- [107] F. Bach, "Learning with Submodular Functions: A Convex Optimization Perspective," 2011.
- [108] S. Fujishige, "Lexicographically Optimal Base of a Polymatroid with Respect to a Weight Vector," *Mathematics of Operations Research*, vol. 5, no. 2, pp. 186–196, 1980.
- [109] P. Wolfe, "Finding the nearest point in A polytope," *Mathematical Programming*, vol. 11, no. 1, pp. 128–149, 1976.
- [110] S. Fujishige, "Submodular systems and related topics," in *Mathematical Programming at Oberwolfach II*, pp. 113–131, 1984.

-
- [111] D. Chakrabarty, P. Jain, and P. Kothari, "Provable Submodular Minimization using Wolfe's Algorithm," in *Advances in Neural Information Processing Systems 27 (NIPS 2014)*, vol. 2014, pp. 1–9, 2014.
- [112] D. G. Luenberger, Y. Ye, *et al.*, *Linear and nonlinear programming*, vol. 2. Springer, 1984.
- [113] A. Ravindran, G. V. Reklaitis, and K. M. Ragsdell, *Engineering optimization: methods and applications*. John Wiley & Sons, 2006.
- [114] J. A. Nelder and R. Mead, "A Simplex Method for Function Minimization," *The Computer Journal*, vol. 7, no. 4, pp. 308–313, 1965.
- [115] W. Spendley, G. R. Hext, and F. R. Himsworth, "Sequential application of simplex designs in optimisation and evolutionary operation," *Technometrics*, vol. 4, no. 4, pp. 441–461, 1962.
- [116] V. J. Torczon, *Multidirectional search: a direct search algorithm for parallel machines*. PhD thesis, Rice University, 1989.
- [117] C. T. Kelley, "Iterative Methods for Optimization," *Siam*, p. 188, 1999.
- [118] M. A. Luersen and R. Le Riche, "Globalized Nelder-Mead method for engineering optimization," *Computers and Structures*, vol. 82, no. 23-26, pp. 2251–2260, 2004.
- [119] S. Singer, "Complexity analysis of Nelder-Mead search iterations," *Conference on Applied Mathematics and Computation*, pp. 185–196, 1999.
- [120] N. B. Mehta, J. Wu, A. F. Molisch, and J. Zhang, "Approximating a sum of random variables with a lognormal," 2007.
- [121] F. Bach, "Learning with Submodular Functions: A Convex Optimization Perspective," *Foundations and Trends in Machine Learning*, vol. 6, no. 2-3, pp. 145–373, 2013.
- [122] F. Bach, "Convex Analysis and Optimization with Submodular Functions: a Tutorial," *arXiv preprint*, 2010.
- [123] L. Lovász, "Submodular Functions and Optimization," 1983.
- [124] S. Boyd and L. Vandenberghe, *Convex Optimization*. Cambridge: Cambridge University Press, 2004.
- [125] S. T. McCormick, *Submodular Function Minimization*, vol. 3a. Elsevier, K. Aardal, G. Nemhauser, and R. Weismantel, editors, 2007.

Appendix A

Submodular Functions Minimization

A.1 Introduction

In this chapter, we show how to minimize a submodular function F over $\{0, 1\}^n$. The process involves several steps. The first step is to extend F to $[0, 1]^n$ using the Lovász extension f . It turns out that this extension is convex when F is submodular and that the minimizers of f and F coincide. This extension is equivalent to the convex closure of F . The second step consists in relating a regularized version of the Lovász extension minimization problem with a regularized version of the original set function minimization problem. This allows to characterize the minimizer of F . The third step consists in studying the dual of the regularized Lovász extension minimization problem and showing that it is equivalent to minimize the norm over a base polyhedron defined from F . The last step is a minimum-norm algorithm to find the solution.

A.2 Submodular Functions

A.2.1 Notations

We consider a finite set $V = \{b_1, \dots, b_n\}$ of n elements and its power set 2^V , composed of the 2^n subsets of V . Every subset S of V can be represented by a vector in $\{0, 1\}^n$ denoted $\mathbf{1}_S$, which has 1 at the positions of the elements of S and 0 elsewhere. Take now $x \in \mathbb{R}^n$, a vector of n real components. We denote x_b the component of x corresponding to the element $b \in V$. We denote also $x(S) = \sum_{b \in S} x_b = \mathbf{1}_S^T x$. A set function F is a function from 2^V to \mathbb{R} ; equivalently, we can write: $F : \{0, 1\}^V \rightarrow \mathbb{R}$. We will always assume in the rest of this chapter that $F(\emptyset) = 0$.

A.2.2 Definitions

Definition 3 ([121]). *The set function $F : 2^V \rightarrow \mathbb{R}$ is submodular if and only if, for all subsets $A, B \subseteq V$, we have: $F(A) + F(B) \geq F(A \cup B) + F(A \cap B)$.*

A function F is *supermodular* if $-F$ is submodular and a function F that is both submodular and supermodular is called *modular*. A function F is modular if and only if there exists $s \in \mathbb{R}^n$ such that $F(A) = \sum_{k \in A} s_k$ for all $A \subseteq V$ and we have $s_k = F(\{k\})$. An equivalent definition of submodularity is the following:

Definition 4 ([121]). *The set function $F : 2^V \rightarrow \mathbb{R}$ is submodular if and only if, for all subsets $A, B \subseteq V$ and $b \in V$ such that $A \subseteq B$ and $b \notin B$, we have: $F(A \cup b) - F(A) \geq F(B \cup b) - F(B)$.*

Two important sets play a role in submodular function minimization.

Definition 5 ([121]). Let F be a submodular function such that $F(\emptyset) = 0$. The submodular polyhedron \mathcal{P}_F and the base polyhedron \mathcal{B}_F are defined as:

$$\begin{aligned} \mathcal{P}_F &= \{x \in \mathbb{R}^n : x(A) \leq F(A) \text{ for all } A \subseteq V\} \\ \mathcal{B}_F &= \{x \in \mathcal{P}_F : x(V) = F(V)\} \end{aligned}$$

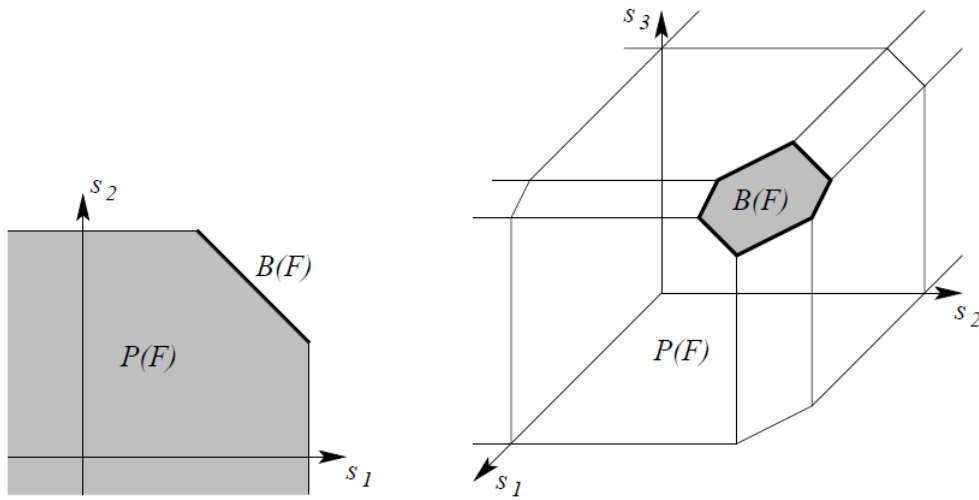


Figure A.1 Submodular Polyhedron $P(F)$ and base polyhedron $B(F)$ for $n = 2$ (left) and $n = 3$ [122].

A.2.3 Submodular Functions Properties

The linear combination of submodular functions is submodular. The multiplication by a positive scalar preserves submodularity. Point-wise minimum or maximum of submodular functions are however not necessary submodular.

A.3 Submodular Function Minimization

A.3.1 Problem Formulation

We consider the following problem:

$$\min_{S \subseteq V} F(S) \tag{A.1}$$

where F is a submodular function such that $F(\emptyset) = 0$. The objective is to find a minimizer set $S \subseteq V$ satisfying $F(S) \leq F(A)$ for every $A \subseteq V$. Exhaustive search is infeasible as the number of subsets grows exponentially with the number of elements in V .

A.3.2 Lovász Extension

The Lovász extension f of a set function F is an extension that is tight in the sense that coincides with F at integer values, and that has the same minimizers as F . When F is submodular, the Lovász extension is equivalent to the convex closure of F , it is however easier to compute.

Definition 6 ([123]). Let $F : 2^V \rightarrow \mathbb{R}$ be a set function such that $F(\emptyset) = 0$. For $x \in \mathbb{R}^n$, let $\{j_1, \dots, j_n\}$ be a permutation of the elements of V such that $x_{j_1} \geq x_{j_2} \geq \dots \geq x_{j_n}$. Then, the Lovász extension of F is the function $f : \mathbb{R}^n \rightarrow \mathbb{R}$ defined as:

$$f(x) = \sum_{k=1}^{n-1} (x_{j_k} - x_{j_{k+1}}) F(\{j_1, \dots, j_k\}) + x_{j_n} F(V) \quad (\text{A.2})$$

$$= \sum_{k=1}^n x_{j_k} (F(\{j_1, \dots, j_k\}) - F(\{j_1, \dots, j_{k-1}\})) \quad (\text{A.3})$$

with the convention that $F(\{j_1, \dots, j_{k-1}\}) = 0$ when $k = 1$.

Lemma 7. Let $F : 2^V \rightarrow \mathbb{R}$ be a set function such that $F(\emptyset) = 0$ and f its Lovász extension. We have:

$$f(x) = \int_{-\infty}^0 [F(\{x \geq z\}) - F(V)] dz + \int_0^{\infty} F(\{x \geq z\}) dz. \quad (\text{A.4})$$

Proof. Note that the function of z , $g(z) \triangleq F(\{x \geq z\})$ is piece-wise linear: $g(z) = 0$ for $z > x_{j_1}$; $g(z) = F(V)$ for $z \leq x_{j_n}$; and $g(z) = F(\{j_1, \dots, j_k\})$ when $x_{j_{k+1}} < z \leq x_{j_k}$. By substituting these expressions in (A.4), we obtain (A.2). \square

Theorem 1 ([121, 123]). Let $F : 2^V \rightarrow \mathbb{R}$ be a submodular function such that $F(\emptyset) = 0$ and $f : \mathbb{R}^n \rightarrow \mathbb{R}$ its Lovász extension. For $x \in \mathbb{R}^n$, let $\{j_1, \dots, j_n\}$ be a permutation of the elements of V such that $x_{j_1} \geq x_{j_2} \geq \dots \geq x_{j_n}$. Define $s^* \in \mathbb{R}^n$ such that:

$$s_{j_k}^* = F(\{j_1, \dots, j_k\}) - F(\{j_1, \dots, j_{k-1}\}). \quad (\text{A.5})$$

We have:

$$f(x) = \max_{s \in \mathcal{B}_F} x^T s = x^T s^* \quad (\text{A.6})$$

$$s^* = \arg \max_{s \in \mathcal{B}_F} x^T s \quad (\text{A.7})$$

Proof. We first verify that s^* is in \mathcal{B}_F when F is submodular. For any $S \subseteq V$, we have:

$$\begin{aligned}
s^*(S) &= s^* \mathbf{1}_S^T \\
&= \sum_{k=1}^n s_{j_k} \mathbf{1}_{j_k \in S} \\
&= \sum_{k=1}^n \mathbf{1}_{j_k \in S} (F(\{j_1, \dots, j_k\}) - F(\{j_1, \dots, j_{k-1}\})) \\
&\stackrel{(a)}{\leq} \sum_{k=1}^n \mathbf{1}_{j_k \in S} (F(S \cap \{j_1, \dots, j_k\}) - F(S \cap \{j_1, \dots, j_{k-1}\})) \\
&\stackrel{(b)}{=} \sum_{k=1}^n (F(S \cap \{j_1, \dots, j_k\}) - F(S \cap \{j_1, \dots, j_{k-1}\})) \\
&= F(S).
\end{aligned}$$

The inequality (a) is obtained by using the definition of submodularity. When $S = V$, we have equality, so that $s(V) = F(V)$. In (b), if $j_k \notin S$, then $F(S \cap \{j_1, \dots, j_k\}) = F(S \cap \{j_1, \dots, j_{k-1}\}) = F(\emptyset) = 0$, so that we don't add new terms on the right side of the equation. We conclude that $s^* \in \mathcal{B}_F$.

We now show that s^* is an optimizer of the problem (A.6) by exhibiting a pair of primal-dual solutions achieving the same value of the primal and dual objective functions $x^T s^*$. The equation (A.6) is a linear program which is equivalent to

$$\min_{s \in \mathbb{R}^n} \{-x^T s, \text{ s.t. } s(S) \leq F(S), \forall S \subseteq V, s(V) = F(V)\}.$$

Its Lagrange dual function is:

$$g(\lambda) = \inf_s (-x^T s + \sum_{S \subseteq V} \lambda_S (s(S) - F(S))) \quad (\text{A.8})$$

$$= \begin{cases} -\sum_{S \subseteq V} \lambda_S F(S) & \text{if } x = \sum_{S \subseteq V} \lambda_S \mathbf{1}_S \\ -\infty & \text{otherwise} \end{cases} \quad (\text{A.9})$$

The dual problem is thus:

$$\max_{\lambda_S} -\sum_{S \subseteq V} \lambda_S F(S) \quad (\text{A.10})$$

$$\text{s.t. } x = \sum_{S \subseteq V} \lambda_S \mathbf{1}_S \quad (\text{A.11})$$

$$\lambda_S \geq 0, \forall S \subsetneq V \quad (\text{A.12})$$

Or equivalently:

$$\min_{\lambda_S} \sum_{S \subseteq V} \lambda_S F(S) \quad (\text{A.13})$$

$$\text{s.t. } x = \sum_{S \subseteq V} \lambda_S \mathbf{1}_S \quad (\text{A.14})$$

$$\lambda_S \geq 0, \forall S \subsetneq V \quad (\text{A.15})$$

Note that the Lagrange multiplier associated to V need not to be positive. Define the dual variables as follows:

$$\lambda_S^* = \begin{cases} x_{j_k} - x_{j_{k+1}} & \text{if } S = \{j_1, \dots, j_k\}, k = 1, \dots, n-1 \\ x_{j_n} & \text{if } S = V \\ 0 & \text{otherwise} \end{cases} \quad (\text{A.16})$$

These variables are positive when $S \neq V$ and verify the first constraint of the dual function:

$$\begin{aligned} \sum_{S \subseteq V} \lambda_S^* \mathbf{1}_S &= \sum_{k=1}^{n-1} (x_{j_k} - x_{j_{k+1}}) \mathbf{1}_{\{j_1, \dots, j_k\}} + x_{j_n} \mathbf{1}_V \\ &= \sum_{k=1}^n x_{j_k} \mathbf{1}_{\{j_1, \dots, j_k\}} - \sum_{k=2}^n x_{j_k} \mathbf{1}_{\{j_1, \dots, j_{k-1}\}} \\ &= x_{j_1} \mathbf{1}_{\{j_1\}} + \sum_{k=2}^n x_{j_k} (\mathbf{1}_{\{j_1, \dots, j_k\}} - \mathbf{1}_{\{j_1, \dots, j_{k-1}\}}) \\ &= x. \end{aligned}$$

Now the dual objective is:

$$\begin{aligned} \sum_{S \subseteq V} \lambda_S^* F(S) &= \sum_{k=1}^{n-1} (x_{j_k} - x_{j_{k+1}}) F(\{j_1, \dots, j_k\}) + x_{j_n} F(V) \\ &= \sum_{k=1}^n x_{j_k} F(\{j_1, \dots, j_k\}) - \sum_{k=2}^n x_{j_k} F(\{j_1, \dots, j_{k-1}\}) \\ &= x_{j_1} F(\{j_1\}) + \sum_{k=2}^n x_{j_k} (F(\{j_1, \dots, j_k\}) - F(\{j_1, \dots, j_{k-1}\})) \\ &= \sum_{k=1}^n x_{j_k} (F(\{j_1, \dots, j_k\}) - F(\{j_1, \dots, j_{k-1}\})) \\ &= x^T s^*. \end{aligned} \quad (\text{A.17})$$

With these definitions of s^* and λ_{s^*} , the primal and dual objective functions are thus equal. As \mathcal{B}_F has a non-empty interior (it contains s^*), we have a pair of primal-dual solutions. We see from (A.17) that the objective value at optimal corresponds to the definition (A.2) of the Lovász extension, this justifies the equivalence of the two definitions.

From the equation:

$$f(x) = \sum_{k=1}^{n-1} (x_{j_k} - x_{j_{k+1}}) F(\{j_1, \dots, j_k\}) + x_{j_n} F(V),$$

we deduce that for any $S \subseteq V$, $f(\mathbf{1}_S) = F(S)$ and that f is indeed an extension of F . \square

Proposition 4. *The Lovász extension is convex if and only if F is submodular.*

Proof. If F is submodular, we have seen that $f(x) = \max_{s \in \mathcal{B}_F} x^T s$, the Lovász extension is thus a point-wise maximum of convex functions over a convex set. It is thus a convex function. Assume now that f is convex and take $A, B \subseteq V$. We have: $\mathbf{1}_A + \mathbf{1}_B = \mathbf{1}_{A \cup B} + \mathbf{1}_{A \cap B}$ and $f(2(0.5\mathbf{1}_A + 0.5\mathbf{1}_B)) = 2f(0.5\mathbf{1}_A + 0.5\mathbf{1}_B) \leq f(\mathbf{1}_A) + f(\mathbf{1}_B)$. The first equality is due to the fact that f is 2-homogeneous and the inequality is by convexity. We have:

$$\begin{aligned} F(A) + F(B) &\stackrel{(a)}{=} f(\mathbf{1}_A) + f(\mathbf{1}_B) \\ &\geq f(\mathbf{1}_{A \cup B} + \mathbf{1}_{A \cap B}) \\ &\stackrel{(b)}{=} F(A \cup B) + F(A \cap B) \end{aligned}$$

(a) results from the fact that f is an extension of F . (b) is from the definition of f : let $x = \mathbf{1}_{A \cup B} + \mathbf{1}_{A \cap B}$. We have:

$$x_i = \begin{cases} 2 & \text{if } i \in A \cap B \\ 1 & \text{if } i \in A \Delta B \\ 0 & \text{otherwise} \end{cases} \quad (\text{A.18})$$

With the notations of the definition: $A \cap B = \{j_1, \dots, j_m\}$, $A \Delta B = \{j_{m+1}, \dots, j_p\}$ and $V \setminus (A \cup B) = \{j_{p+1}, \dots, j_n\}$ for some integers m and p . Now:

$$\begin{aligned} f(x) &= \sum_{k=1}^{n-1} (x_{j_k} - x_{j_{k+1}}) F(\{j_1, \dots, j_k\}) + x_{j_n} F(V) \\ &= F(\{j_1, \dots, j_m\}) + F(\{j_1, \dots, j_p\}) \\ &= F(A \cup B) + F(A \cap B). \end{aligned} \quad (\text{A.19})$$

\square

Proposition 5. Let F be a submodular function such that $F(\emptyset) = 0$ and f its Lovász extension. Then:

$$\min_{S \subseteq V} F(S) = \min_{x \in [0;1]^n} f(x). \quad (\text{A.20})$$

Proof. It is clear that $\min_{S \subseteq V} F(S) \geq \min_{x \in [0;1]^n} f(x)$. Now we have for $x \in [0;1]^n$:

$$\begin{aligned} f(x) &= \sum_{k=1}^{n-1} (x_{j_k} - x_{j_{k+1}}) F(\{j_1, \dots, j_k\}) + x_{j_n} F(V) \\ &\geq \sum_{k=1}^{n-1} (x_{j_k} - x_{j_{k+1}}) \min_{S \subseteq V} F(S) + x_{j_n} \min_{S \subseteq V} F(S) \\ &= x_{j_1} \min_{S \subseteq V} F(S) \\ &\geq \min_{S \subseteq V} F(S). \end{aligned}$$

The last inequality is obtained by noticing that $x_{j_1} \in [0;1]$ and $\min_{S \subseteq V} F(S) \leq F(\emptyset)$, i.e., $\min_{S \subseteq V} F(S) \leq 0$. \square

A.3.3 Convex Closure

There is a relationship between the Lovász extension and a classical way of dealing with the minimization of a discrete function F , which is to consider its convex closure f^- . The convex closure of F is the point-wise greatest convex function underestimating F . When F is submodular, the Lovász extension and the convex closure coincide.

Proposition 6. Let $F : 2^V \rightarrow \mathbb{R}$ be a set function. The value of the convex closure $f^- : [0,1]^n \rightarrow \mathbb{R}$ in x is the solution of the following problem:

$$\min_{\lambda_S, S \subseteq V} \sum_{S \subseteq V} \lambda_S F(S) \quad (\text{A.21})$$

$$s.t. \quad \sum_{S \subseteq V} \lambda_S \mathbf{1}_S = x \quad (\text{A.22})$$

$$\sum_{S \subseteq V} \lambda_S = 1 \quad (\text{A.23})$$

$$\lambda_S \geq 0, \forall S \in V. \quad (\text{A.24})$$

Proof. 1) f^- is tight at F : If $x = \mathbf{1}_S$ for some S , then $\lambda_S = 1$ and $\lambda_{S'} = 0$ for $S' \neq S$ and the objective is $F(S)$ so that $f^-(\mathbf{1}_S) = F(S)$.

2) f^- is convex: Take $x, y, z \in [0,1]^n$ and $\theta \in [0,1]$ such that $z = \theta x + (1 - \theta)y$. Let λ_S and λ'_S be the minimizing coefficients associated to x and y respectively. Let

$\mu_S = \theta \lambda_S + (1 - \theta) \lambda'_S$. We have: $\sum \mu_S = 1$, $\mu_S \geq 0$ and $\sum \mu_S \mathbf{1}_S = z$. So by definition of $f^-(z)$:

$$f^-(z) \leq \sum \mu_S F(S) \quad (\text{A.25})$$

$$= \theta f^-(x) + (1 - \theta) f^-(y). \quad (\text{A.26})$$

3) f^- is the point-wise greatest convex function underestimating F : Take g a convex function underestimating F and $x \in [0, 1]^n$. Let λ_S be the coefficients defining x in the minimization problem above. We have:

$$g(x) = g\left(\sum \lambda_S \mathbf{1}_S\right) \quad (\text{A.27})$$

$$\leq \sum_S \lambda_S g(\mathbf{1}_S) \quad (\text{A.28})$$

$$= \sum_S \lambda_S F(S) \quad (\text{A.29})$$

$$= f^-(x). \quad (\text{A.30})$$

The first inequality is obtained by the convexity of g and the third equality is from the fact that g and F coincide on $\{0, 1\}^n$. \square

Remark 1. The function f^- is the Fenchel bi-conjugate of the function $g : \mathbb{R}^n \rightarrow \mathbb{R}$, such that $g(\mathbf{1}_S) = F(S)$ and $g(x) = -\infty$ if x is not the indicator function of a subset of V .

Proposition 7. Let $F : 2^V \rightarrow \mathbb{R}$ be a set function and $f^- : [0, 1]^n \rightarrow \mathbb{R}$ its convex closure. We have: (i)

$$\min_{A \subseteq V} F(A) = \min_{x \in [0, 1]^n} f^-(x); \quad (\text{A.31})$$

(ii) the minimizers of F on $\{0, 1\}^n$ are also minimizers of f^- on $[0, 1]^n$; (iii) if x is a minimizer of f^- , every subset in the support of $\{\lambda_S\}$ such that $x = \sum_{S \subseteq V} \lambda_S \mathbf{1}_S$ is a minimizer of F .

Proof. (i) Clearly $\min_{A \subseteq V} F(A) \geq \min_{x \in [0, 1]^n} f^-(x)$ as F and f^- coincide on $\{0, 1\}^n$. On the other hand, $f^-(x)$ can be seen in (A.31) as the expected value of F with respect to a random variable over $\{0, 1\}^n$ with probability mass function defined by the λ_S . As a consequence, $f^-(x)$ cannot be less than the smallest value of F , i.e., for all $x \in [0, 1]^n$, $f^-(x) \geq \min_{A \subseteq V} F(A)$ and $\min_{x \in [0, 1]^n} f^-(x) \geq \min_{A \subseteq V} F(A)$. (ii) Using the same interpretation, we see that the minimizers of f^- necessary includes extreme points in $\{0, 1\}^n$, i.e., points that are minimizers of F . (iii) Let x be a minimizer of f^- with $f^-(x) = \sum_S \lambda_S F(S)$. Assume that there are two sets S_1 and S_2 such that $\lambda_{S_1} \neq 0$, $\lambda_{S_2} \neq 0$ and $F(S_1) < F(S_2)$. Define $\tilde{x} = \sum_S \tilde{\lambda}_S F(S)$ with $\tilde{\lambda}_S = \lambda_S$ for all $S \notin \{S_1, S_2\}$, $\tilde{\lambda}_{S_2} = 0$, and $\tilde{\lambda}_{S_1} = \lambda_{S_1} + \lambda_{S_2}$. Then

$f^-(\tilde{x}) < f^-(x)$ which is a contradiction. As a consequence, in the definition of $f^-(x)$ all $F(S)$ are equal and the conclusion follows. \square

We see that the convex closure of F is an extension of F that allows to relax the discrete problem on $\{0, 1\}^n$ to a continuous problem on $[0, 1]^n$. However, as it is defined as the result of an optimization problem, the convex closure is still difficult to handle and to optimize. When F is submodular however, we have the following result (we refer to [121] for the proof).

Proposition 8. *The Lovász extension coincides with the convex closure when F is submodular, i.e., $f^- = f$.*

A.4 Equivalent Optimization Problems

In this section, we make a detour through a related set of optimization problems, namely $\min_S F(S) + \alpha|S|$. Note that this set includes our original problem by setting $\alpha = 0$. When $\alpha \neq 0$, the problem is a regularized version of the original problem, where a penalty is put on the cardinality of the set S . Although the problem looks more difficult, we will see that it will allow us to easily find a minimal minimizer of F , i.e., a set S that minimizes F and is of minimum cardinality among the minimizers of F .

A.4.1 Minimal Minimzer

We start by defining the set of regularized problems and by showing how we can compute the solutions from the solution to its extension in \mathbb{R}^n .

Proposition 9. *Let F be a submodular function and f its Lovász extension. For $\alpha \in \mathbb{R}$, consider the related following problems:*

$$\min_{x \in \mathbb{R}^n} f(x) + \frac{1}{2} \|x\|_2^2 \quad (\text{A.32})$$

$$\min_{S \subseteq V} F(S) + \alpha|S| \quad (\text{A.33})$$

Let S_α^* be a solution of (A.33), i.e., $S_\alpha^* \in \arg \min_{S \subseteq V} F(S) + \alpha|S|$ and define $u^* \in \mathbb{R}^n$ by $u_j^* = \sup\{\alpha \in \mathbb{R} \mid j \in S_\alpha^*\}$, $j = 1, \dots, n$. We have the following results:

1. If $\alpha < \beta$ then $S_\beta^* \subseteq S_\alpha^*$.
2. $\{j \mid u_j^* > \alpha\} \subseteq S_\alpha^* \subseteq \{j \mid u_j^* \geq \alpha\}$

3. u^* is the unique solution of (A.32).

4. The set $\{j \in V | u_j^* > \alpha\}$ is the minimal minimizer of (A.33).

Proof. Note first that for a α sufficiently small, $S_\alpha^* = V$ and any j belongs to S_α^* , so that the set $\{\alpha \in \mathbb{R} | j \in S_\alpha^*\}$ is non empty. We have also $S_\alpha^* = \emptyset$ for α sufficiently large, so that the $\{\alpha \in \mathbb{R} | j \in S_\alpha^*\}$ is upper bounded. This means that u_j^* is well-defined and finite.

(1): It is easy to check that if $\alpha < \beta$ then $S_\beta^* \subseteq S_\alpha^*$.

(2): Take some $j \in \{j | u_j^* > \alpha\}$. As $u_j^* > \alpha$, there exists $\beta \in (\alpha, u_j^*)$. As $\beta < u_j^*$, $j \in S_\beta^*$ by definition of u_j^* . By (1), we have $S_\beta^* \subseteq S_\alpha^*$, so that $j \in S_\alpha^*$. Take some j such that $u_j^* < \alpha$. By definition of u_j^* , $j \notin S_\alpha^*$, so that $S_\alpha^* \subseteq \{j | u_j^* \geq \alpha\}$.

(3) Let $w \in \mathbb{R}^n$. Define $\beta = \min\{w_j, u_j^* | j = 1, \dots, n\}$. Define $\Phi(x_j) = \frac{1}{2}x_j^2$, so that $\Phi'(x_j) = x_j$ and $f(x) + \frac{1}{2}\|x\|^2 = f(x) + \sum_{j=1}^n \Phi(x_j)$. We have the following equalities from basic integration and the definition of the Lovász extension (see A.4):

$$\begin{aligned} \Phi(u_j^*) &= \Phi(\beta) + \int_{\beta}^{u_j^*} \Phi'(\alpha) d\alpha = \Phi(\beta) + \int_{\beta}^{\infty} \Phi'(\alpha) \mathbf{1}\{\alpha \leq u_j^*\} d\alpha \\ f(u^*) &= \int_{\beta}^0 [F(\{u^* \geq \alpha\}) - F(V)] d\alpha + \int_0^{\infty} F(\{u^* \geq \alpha\}) d\alpha \\ &= \int_{\beta}^0 F(\{u^* \geq \alpha\}) d\alpha + \beta F(V). \end{aligned}$$

We have now:

$$\begin{aligned} f(u^*) + \sum_{j=1}^n \Phi(u_j^*) &= C + \int_{\beta}^{\infty} [F(\{u^* \geq \alpha\}) + \sum_{j=1}^n \Phi'(\alpha) \mathbf{1}\{\alpha \leq u_j^*\}] d\alpha \\ &= C + \int_{\beta}^{\infty} (F(S_\alpha^*) + \alpha |S_\alpha^*|) d\alpha \\ &\leq C + \int_{\beta}^{\infty} [F(\{w \geq \alpha\}) + \sum_{j=1}^n \Phi'(\alpha) \mathbf{1}\{w \geq \alpha\}] d\alpha \\ &= f(w) + \sum_{j=1}^n \Phi(w_j), \end{aligned} \tag{A.34}$$

where $C = n\Phi(\beta) + \beta F(V)$. The second equality uses the fact that $\{j | u_j^* > \alpha\} \subseteq S_\alpha^* \subseteq \{j | u_j^* \geq \alpha\}$ (whether the inequality is strict or not doesn't play any role when integration is considered). The inequality is obtained by noticing that for every α , S_α^* minimizes $F(S) + \alpha|S|$. The last inequality is obtained by performing the same sequence of steps for w as for u^* . We conclude that u^* is the unique minimizer of (A.32).

(4) If α is not a value taken by some u_j^* , then S_α^* is uniquely defined as $\{j|u_j^* > \alpha\} = S_\alpha^* = \{j|u_j^* \geq \alpha\}$ and $\{j|u_j^* > \alpha\}$ is indeed a minimal minimizer of (A.33). Otherwise, by taking the limit of S_β^* when $\beta \rightarrow \alpha^+$, we see that $\{j|u_j^* > \alpha\}$ is indeed a minimizer of (A.33). \square

From this proposition, we see that if we have the unique solution u^* of (A.32), we can deduce the minimal minimizer of (A.33) for any α . In particular, $\{u > 0\}$ is the minimal minimizer of $\min_{S \subseteq V} F(S)$. But it turns out that (A.32) can be efficiently solved using the mini-max theorem (or saddle-point property) as shown below.

Lemma 8. *Let F be a submodular function and f its Lovász extension. The two following problems are dual from each other:*

$$\min_{x \in \mathbb{R}^n} f(x) + \frac{1}{2} \|x\|_2^2 \quad (\text{A.35})$$

$$-\min_{s \in \mathcal{B}_F} \frac{1}{2} \|s\|_2^2 \quad (\text{A.36})$$

Proof. Recall from [124] that if $g : X \times Y \rightarrow \mathbb{R}$ is continuous convex-concave, i.e., $g(\cdot, y)$ is convex for every given y and $g(x, \cdot)$ is concave for any given x , and if the sets X and Y are convex, then: $\min_{x \in X} \max_{y \in Y} g(x, y) = \max_{y \in Y} \min_{x \in X} g(x, y)$. As a consequence:

$$\begin{aligned} \min_{x \in \mathbb{R}^n} f(x) + \frac{1}{2} \|x\|_2^2 &= \min_x \max_{s \in \mathcal{B}_F} s^T x + \frac{1}{2} \|x\|_2^2 \\ &= \max_{s \in \mathcal{B}_F} \min_x s^T x + \frac{1}{2} \|x\|_2^2, \end{aligned}$$

because $g(x, s) = s^T x + \frac{1}{2} \|x\|_2^2$ is convex in x and concave (linear) in s , g is continuous and \mathbb{R} and \mathcal{B}_F are convex sets. By differentiating g with respect to x , it is easy to see that:

$$\begin{aligned} \max_{s \in \mathcal{B}_F} \min_x s^T x + \frac{1}{2} \|x\|_2^2 &= \max_{s \in \mathcal{B}_F} -\frac{1}{2} \|s\|_2^2 \\ &= -\min_{s \in \mathcal{B}_F} \frac{1}{2} \|s\|_2^2, \end{aligned} \quad (\text{A.37})$$

which concludes the proof. \square

Summarizing the previous results, we obtain the following proposition.

Proposition 10. *Let F be a submodular function and f its Lovász extension. Let u^* be the unique minimizer of the function $x \rightarrow f(x) + \frac{1}{2} \|x\|_2^2$. Then: (a) $s^* = -u^*$ is the point of \mathcal{B}_F with minimum norm; (b) The unique minimal minimizer of F is $\{j|s_j^* < 0\}$.*

A.4.2 Linear Optimization over the Base Polyhedron

We have seen that our problem now reduces to finding a point in the base polyhedron with minimum norm. An extreme point of \mathcal{B}_F can be easily computed using the Algorithm 3, which can be used also to compute the Lovász extension at some point x . This algorithm, of $O(n \log n)$ complexity, performs a linear minimization over the base polyhedron, obtained by sorting the coordinates of x in increasing order. The justification of the algorithm is given by Theorem 1. Thus, we see that x plays a role only through the ordering of its coordinates.

Proposition 11. *All extreme points of \mathcal{B}_F can be obtained using Algorithm 3, using all possible ordering of x coordinates.*

An exhaustive search for the norm minimization over the base polyhedron (A.36) would then require at most $n!$ runs of this algorithm. The min-norm algorithm presented in the next section provides a much faster solution.

A.5 Min-Norm Algorithm

In this section, we provide further details of the different steps of the min-norm algorithm, described in Algorithm 4.

A.5.1 Initialization

At the initialization of the algorithm, it is required to start with a vertex of \mathcal{B}_F . According to Theorem 2.1 of [125], every minimization problem of the form $\min_{x \in \mathcal{B}_F} p^T x$ provides a vertex of \mathcal{B}_F . As this minimization problem is solved using the Algorithm 3, every permutation of $\{1, 2, \dots, n\}$ generates a vertex of \mathcal{B}_F (Proposition 11). So for the initialization of the algorithm, we can choose the identity permutation. As a result, defining for $k = 1, \dots, n$:

$$q_k = F(\{1, \dots, k\}) - F(\{1, \dots, k-1\}) \quad (\text{A.38})$$

provides a vertex of \mathcal{B}_F . Above, by definition we set $F(\{1, \dots, k-1\}) = F(\emptyset) = 0$ when $k = 1$.

A.5.2 Linear Optimization over the Base Polyhedron

As we have seen in the previous sections, in order to solve: $q = \arg \min_{p \in \mathcal{B}_F} x^T p$, we can use Algorithm 3.

A.5.3 Optimality Test

The optimality test is given by $\|x\|^2 \leq x^T q + \epsilon$, where $\epsilon > 0$. The explanation is given in [109] and is as follows. Note that $x \in \mathcal{B}_F$ and take some $y \in \mathcal{B}_F$ and $0 \leq \theta \leq 1$. Let define $z_\theta = x + \theta(y - x)$. We have $z_\theta \in \mathcal{B}_F$ because \mathcal{B}_F is convex. We have also: $\|z_\theta\|^2 = \|x\|^2 + 2\theta(x^T y - x^T x) + \theta^2\|y - x\|^2$

We now claim that x is of minimum norm in \mathcal{B}_F iff $x^T y - x^T x \geq 0$ for all y . Indeed:

- If there exists a y s.t. $x^T y - x^T x < 0$, we can find z_θ with lower norm than x for sufficiently small θ .
- If for all y , $x^T y - x^T x \geq 0$, then take any y and set $\theta = 1$ so that $z_1 = y$. We have: $\|y\|^2 = \|x\|^2 + 2(x^T y - x^T x) + \|y - x\|^2 > \|x\|^2$.

Equivalently, we claim that: x is of minimum norm in \mathcal{B}_F iff $\min_y x^T y \geq \|x\|^2$. Equivalently: x is of minimum norm in \mathcal{B}_F iff $x^T q \geq \|x\|^2$. Equivalently: x is of minimum norm in \mathcal{B}_F iff $x^T q = x^T x$ (since $x \in \mathcal{B}_F$).

A.5.4 Norm Minimization over the Affine Hull

At this step, we want to minimize the norm over the affine hull. Let thus consider the following generic problem:

$$\begin{aligned} \min \quad & \frac{1}{2}x^T A x + b^T x + c \\ \text{s.t.} \quad & Hx = d \\ & x \in \mathbb{R}^n \end{aligned}$$

with A invertible. KKT conditions are [124]: $Hx^* = d$ and $Ax^* + b + H^T \lambda^* = 0$. Let $B = (HA^{-1}H^T)^{-1}$, then:

$$\begin{aligned} x^* &= A^{-1}H^T B(HA^{-1}b + d) - A^{-1}b \\ \lambda^* &= -B(HA^{-1}b + d) \end{aligned}$$

Let us use this result to solve: $y = \arg \min_{z \in \text{aff}(S)} \|z\|$. Let $S = \{q_1, \dots, q_m\}$, $\alpha = [\alpha_1 \dots \alpha_m]^T$, $Q = [q_1 q_2 \dots q_m]$, and $A = 2Q^T Q$. Define the affine hull of S as follows: $\text{aff}(S) \triangleq \{\sum_{i=1}^m \alpha_i q_i \mid q_i \in S \text{ and } \sum_{i=1}^m \alpha_i = 1\}$. We note that: $\|\sum_{i=1}^m \alpha_i q_i\|^2 = \|Q\alpha\|^2 =$

$(Q\alpha)^T(Q\alpha) = \alpha^T Q^T Q \alpha$. Thus, our problem becomes:

$$\begin{aligned} \min \quad & \frac{1}{2} \alpha^T A \alpha \\ \text{s.t.} \quad & \mathbf{1}^T \alpha = 1, \alpha \in \mathbb{R}^n \end{aligned}$$

There is a unique solution iff the matrix $\begin{bmatrix} 0 & \mathbf{1}^T \\ \mathbf{1} & Q^T Q \end{bmatrix}$ is non singular, i.e., if the points of

Q are affinely independent. Using previous results, the solution is: $\alpha^* = \frac{A^{-1}\mathbf{1}}{\mathbf{1}^T A^{-1}\mathbf{1}}$, so that $y = Q\alpha^*$ and $\|y\|^2 = \frac{1}{2} \frac{1}{\mathbf{1}^T A^{-1}\mathbf{1}}$. Take any $v := Q\alpha$ with $\mathbf{1}^T \alpha = 1$ (i.e., in the affine hull of S), then $v^T y = \alpha^T Q^T Q \alpha^* = \frac{1}{2} \frac{\alpha^T A \alpha^*}{\mathbf{1}^T A^{-1}\mathbf{1}} = \|y\|^2$.

A.5.5 Line Search

We provide here the justification for the following steps (13-14) of the algorithm:

$$\begin{aligned} \theta &\leftarrow \min_{i:\alpha_i < \lambda_i} \lambda_i / (\lambda_i - \alpha_i); \\ x &\leftarrow \theta y + (1 - \theta)x; \lambda \leftarrow \theta \alpha + (1 - \theta)\lambda : \end{aligned}$$

Note that first we have always $\lambda_i \geq 0$ for all i because x is always in the convex hull of S . Let $z_\theta = \theta y + (1 - \theta)x$ and $\lambda'_i(\theta) = \theta \alpha_i + (1 - \theta)\lambda_i$ s.t. $z_\theta = \sum_i \lambda'_i(\theta) q_i$. Clearly z_θ is on the line (x, y) . It is also in $\text{conv}(S)$ if $\lambda'_i(\theta) \geq 0$ for all i . Choose $\theta = \min_{j:\alpha_j < \lambda_j} \lambda_j / (\lambda_j - \alpha_j)$ and notice that $0 \leq \theta < 1$. Now, if $\alpha_i \geq \lambda_i$, then $\lambda'_i(\theta) = \theta(\alpha_i - \lambda_i) + \lambda_i \geq 0$ because $\theta \geq 0$ and $\lambda_i \geq 0$. If on the contrary $\alpha_i \leq \lambda_i$, then $\lambda'_i(\theta) \geq \frac{\lambda_i}{\lambda_i - \alpha_i}(\alpha_i - \lambda_i) + \lambda_i$ (using the definition of θ), i.e., $\lambda'_i(\theta) \geq 0$. As a conclusion: with this θ , $\lambda'_i(\theta) \geq 0$ in all cases (for all i) and z_θ is in $\text{conv}(S)$. Moreover, there is at least one k ($k = \arg \min_{i:\alpha_i < \lambda_i} \lambda_i / (\lambda_i - \alpha_i)$) such that $\lambda'_k(\theta) = 0$. This justifies step 15 of the algorithm.

A.5.6 Algorithm Termination

We now show that the min-norm algorithm always terminates. A loop invariant is that all points of S are affinely independent. Suppose it is true at the beginning of a major cycle. A new point q is added to S if and only if $\|x\|^2 \neq x^T q$, where x is the affine minimizer of S . As we have: $\forall v \in \text{aff}(S), x^T v = \|x\|^2, q \notin \text{aff}(S)$. Then, during minor cycles, points are removed from S so that remaining points remain affinely independent. From this, we deduce that $S \leq n + 1$ is another invariant of the algorithm.

During every line search in the minor cycle, at least one point is removed from S : let $j = \arg \min_{i: \alpha_i < \lambda_i} \lambda_i / (\lambda_i - \alpha_i)$, then $\lambda_j \leftarrow 0$ at the next step of the algorithm, so that q_j will be removed from S . If S is a singleton, then the affine minimizer is also in the convex hull and the minor cycle stops at step 11. This means that there cannot be more than n minor cycles within a major cycle.

It is thus now sufficient to show that the number of major cycles is bounded. For that, we start by showing that the norm of x strictly decreases. If we do not perform line search (step 11), then $\|y\|^2 \leq \|x\|^2$ (because y is an affine minimizer) and $y \neq x$ (because $y^T q = \|y\|^2$ from the affine minimizer property while $x^T q \neq \|x\|^2$ from step 6). If a line search is performed (step 13), let $x' = \theta y + (1 - \theta)x$. If $\theta = 0$, i.e., there is some $\lambda_i = 0$, then q_i is removed and this cycle is immediately followed by another minor cycle. We can thus assume that $\theta > 0$. As y is the affine minimizer, which is unique and $y \notin \text{conv}(S)$, $\|y\| < \|x\|$. Then, $\|x'\| \leq \theta \|y\| + (1 - \theta)\|x\| < \|x\|$ because $\theta > 0$. As a consequence, every major cycle starts with a different corral. As the number of corrals is finite, the algorithm terminates.

Glossary

2G	Second Generation
3G	Third Generation
3GPP	3rd Generation Partnership Project
4G	Fourth Generation
5G	Fifth Generation
APCO P25	Association of Public-safety Communications Officials-Project 25
ARQ	Automatic Repeat re-Quest
AWGN	Additive White Gaussian Noise
BLER	Block Error Rate
BS	Base Station
BSs	Base Stations
CC	Chase Combining
CDF	Cumulative Distribution Function
CoMP	Coordinated MultiPoint
CP	Cyclic Prefix
CQI	Channel Quality Indicator
CSA	Common Subframe Allocation
CSI	Channel State Information
D2D	Device-To-Device
eBM-SC	evolved Broadcast/Multicast Service Center
ECR	Effective Code Rate
EESM	Exponential Effective SNR Mapping

eMBMS	evolved Multimedia Broadcast/Multicast Service
eMBMS-GW	eMBMS GateWay
EPA	Extended Pedestrian A
EPC	Evolved Packet Core
ETU	Extended Typical Urban
EUTRAN	Evolved Universal Terrestrial Radio Access Network
EVA	Extended Vehicular A
FDD	Frequency Division Duplex
FRMCS	Future Railway Mobile Communication System
GCSE	Group Communication System Enabler
gNB	next generation Node-B
GSM	Global System for Mobile communications
HARQ	Hybrid Automatic Repeat re-Quest
ICI	Inter-Cell Interference
IoT	Internet of Things
IR	Incremental Redundancy
ISI	Inter-Symbol Interference
LTE	Long Term Evolution
LTE-A	Long Term Evolution Advanced
MAC	Medium Access Control
MBB	Mobile BroadBand
MBMS	Multimedia Broadcast/Multicast Service
MBSFN	Multicast/Broadcast Single Frequency Network
MCCH	Multicast Control CHannel
MCDData	Mission-Critical Data
MCE	Multi-cell/multicast Coordination Entity
MCH	Multicast CHannel
MCPTT	Mission-Critical Push-To-Talk

MCS	Modulation and Coding Scheme
MCSs	Modulation and Coding Schemes
MVideo	Mission-Critical Video
MIC	Mean Instantaneous Capacity
MIMO	Multiple Input Multiple Output
MME	Mobility Management Entity
mMTC	Massive Machine-Type Communications
MRC	Maximum Ratio Combining
MSA	MCH Subframe Allocation
MTC	Machine-Type Communications
MTCH	Multicast Traffic CHannel
NACK	Non-ACKnowledgement
NB-IoT	NarrowBand-Internet of Things
NM	Nelder-Mead
OFDM	Orthogonal Frequency-Division Multiplexing
PDCCH	Physical Downlink Control CHannel
PDSCH	Physical Downlink Shared CHannel
PMCH	Physical Multicast CHannel
PMR	Professional Mobile Radio
ProSe	Proximity Services
PSNR	Peak Signal to Noise Ratio
PTM	Point-To-Multipoint
PTP	Point-To-Point
PTT	Push-To-Talk
QAM	Quadrature Amplitude Modulation
QoE	Quality of Experience
QoS	Quality of Service
QPSK	Quadrature Phase Shift Keying
RB	Resource Block
RBs	Resource Blocks
RLC	Radio Link Control

RMS	Root Mean Square
RNTI	Radio Network Temporary Identifier
SC-PTM	Single-Cell Point-To-Multipoint
SE	Spectral Efficiency
SINR	Signal to Interference plus Noise Ratio
SIR	Signal to Interference Ratio
SISO	Single Input Single Output
SNR	Signal to Noise Ratio
SSE	System Spectral Efficiency
SSIM	Structural SIMilarity
TETRA	TERrestrial Trunked RADio
TETRAPOL	TETRA for POLice
TTI	Transmission Time Interval
UE	User Equipment
UEs	User Equipments
UIC	International Union of Railway
UM	Unacknowledged Mode
uMTC	Ultra-reliable Machine-Type Communications
UMTS	Universal Mobile Telecommunication System
URLLC	Ultra-Reliable Low Latency Communications
UTRAN	Universal Terrestrial Radio Access Network
V2X	Vehicule-to-anything

Title: Optimizing Cellular Networks for Business and Mission-Critical Communications

Keywords: Critical Communications; PMR; MBMS; Optimization.

Abstract: Business- and mission-critical communications are communications between professional users either from the public safety sector or operating critical infrastructures. Owing to special coverage, priority access, reliability and resilience requirements, as well as additional services for professional users, these communications are conveyed by Professional Mobile Radio (PMR) networks. Driven by the demand growth, significant changes are taking place in the PMR industry. The existing PMR technologies are indeed not well suited to provide high data rates mobile services like video and photo transfers; hence, the adoption of commercial technologies for mission-critical communications is gaining strong momentum. On the other hand, the next generation cellular networks are envisioned to support a large variety of applications and services with heterogeneous performance requirements, i.e., enhanced Mobile BroadBand (eMBB), massive Machine-Type Communications (mMTC) and Ultra-Reliable Low Latency Communications (URLLC). Recently, mission-critical communications have been classified in a URLLC use case family, characterized by the need to a higher priority over other communications in the networks.

In this context, we focus on enhancing the coverage of wireless networks providing group communications, the main service allowed by PMR networks, taking advantage of the current technologies (e.g. Multimedia Broadcast/Multicast Service), to meet the mission-critical communications needs. First, we evaluate the performance of unicast and multicast transmission tech-

niques, i.e., the Multicast/Broadcast Single Frequency Network (MBSFN) and Single-Cell Point-To-Multipoint (SC-PTM), in terms of radio quality, system spectral efficiency and cell coverage, assuming static MBSFN configurations. Then, we introduce an analytical model to derive an approximate closed-form formula of the Signal to Interference plus Noise Ratio (SINR) in a MBSFN network.

Furthermore, we propose a simple repetition scheme without request, as an alternative to Hybrid Automatic Repeat re-Quest (HARQ), in the aim of improving the network coverage in presence of group communications. By considering the wireless channel characteristics, as well as the service delay constraints, we show that our proposed scheme provides significant gains over traditional repetition schemes.

Finally, we assess the trade-off in the cluster's size of serving cells which arises between network coverage and capacity in multi-point transmissions. We formulate an optimization problem to maintain an acceptable system blocking probability, while maximizing the average SINR of the multicast group users. For group calls, a dynamic cluster of cells is selected based on the minimization of a submodular function that takes into account the traffic in every cell through some weights and the average SINR achieved by the group users. Traffic weights are then optimized using a Nelder-Mead simplex method with the objective of tracking a blocking probability threshold. Results show the importance of dynamic clustering in improving system capacity and coverage.

Titre: Optimisation des réseaux cellulaires pour les communications professionnelles critiques.

Mots clés: Communications critiques; PMR; MBMS; Optimisation.

Résumé: Les communications professionnelles et critiques sont établies soit entre utilisateurs du secteur de la sécurité publique soit entre acteurs opérants des infrastructures critiques. Du fait des fortes exigences en termes de couverture, de priorité d'accès, de fiabilité et de résilience, sans oublier les services supplémentaires pour les utilisateurs professionnels, ces communications utilisent généralement les technologies PMR (*Professional Mobile Radio*). Vu la croissance des demandes de services, des changements importants auront lieu dans la PMR. Les technologies PMR historiques échouent cependant à fournir des services à débits de données élevés, tels que les services vidéos et le transfert de photos. Ainsi, l'adaptation des technologies utilisées par les opérateurs commerciaux à la PMR apparaît comme une solution prometteuse. D'autre part, la prochaine génération de réseaux cellulaires prévoit une nouvelle variété d'applications et de services, dont les exigences de performances sont extrêmement hétérogènes, i.e., *enhanced Mobile BroadBand* (eMBB), *massive Machine-Type Communications* (mMTC) et *Ultra-Reliable Low Latency Communications* (URLLC). Récemment, les communications critiques ont été classées dans une famille de cas d'usage, caractérisé par un fort besoin de priorité par rapport aux autres communications dans le réseau.

Dans ce contexte, nous allons nous concentrer à renforcer la couverture des réseaux radio fournissant des communications de groupe, service essentiel fourni par les technologies PMR, pour parvenir les besoins des communications critiques. Tout d'abord, on évalue la performance des transmissions unicast et multicast, i.e., les transmissions *Multicast/Broadcast Single Frequency Network* (MBSFN) et *Single-Cell Point-To-Multipoint* (SC-PTM), en

termes de qualité radio, d'efficacité spectrale du système et de couverture de cellules, tout en considérant des configurations MBSFN statiques. Puis, nous étudions un modèle analytique pour estimer le *Signal to Interference plus Noise Ratio* (SINR) dans un réseau MBSFN.

En outre, nous proposerons un algorithme simple de répétitions sans requête, comme alternative à l'algorithme *Hybrid Automatic Repeat re-Quest* (HARQ), afin d'améliorer la couverture du réseau en présence de communications de groupe. En considérant les caractéristiques du canal radio, ainsi que les contraintes de délai de service, nous justifierons que notre modèle fournit un important gain par rapport aux algorithmes de répétitions traditionnels.

Enfin, on évalue le compromis entre la couverture et la capacité d'un réseau utilisant les transmissions *Coordinated Multi-Point* (CoMP), qui évolue en fonction de la taille du *cluster* de stations serveuses. On formule alors un problème d'optimisation dont l'objectif est de maintenir une probabilité de blocage acceptable du système, tout en maximisant le SINR moyen du groupe d'utilisateurs. Pour chaque groupe, on choisit le *cluster* de cellules d'une manière dynamique, en se fondant sur la minimisation d'une fonction sous-modulaire, qui prend en compte le trafic de chaque cellule du réseau à travers certains poids, ainsi que le SINR moyen du groupe. Ces poids sont optimisés au moyen de la méthode Nelder-Mead, dans le but de diriger la probabilité de blocage vers un certain seuil. Les résultats obtenus montrent l'importance du regroupement dynamique des cellules dans l'amélioration de la capacité et la couverture du système.